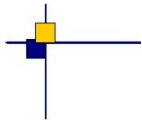




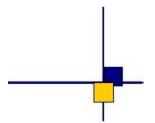
CalVal Jason-1



Jason-1 - GDR-E release

Global assessment over ocean

Contract No 104685/00 TC6



Nomenclature : SALP-RP-MA-EA-22426-CLS

Issue : 1rev 1

Date : February 3, 2017

Chronology Issues :		
Issue :	Date :	Reason for change :
1.0	09/09/2016	document creation
1.1	02/02/2017	Updated after CNES review (Nicolas Picot and Jean-Damien Desjonqueres)

People involved in this issue:				
	AUTHORS	COMPANY	DATE	INITIALS
WRITTEN BY	H. Roinard S. Philipps	CLS CLS		
CHECKED BY	S. Rouge	CLS		
APPROVED BY	J.P. Dumont	CLS CLS		
APPLICATION AUTHORISED BY				

Index sheet :	
Context	
Keywords	Jason-2, Jason-1, Calval, Reprocessing
hyperlink	

Distribution :		
Company	Means of distribution	Names
CLS	electronic copy	V. Rosmorduc J.P. Dumont
CNES	electronic copy	emilie.bronner@cnes.fr francoise.bailly-poirot@cnes.fr Jean-Damien.Desjonqueres@cnes.fr nicolas.picot@cnes.fr thierry.guinle@cnes.fr aqgp_rs@cnes.fr

List of tables and figures :

List of Tables

1	Models and standards adopted for the Jason-1 product version “C” and “E”	7
2	Editing criteria	13
3	Used Jason-1 and Jason-2 data for crossover analysis	17
4	SLA global bias between repetitive and geodetic Jason-1 phases	47
5	Table of uncertainties on Jason-1 summarize	56

List of Figures

1	Top: Number of ocean data available for GDR-E and GDR-C products. Bottom: Number of data difference GDR-E - GDR-C.	9
2	Top left: Percentage per cycle of rejected data in GDR-C and GDR-E. Top right: Difference of percentage of rejected data (GDR-E - GDR-C). Bottom: Maps of valid measurements with one dataset that are rejected considering the other dataset over year 2002. Left: Valid with GDR-C and rejected with GDR-E. Right: Valid with GDR-E and rejected with GDR-C.	10
3	Left: Percentage per cycle of rejected data in GDR-C and GDR-E on all thresholds criteria. Right: Difference of percentage of rejected data (GDR-E - GDR-C).	11
4	Difference of number of points rejected on thresholds criteria: Left: sea state bias Right: ionospheric correction	11
5	Difference of number of points rejected on thresholds criteria: Top left: ocean tide (Got4.10 vs Got00) Top right: Radiometer wet troposphere correction Bottom left: Wind speed Bottom right: Sea Level Anomaly	12
6	For monitorings, crossovers are only selected for open ocean (latitude less than $\pm 50^\circ$, bathymetry less than -1000 m and oceanic variability less than 20 cm). Top: Cycle per cycle monitoring of mean (left) and standard deviation (right) of SSH difference at crossovers with GDR-E (red) and GDR-C (blue) standards. Bottom left: Difference of SSH variance at crossovers between GDR-E and GDR-C. Bottom right: Map of difference of SSH variances (variance SSH_{GDR-E} - variance SSH_{GDR-C}).	16
7	Bottom left: Difference of SSH variance at crossovers between GDR-E and pseudo GDR-D. Crossovers are only selected for open ocean (latitude less than $\pm 50^\circ$, bathymetry less than -1000 m and oceanic variability less than 20 cm). Bottom right: Map of difference of SSH variances (variance SSH_{GDR-E} - variance SSH_{GDR-D}).	16
8	Mean at SSH crossovers for Jason-1 whole period Left: GDR-C. Right: GDR-E.	17
9	Monitoring of mean (left) and standard deviation (right) of Jason-1 minus Jason-2 SSH crossovers.	18
10	Left: Cycle per cycle monitoring of pseudo time-tag bias estimated cycle by cycle from GDR-C and GDR-E products for Jason-1. Unit is in seconds. Right: Periodogram of pseudo time tag bias.	19
11	Left: Cycle per cycle mean of SLA with GDR-C (blue) and GDR-E (red) standards. Right: Monitoring per cycle of the difference of GDR-E SLA and GDR-C SLA	20
12	Cycle per cycle standard deviation of along track SLA with GDR-C (blue) and GDR-E (red) standards.	21

13	<i>SLA differences between Jason-1 and Jason-2 (before applying orbit error correction),</i> Left: <i>with GDR-D standards for Jason-2 and updated GDR-C standards for Jason-1,</i> Right: <i>with GDR-E standards for Jason-1 and updated GDR-D standards for Jason-2.</i> Bottom: <i>SLA differences between Jason-1 and Jason-2 (without any correction) with GDR-E standards.</i>	22
14	<i>Main changes in final POE-E orbit standard compared to POE-D.</i>	24
15	<i>Final POE-E orbit standard. Difference of variance at crossovers</i>	24
16	<i>Final POE-E orbit standard. Global Mean Sea Level</i>	25
17	<i>Final POE-E orbit standard. Regional Mean Sea Level: location of studied boxes.</i>	26
18	<i>Final POE-E orbit standard. Regional Mean Sea Level: East/West differences in boxes.</i>	26
19	<i>Cycle per cycle monitoring of radiometer minus model wet troposphere differences. Radiometer minus model for Jason-1 GDR-E and GDR-C.</i>	28
20	Left: <i>Difference of radiometer minus ECMWF model wet troposphere correction as a function of coast distance for Jason-1 cycle 250 (Jason-2 cycle 011).</i> Right: <i>: Difference of SLA variances - computed by using successively GDR-E and GDR-C radiometer wet troposphere - as a function of coastal distances between 0 and 100 km.</i> Bottom: <i>Map of differences between GDR-E - GDR-C radiometer wet troposphere</i>	29
21	<i>Mean of Jason-1 - Jason-2 wet troposphere differences over tandem phase. Top left:</i> <i>Map with J1 updated GDR-C and J2 GDR-D. Top right:</i> <i>Map with J1 GDR-E and J2 updated GDR-D. Bottom left:</i> <i>Daily monitoring Bottom right:</i> <i>Cyclic monitoring</i>	30
22	<i>Cycle per cycle monitoring of radiometer minus model wet troposphere differences. Left:</i> <i>radiometer minus ERA or ECMWF operational model wet troposphere difference for GDR-E Jason-1. Right:</i> <i>radiometer or ERA model minus ecmwf wet troposphere model, and ecmwf model changes.</i>	31
23	<i>GDR-E minus GDR-C difference over Jason-1 cycle 250.</i>	31
24	<i>Mean of Jason-1 - Jason-2 atmospheric attenuation differences over tandem phase. Left:</i> <i>J1 GDR-C and J2 GDR-D. Right:</i> <i>J1 GDR-E and J2 GDR-D.</i>	32
25	Top: <i>Mean of Jason-1 - Jason-2 sigma0 differences over tandem phase. Left:</i> <i>J1 updated GDR-C and J2 GDR-D. Right:</i> <i>J1 GDR-E and J2 updated GDR-D. Bottom left:</i> <i>GDR-E minus GDR-C difference over Jason-1 cycle 250. Bottom right:</i> <i>Daily mean and standard deviation of Jason1 - Jason2 Ku-band backscattering coefficient difference over the tandem phase.</i>	33
26	<i>Mean of Jason-1 - Jason-2 wind speed differences over tandem phase. Left:</i> <i>J1 updated GDR-C and J2 GDR-D. Right:</i> <i>J1 GDR-E and J2 updated GDR-D Bottom left:</i> <i>GDR-E minus GDR-C difference over Jason-1 cycle 250. Bottom right:</i> <i>Daily mean and standard deviation of Jason1 - Jason2 Ku-band altimeter wind speed difference over the tandem phase.</i>	34
27	Top: <i>Mean of Jason-1 - Jason-2 ssb (Ku band) differences over tandem phase. Bottom:</i> <i>Mean of Jason-1 - Jason-2 ssb (C band) differences over tandem phase. Left:</i> <i>J1 GDR-C and J2 GDR-D. Right:</i> <i>J1 GDR-E and J2 Tran2012</i>	35
28	Top: <i>Mean of Jason-1 - Jason-2 dual frequency ionosphere correction differences over tandem phase. Left:</i> <i>J1 updated GDR-C and J2 GDR-D. Right:</i> <i>J1 GDR-E and J2 updated GDR-D Bottom left:</i> <i>GDR-E minus GDR-C difference over Jason-1 cycle 250. Bottom right:</i> <i>Daily mean and standard deviation of Jason1 - Jason2 ionosphere correction difference over the tandem phase.</i>	36

29	<i>Cycle by cycle monitoring of the difference of variance at crossover points with selection on bathy < -1000m, LAT < 50°, and oceanic variability < 0.2m. Impact of SSB + IONO</i>	37
30	<i>Difference of valid measurements with ocean tide GOT thresholds criterion over cycle 250.</i>	37
31	Left: <i>Monitoring of mean of GDR-E (Got4.10) minus GDR-C (Got00) Jason-1 ocean tide differences. Right:</i> <i>Map of the difference</i>	38
32	Left: <i>Map of differences of SSH variances (SSH variance using GOT4.10 - SSH variance using GOT00) Right:</i> <i>cyclic monitoring of this difference.</i>	38
33	<i>Difference of SLA variances - computed by using successively GDR-E GOT4.10 and GDR-C GOT00.2 tide model Left:</i> <i>plotted in function of coastal distances between 0 and 100 km. Right:</i> <i>Map of the difference</i>	39
34	<i>Periodogram of SLA using different ocean tide solutions close to 59 days signal.</i>	39
35	Left: <i>Map of differences of SSH variances (SSH variance using FES2014 - SSH variance using GOT4.10) Right:</i> <i>cyclic monitoring of this difference.</i>	40
36	<i>Difference of SLA variances - computed by using successively GDR-E GOT4.10 and FES2014 tide model Left:</i> <i>plotted in function of coastal distances between 0 and 100 km. Right:</i> <i>Map of the difference</i>	40
37	<i>GDR-E minus GDR-C pole tide difference over Jason-1 cycle 355.</i>	41
38	<i>GDR-E minus GDR-C long period non equilibrium tide difference over Jason-1 cycle 250.</i>	41
39	Left: <i>Map of differences between MSS2011 referenced over 20 years and MSS2001 for Jason-1 cycle 250 Right:</i> <i>Map of differences between MSS2011 referenced over 20 years and MSS2011 for Jason-1 cycle 250 Bottom:</i> <i>Difference of variance of SLA for repetitive phase.</i>	42
40	<i>SLA spectrum computed with one Jason-1 cyle (1Hz GDR data) Left:</i> <i>Cycle 250: Historical ground-track Middle:</i> <i>Cycle 300: interleaved ground-track Right:</i> <i>Cycle 510: geodetic ground-track</i>	43
41	<i>GDR-E minus GDR-C MDT difference over Jason-1 cycle 250.</i>	43
42	<i>GDR-E minus GDR-C geoid difference over Jason-1 cycle 355.</i>	44
43	<i>GDR-E minus GDR-C bathymetry difference over Jason-1 cycle 355.</i>	44
44	<i>Cycle per cycle mean of model dry tropospheric correction from ERA Interim products</i>	45
45	<i>Cycle per cycle mean of Left:</i> <i>high frequency fluctuations of the sea surface topography derived from ERA Interim products. Right:</i> <i>inverted barometer height correction from ERA Interim products. Bottom:</i> <i>mog2d from ERA Interim products</i>	46
46	<i>Cycle per cycle mean of model wind vector from ERA Interim products Left:</i> <i>U component. Right:</i> <i>V component.</i>	46
47	<i>Global Mean Sea Level difference between odd and even passes, annual and semi-annual signals removed. Left:</i> <i>GDR-C Right:</i> <i>GDR-E</i>	48
48	Top: <i>Global MSL trends for J1 GDR-E versus GDR-C (annual and semi-annual signals are removed) Left:</i> <i>limited to repetitive phase Right:</i> <i>including geodetic phase, bias between repetitive and geodetic phase presented on dedicated part are applied. Bottom:</i> <i>Global MSL trends difference between J1 GDR-E and GDR-C</i>	49
49	Top: <i>Global MSL trends for J1 versus J2 (annual and semi-annual signals are removed) over common inflight period. Jump value in Jason-1 SLA is applied (bias presented on dedicated part are applied). Bottom:</i> <i>Maps of the Jason-1 minus Jason-2 MSL difference of trends. Left:</i> <i>J1 GDR-C and J2 GDR-D Right:</i> <i>J1 GDR-E and J2 updated GDR-D (GDR-E like).</i>	50

50	<i>Global MSL trends for J1 versus J2 (annual and semi-annual signals are removed) over common inflight period. Jump value in Jason-1 SLA is applied (bias presented on dedicated part are applied). Data used are J1 GDR-E and J2 updated GDR-D (GDR-E like). Top left: Whole common inflight period Top right: without year 2013. Bottom left: using ECMWF wet tropospheric correction. Bottom right: using ERA-Interim wet tropospheric correction.</i>	51
51	<i>Time series of global average differences between Jason-1 GDR-C (blue) or GDR-E (red) and tide gauges Top Left: Repetitive Phasis, no signal ajustment. Top Right: Repetitive Phasis, annual and semi-annual signals ajustments. Bottom:Whole Jason-1 mission.</i>	52
52	<i>Rms of elementary Ku-band range measurements left: Mean per cycle monitoring. right: in function of significant wave height for Jason-1 GDR-E over 2011.</i>	57
53	<i>Rms of elementary C-band range measurements in function of significant wave height for Jason-1 GDR-E over 2011.</i>	58
54	<i>Cycle per cycle monitoring (mean and standard deviation) of the Jason-1 minus Jason-2 unfiltered (top) and filtered (bottom) dual-frequency ionospheric correction.</i>	59
55	<i>Cycle per cycle monitoring (mean and standard deviation) of the Jason-1 minus Jason-2 non-parametric sea state bias correction.</i>	60
56	<i>Cycle per cycle monitoring (mean and standard deviation) of the Jason-1 minus Jason-2 radiometer wet tropospheric correction.</i>	61
57	<i>Cycle per cycle monitoring of the radiometer minus model (ECMWF or ERA-Interim) wet tropospheric correction difference for Jason-1 GDR. Vertical lines indicate a change in ECMWF model. Left: mean. Right: standard deviation.</i>	62
58	<i>Rms of elementary Ku-band SWH measurements in function of significant wave height for Jason-1 GDR-E over 2011.</i>	62
59	<i>Cycle per cycle monitoring (mean and standard deviation) of the Jason-1 minus Jason-2 significant wave height.</i>	63
60	<i>Rms of elementary Ku-band Sigma0 measurements in function of significant wave height for Jason-2 GDR over 2011.</i>	63
61	<i>Cycle per cycle monitoring (mean and standard deviation) of the Jason-1 minus Jason-2 backscattering coefficient.</i>	64
62	<i>Cycle per cycle monitoring of std of altimeter - model wind speed for Jason-1 GDR-E over 2011.</i>	64
63	<i>Cycle per cycle monitoring (mean and standard deviation) of the Jason-1 minus Jason-2 altimeter wind speed.</i>	65
64	<i>Cycle per cycle monitoring (standard deviation) of the Jason-1 minus Jason-2 sea level anomaly.</i>	66
65	<i>Cycle per cycle monitoring standard deviation of ascending / descending sea surface height differences for Jason-2 OGDR, IGDR and GDR products.</i>	66
66	<i>MSL trend uncertainties from 1993 to 2008 for each correction or model impacting the MSL calculation.</i>	67

Contents

1. Introduction	1
2. Data used and processing	3
2.1. Data used	3
2.2. GDR standards	4
2.3. Jason-2 data used for comparison	7
3. Missing and invalidated measurements	8
3.1. Missing measurements	8
3.2. Invalidated measurements	9
4. Quality overview/Performances	14
4.1. Performances at crossovers	14
4.1.1. Jason-1/Jason-2 SSH crossover differences	17
4.1.2. Estimation of pseudo time-tag bias	18
4.2. Along-track performances of Sea Level Anomaly	20
4.2.1. SLA differences between GDR-E and GDR-C	20
4.2.2. SLA differences between Jason-1 and Jason-2	21
5. Details of the changes in GDR-E standard	23
5.1. Concerning the datation of GDR-E products	23
5.2. Concerning the standard of GDR-E Precise Orbit Ephemeris (POE-E)	23
5.2.1. Comparison between GDR-E orbit and GDR-D orbit	23
5.2.1.1. Crossovers	24
5.2.1.2. Impact on Global and Regional Mean Sea Level	25
5.2.1.3. Global Mean Sea Level	25
5.2.1.4. Regional Mean Sea Level	25
5.2.1.5. Conclusions	26
5.2.2. Conclusions about the evolutions from GDR-C orbit to GDR-E orbit	27
5.3. Concerning the radiometer related parameters	27
5.3.1. Radiometer wet troposphere correction	28
5.3.2. Atmospheric attenuation	31
5.4. Concerning the altimeter related parameters and corrections derived from the altimeter related parameters	32
5.4.1. Altimeter Ku-band range	32
5.4.2. Ku-band sigma0	32
5.4.3. Altimeter wind speed	33
5.4.4. Sea State Bias and Dual-frequency ionosphere correction	34
5.5. Concerning other corrections	37
5.5.1. New global tide model (GOT4.10 and FES2014)	37
5.5.2. Pole tide correction	41
5.5.3. Long period non equilibrium tide	41
5.5.4. Mean sea surface	42
5.5.5. Mean dynamic topography	43
5.5.6. Geoid based on EGM2008	44
5.5.7. Bathymetry from DTM2000.1	44
5.5.8. Meteorological data: ERA-INTERIM	45

.....	
6. Long Term Monitoring	47
6.1. From J1 repetitive mission to geodetic drifting mission	47
6.2. Global and Regional Mean Sea Level Trend	47
6.3. Tide Gauges Comparison	52
7. Table of uncertainties	53
7.1. Comments	53
7.1.1. Description of the uncertainties sources	53
7.1.2. Methods to determine the uncertainties	54
7.1.2.1. Using tandem flight phase of Jason-2 with Jason-1	54
7.1.2.2. Spectral Analysis	54
7.1.2.3. Analyzing rms of 20 Hz data	55
7.1.2.4. Comparison with other corrections	55
7.1.2.5. Intercalibration with other altimeter missions	55
7.1.2.6. Bibliography and theoretical considerations	55
7.2. Jason-1 uncertainties summarize	56
7.3. Details	57
7.3.1. Altimeter Noise	57
7.3.2. Ionosphere	58
7.3.3. Sea State Bias	59
7.3.4. Dry Troposphere Correction	60
7.3.5. Wet Troposphere Correction	61
7.3.6. Significant Wave Height	62
7.3.7. Backscattering coefficient	63
7.3.8. Altimeter wind speed	64
7.3.9. Uncertainty on the raw Sea Surface Height (for time scales less than 10 days)	65
7.3.10. Uncertainty on the final SSH (for timescales less than 10 days)	66
7.3.11. System drift	67
8. Conclusion	68
9. References	69

LIST OF ACRONYMS

AMR	Advanced Microwave Radiometer
DEM	Digital Elevation Model
ECMWF	European Center for Medium range Weather Forecasts
GDR-C	Geophysical Data Record version C
GDR-D	Geophysical Data Record version D
GDR-E	Geophysical Data Record version E
GMSL	Global Mean Sea Level
JMR	Jason-1 Microwave Radiometer
LTM	Long Term Monitoring
MQE	Mean Quadratic Error
MSL	Mean Sea Level
MSS	Mean Sea Surface
MWT	Model Wet Troposphere
POE	Precise Orbit Ephemeris
PRF	Pulse Repetition Frequency
RWT	Radiometer Wet Troposphere
SHM	Safe Hold Mode
SLA	Sea Level Anomalies
SSB	Sea State Bias
SSH	Sea Surface Height
SWH	Significant Wave Height

1. Introduction

This document presents the synthesis report concerning validation activities of Jason-1 GDR-E under SALP contract (“N° 104685/00 TC6 tache3”) supported by CNES at the CLS Space Oceanography Division.

Since the beginning of the mission, Jason-1 data have been analyzed and monitored in order to assess the quality of Jason-1 GDR products (AVISO and PODAAC User handbook, [1]) for oceanographic applications. Since May 2012, Jason-1 was on a geodetic orbit. To distinguish this geodetic phase from the previous repeat ground-track, numbering of the geodetic orbit period starts with cycle 500. The repeat period of the geodetic orbit is 406 days, but GDRs are distributed using the 10.9 days sub-cycle. Therefore Jason-1 GDRs during the geodetic phase contain 280 tracks per cycle. For more information about the Jason-1 geodetic mission, see the technical note issued by E. Bronner and G. Dibarboue [4]. This report is basically concerned with long-term monitoring of the Jason-1 altimeter system, from all GDR data until the end of the mission, that is for 10 years of data on repetitive orbit (cycles 1 to 374, corresponding to period from January 2002 to March 2012) and 14 months of data on geodetic orbit (cycles 500 to 537, corresponding to period from May 2012 to June 2013). After loss of telemetry on 21 June 2013, Jason-1 was passivated and decommissioned on 01 July 2013, with the last command sent at 16:37:40 UTC.

The whole Jason-1 data had been computed in GDR-C since 2009, except from cycle 500 onwards: the orbit standard is switched to POE standard D and the mean sea surface available in the GDRs is CNES-CLS-2011. The present global report deals with the last complete reprocessed period (cycles 1 to 537) of the Jason-1 mission, thanks to comparison with previous Jason-1 GDR-C standard. It also contains the impact of the reprocessing on the mean sea level trend.

The work performed in terms of data quality assessment over ocean also includes cross-calibration analyzes, mainly with Jason-2.

Note that in this report, on figures showing cycle per cycle monitoring, the x-axis was shifted for the geodetic period by 119 cycles, in order to prevent a (artificial) gap between the last cycle on the repeat ground-track (cycle 374) and the first cycle on the geodetic orbit (cycle 500).

The report is split into 6 main sections, after this introduction describing the keys of the reprocessing campaign:

- first, the **data used** are presented, with a status of the geophysical content of the fields that have changed between GDR-C and GDR-E.
- the **data coverage** and measurement validity issues are then presented.
- a global **overview** of the performances improvement is then synthesized.
- then, the **impact of the reprocessing on the main altimeter and radiometer parameters** is presented.
- the impact of the reprocessing on **Mean Sea Level** issues, through cross calibration results is detailed on the **global** and **regional** drift.
- finally the error budget of the mission is presented.

2. Data used and processing

The whole Jason-1 data had been computed in GDR-C since 2009, except from cycle 500 onwards: the orbit standard is switched to POE standard D and the mean sea surface available in the GDRs is CNES-CLS-2011. The OSTST community requested several modifications in order to correct for some problems in the GDR-C and to improve the consistency with Jason-2 mission. The following updates are applied to the GDR-E data:

- Time tag bias and range bias correction
- New orbit (POE-E)
- Geophysical fields : Tides (FES 2014, GOT4.10), MSS (CNES&CLS_2011), MDT (CNES&CLS_2013)
- Additional corrections that may be useful for long term studies (ERA Interim, Mog2D...)
- Radiometer corrections
- Netcdf format compliant with Jason-2&3

After taking into account these requests, the reprocessing of the Jason-1 mission in GDR-E version started in 2014. As some anomalies had been detected in the first version of data during 2015, a second version of the products have been computed (final delivery to OSTST users on 09 May 2016 (<ftp://avisoftp.cnes.fr/AVISO/pub/jason-1/>)). It has been performed within the frame of the CNES Altimetry Ground Segment (SALP) activities (SALP contract N ° 104685/00).

2.1. Data used

This document deals with the global impact of Jason-1 altimeter mission reprocessing in version GDR-E.

- cycle 001 to 374 on its repetitive orbit covering the period from 15th of January 2002 to 3rd of March 2012,
- cycle 500 to 537 on its geodetic orbit covering the period from 7th of May 2012 to 21st of June 2013.

For any information concerning the data of previous GDR versions, please refer to the Jason-1 yearly reports [3]. Previously, the whole mission of Jason-1 (GDR products) was available in version “C” of CMA ground processing software. The different models and standards used for GDR-C and GDR-E versions are detailed in table 1.

The purpose of this document is to report the major features of the data quality from the Jason-1 mission thanks to the last reprocessing campaign (GDR-E).

2.2. GDR standards

Model	Product Version "C"	Product Version "E"
Orbit	<p>EIGEN-GL04S with time-varying gravity</p> <p>DORIS tracking data for IGDRs</p> <p>DORIS+SLR+GPS tracking data for GDRs with increased weight of D/L</p> <p>from cycle 500 onwards, switched to POE standard D (EIGEN-GRGS_RL02bis_MEAN-FIELD (2011))</p>	<p>EIGEN+GRGS.RL03-v2.MEAN-FIELD gravity</p> <p>Doris/GPS till cycle 169, Doris after cycle 169</p> <p>Improvements in optical coefficients</p>
Altimeter Retracking	<p>MLE4 + 2nd order Brown model : MLE4 simultaneously retrieves the 4 parameters that can be inverted from the altimeter waveforms: epoch, SWH, Sigma0 and mispointing angle. This algorithm is more robust for large off-nadir angles (up to 0.8°).</p>	<p>Updated for correction of Ku-band internal path delay. Except for range bias and a time tag bias (fix, but two values against repetitive or geodetic phase), ranges are identical.</p>
Altimeter Instrument Corrections	<p>Consistent with MLE4 retracking algorithm. A new correction is available in the product to account for the apparent datation bias (field 28). Users are advised to add this correction to the Ku-band altimeter range, as it is not a component of the net instrument correction that has already been applied to the provided Ku-band range</p>	<p>identical for swh and sig0</p> <p>updated for range</p> <p>no need of apparent datation bias correction with this version.</p>
Jason Microwave Radiometer Parameters	<p>Using calibration parameters derived from cycles 1-227.</p>	<p>using JMR calibration performed at NASA/JPL in 2014</p>

.../...

Model	Product Version "C"	Product Version "E"
	From GDR cycle 500 onwards, a new calibration file is applied.	
Dry Troposphere Range Correction	From ECMWF atmospheric pressures and model for S1 and S2 atmospheric tides. Uses new ECMWF delivery to correct for spurious oscillation effects.	identical
Wet Troposphere Range Correction from Model	From ECMWF model.	identical
Back up model for Ku-band ionospheric range correction.	Derived from JPL's Global Ionosphere Model (GIM) maps	computed from updated range and ssb
Sea State Bias Model	Empirical model derived from cycles 11-100 of MLE4 altimeter data with version "C" geophysical models	2015 Tran model, derived from cycles 1-111 of data with version 'E' geophysical models.
Mean Sea Surface Model	CLS01 until cycle 374, and switched to CNES-CLS-2011 [1993,1999 reference period] from cycle 500 onwards	CNES-CLS-2011 with [1993,2012] reference period
Along Track Mean Sea Surface Model	None (set to default)	
Geoid	EGM96	EGM2008
Bathymetry Model	DTM2000.1	identical
Mean Dynamic Topography	Rio 2005 solution	CNES-CLS 2013 with [1993,2012] reference period
Inverse Barometer Correction	Computed from ECMWF atmospheric pressures after removing model for S1 and S2 atmospheric tides, using new ECMWF delivery to correct for spurious oscillation effects	identical
Non-tidal High-frequency De-aliasing Correction	High resolution Mog2D model for both IGDR and GDR products	identical
.../...		

Model	Product Version "C"	Product Version "E"
Tide Solution 1	GOT00.2 + S1 ocean tide . S1 load tide ignored.	GOT4.10
Tide Solution 2	FES2004 + S1 and M4 ocean tides. S1, K2 and loading tides have been updated	FES2014 (using GOT4.8ac load tide as FES2014 load tide were not available early 2016)
Equilibrium long-period ocean tide model.	From Cartwright and Taylor tidal potential.	identical
Non-equilibrium long-period ocean tide model.	Mm, Mf, Mtm, and Msqm from FES2004.	derived from FES2014
Solid Earth Tide Model	From Cartwright and Taylor tidal potential.	identical
Pole Tide Model	Equilibrium model	identical.
Wind Speed from Model	ECMWF model	identical
Altimeter Wind Speed	Table derived from version "A" Jason-1 GDR data.	computed with the updated sig0 values.
Rain Flag	Derived from version "B" Jason-1 GDRs using the AGC instead of sigma naught values	computed from AGC and JPL-JMR . Derived from comparisons to thresholds of the radiometer-derived integrated liquid water content and of the difference between the measured and the expected Ku-band backscatter coefficient.
Ice Flag	New flag based on the comparison of the model wet tropospheric correction and of a radiometer bi frequency wet tropospheric correction (derived from 23.8 GHz and 34.0 GHz), accounting for a backup solution based on climatologic estimates of the latitudinal boundary of the ice shelf, and from altimeter wind speed.	identical
.../...		

Model	Product Version "C"	Product Version "E"
		Note that in addition to ECMWF models, ERA-Interim solutions are available in GDR-E products (dry troposphere correction, wet troposphere correction, inverted barometer height, high frequency fluctuations of the sea surface topography, U and V components of the model wind vector).

Table 1: Models and standards adopted for the Jason-1 product version "C" and "E"

2.3. Jason-2 data used for comparison

The tandem phase with Jason-2 (Jason-1 cycles 240 to 259 / Jason-2 cycles 001 to 020) is specially suited for intercomparison between Jason-2 and Jason-1, as both satellites were only 55 seconds apart on the same ground track. In the current report, Jason-2 GDR-D standards were used to compare to Jason-1, but several corrections for Jason-2 were as much as possible updated to be as homogeneous as possible with the Jason-1 reprocessed data. The following corrections were therefore updated for Jason-2 (when compared to Jason-1 GDR-E):

- POE orbit standard E provided by CNES
- GOT 4.10 ocean tide
- FES 2014 ocean tide (using GOT4.8ac load tide)
- Mean Sea Surface CNES_CLS_2011 (computed on a 20 years reference period)
- Sea State Bias correction is the Tran 2012 version presented in [7].
- recomputed ionospheric correction, using Tran2012 sea state bias correction.

3. Missing and invalidated measurements

This part consists in analyzing the availability of data for level 2 products over oceans before and after the reprocessing exercise. Furthermore the edited (=invalidated) measurements are monitored.

As expected, data availability of GDR-E products is the same as the data availability of GDR-C products, except for cycle 175 (one pass intentionally removed from GDR-E). Percentage of invalidated data is similar between GDR-E and GDR-C. Nevertheless, GDR-E products have about 0.04% more valid data. In particular, there are more valid measurements near coasts and over lakes using GOT4.10 ocean tide (detailed in part 5.5.1).

3.1. Missing measurements

Determination of missing measurements relative to the theoretically expected orbit ground pattern is used to detect missing telemetry in Jason-1 datasets due to altimetry events for instance. This procedure is applied cycle per cycle. The top panel figure 1 represents the number of available measurements. A small annual cycle is visible, which is due to sea ice (as Jason-1 does not track very well over sea ice).

The reprocessed GDR-E data are globally as available as in the GDR-C data set (see bottom of figure 1). Particular events during GDR-E processing are:

- On cycle 146, compared to GDR-C, one erroneous time tag has been removed for pass 231.
- On cycle 175, pass 217 is missing. It was intentionally removed from GDR-E due to lack of corresponding SGDR-C files in CNES and JPL archives.

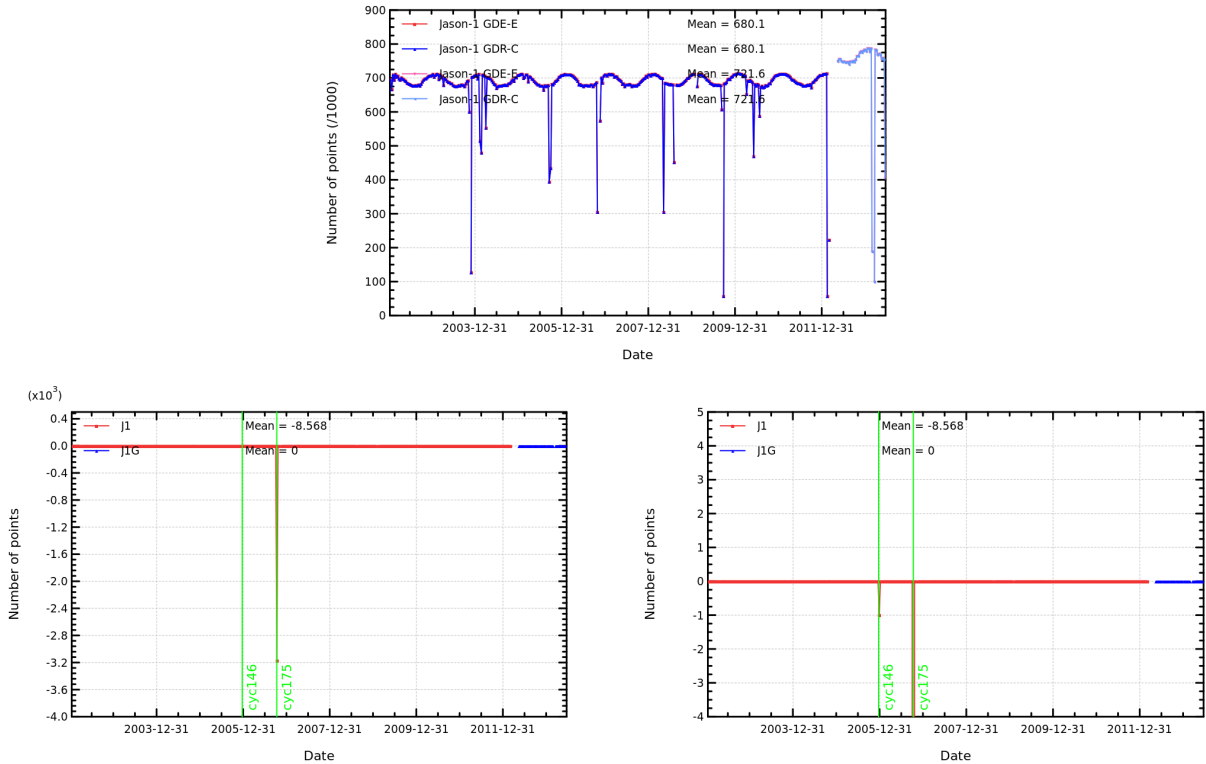


Figure 1: **Top:** Number of ocean data available for GDR-E and GDR-C products. **Bottom:** Number of data difference GDR-E - GDR-C.

3.2. Invalidated measurements

Editing criteria are used to select valid measurements over ocean. Data editing is necessary to remove altimeter measurements having lower accuracy. Once data over land are excluded, it consists in:

- First: removing the data corrupted by sea ice and ice.
- Then, removing the measurements out of thresholds tuned for several parameters. The applied thresholds can be found in the Jason-1 User Handbook ([1]). Threshold criteria are applied on altimeter, radiometer and geophysical parameters and are described in table 2. For each criterion, the cycle per cycle percentage of edited measurements has been monitored. This allows detection of anomalies in the number of removed data, which could come from instrumental, geophysical or algorithmic changes.
- The third step uses cubic splines adjustments to the Sea Surface Height (SSH) to detect remaining spurious measurements.
- The last step consists in removing an entire pass if SSH-MSS mean and standard deviation have higher values than a certain threshold. This criterion is used to detect problems such as bad orbit quality or time tag problems.

The percentage of edited data per cycle is monitored for GDR-E and GDR-C products on the top

left panel of figure 2. The main difference of this percentage between GDR-E and GDR-C (top right of figure 2) is for editing on thresholds criterion for cycle 315 (see details after in this part).

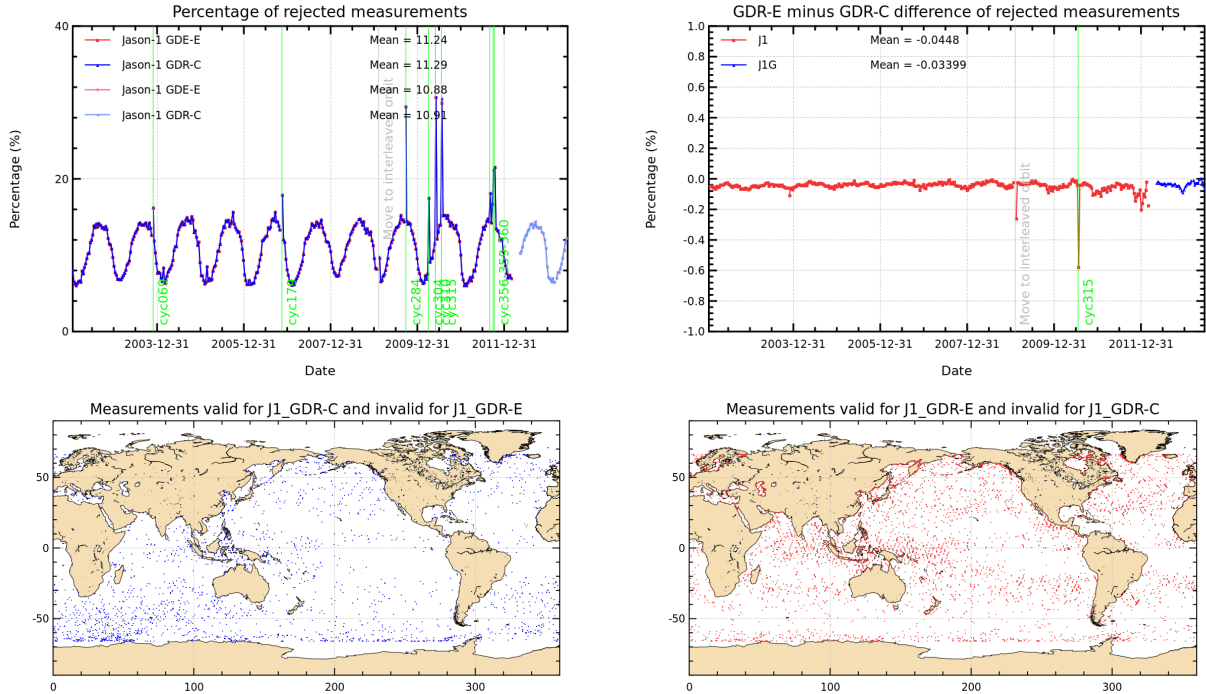


Figure 2: **Top left:** Percentage per cycle of rejected data in GDR-C and GDR-E. **Top right:** Difference of percentage of rejected data (GDR-E - GDR-C). **Bottom:** Maps of valid measurements with one dataset that are rejected considering the other dataset over year 2002. **Left:** Valid with GDR-C and rejected with GDR-E. **Right:** Valid with GDR-E and rejected with GDR-C.

Bottom left and right of figure 2 represents the location where points are lost or gained over year 2002.

Concerning rejected measurements on thresholds criteria:

The number of measurements edited on thresholds criteria decreases for GDR-E compared to GDR-C. Each criterion percentage is detailed on Table 2.

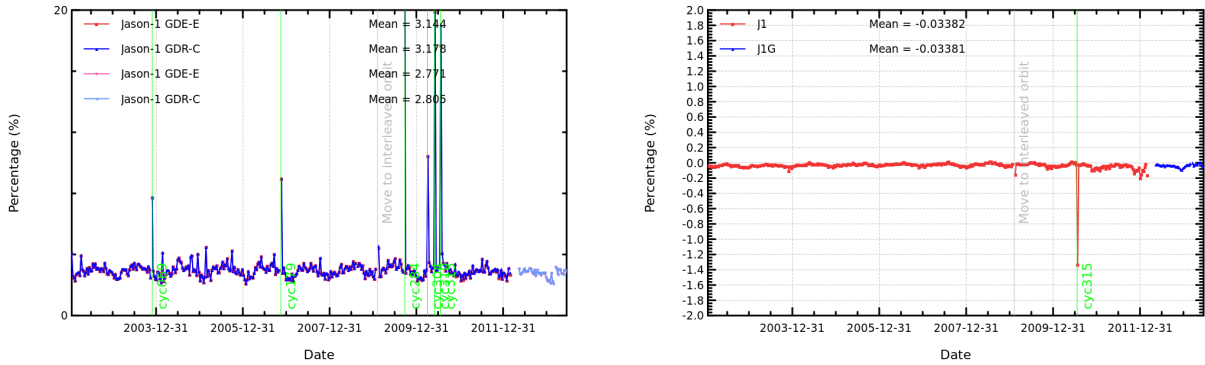


Figure 3: **Left:** Percentage per cycle of rejected data in GDR-C and GDR-E on all thresholds criteria. **Right:** Difference of percentage of rejected data (GDR-E - GDR-C).

Splitting the monitoring against each criterion leads to figure 4 and figure 5. The number of measurements edited by sea state bias and ionophere correction thresholds criteria is slightly increased (figure 4). The number of measurements edited by sla, radiometer wet troposphere, ocean tide and wind speed thresholds criteria is slightly decreased (figure 5).

On **cycle 262** (move to interleaved orbit): compared to GDR-C, part of pass 120 that were rejected because of a last orbit change maneuver during passes 116 to 119 have valid points in GDR-E (bottom right of figure 5). This was already observed with POE-D orbit solution.

On **cycle 315**, part of pass 177 and pass 178 with radiometer at default values in GDR-C have radiometer values in GDR-E, so that parts of pass 177 which had rejected measurements in GDR-C are now available in GDR-E (top right of figure 5). In addition, (bottom right of figure 5) part of passes 30, 57, 136 and 160 of this cycle have additional valid measurements compared to GDR-C thanks to a better estimation of orbit between maneuvers.

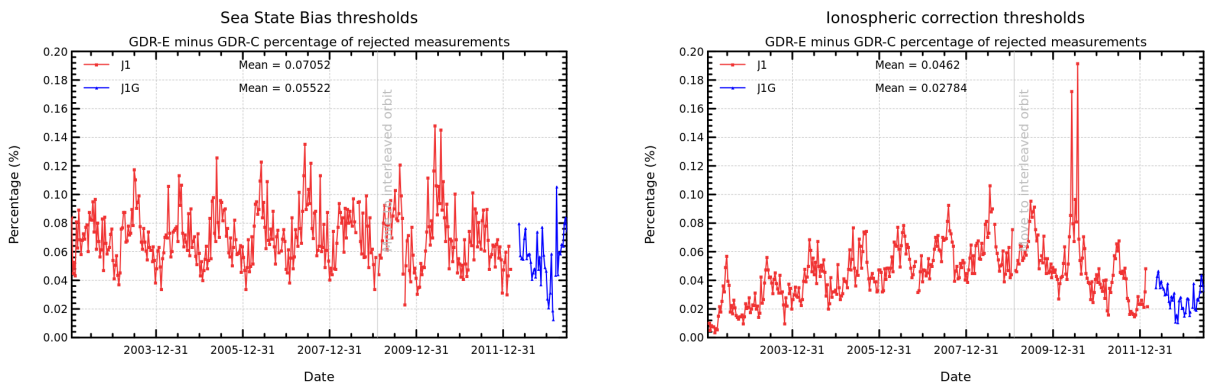


Figure 4: Difference of number of points rejected on thresholds criteria: **Left:** sea state bias **Right:** ionospheric correction

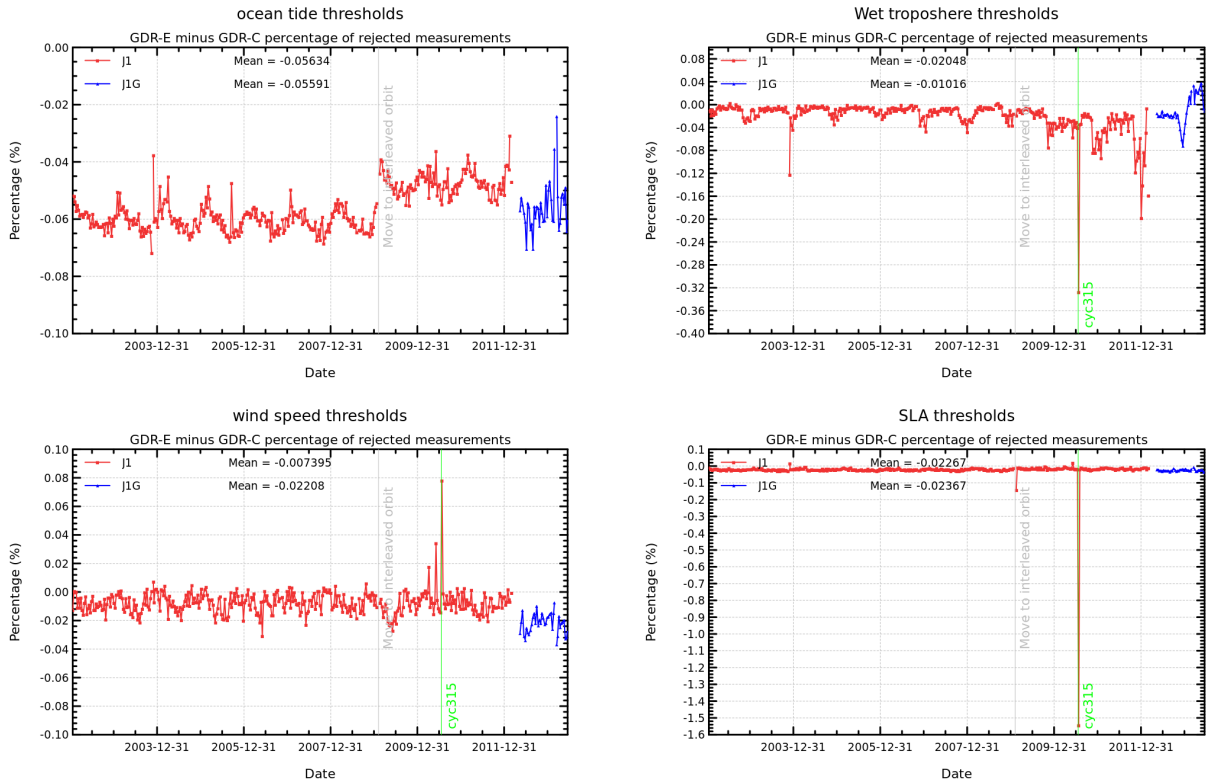


Figure 5: Difference of number of points rejected on thresholds criteria: **Top left:** ocean tide (Got4.10 vs Got00) **Top right:** Radiometer wet troposphere correction **Bottom left:** Wind speed **Bottom right:** Sea Level Anomaly

Parameter	Min thresh-olds	Max thresh-olds	mean edited on repetitive orbit period (GDR-C)	mean edited on repetitive orbit period (GDR-E)	mean edited on geodetic orbit period (GDR-C)	mean edited on geodetic orbit period (GDR-E)
Sea surface height	-130 m	100 m	0.93%	0.93%	0.77%	0.77%
Sea level anomaly	-10 m	10.0 m	1.17%	1.15%	0.88%	0.86%
Number measurements of range	10	Not applicable	1.29%	1.29%	1.11%	1.11%
Standard deviation of range	0 m	0.2 m	1.47%	1.47%	1.31%	1.31%
Square off-nadir angle	-0.2deg ²	0.64deg ²	0.68%	0.68%	0.50%	0.50%
.../...						

Parameter	Min thresholds	Max thresholds	mean edited on repetitive orbit period (GDR-C)	mean edited on repetitive orbit period (GDR-E)	mean edited on geodetic orbit period (GDR-C)	mean edited on geodetic orbit period (GDR-E)
Dry troposphere correction	-2.5 m	-1.9 m	0.00%	0.00%	0.00%	0.00%
Inverted barometer correction	-2.0 m	2.0 m	0.00%	0.00%	0.00%	0.00%
JMR wet troposphere correction	-0.5m	-0.001m	0.15%	0.13%	0.06%	0.05%
Ionosphere correction	-0.4 m	0.04 m	1.26%	1.30%	1.05%	1.08%
Significant waveheight	0.0 m	11.0 m	0.71%	0.71%	0.57%	0.57%
Sea State Bias	-0.5 m	0.0 m	0.62%	0.70%	0.49%	0.54%
Number measurements of Ku-band Sigma0	10	Not applicable	1.28%	1.28%	1.10%	1.10%
Standard deviation of Ku-band Sigma0	0 dB	1.0 dB	1.80%	1.80%	1.59%	1.59%
Ku-band Sigma0 ¹	7.0 dB	30.0 dB	0.66%	0.66%	0.52%	0.52%
Ocean tide	-5.0 m	5.0 m	0.06%	<0.01%	0.06%	<0.01%
Equilibrium tide	-0.5 m	0.5 m	0.00%	0.00%	0.00%	0.00%
Earth tide	-1.0 m	1.0 m	0.00%	0.00%	0.00%	0.00%
Pole tide	-15.0 m	15.0 m	0.00%	0.00%	0.00%	0.00%
Altimeter wind speed	0 m.s ⁻¹	30.0m.s ⁻¹	1.07%	1.06%	0.93%	0.90%
All together	-	-	3.18%	3.14%	2.81%	2.77%

Table 2: Editing criteria

4. Quality overview/Performances

In this chapter the performances of Jason-1 GDR-E data are analyzed at crossovers and along-track. Therefore comparison to previous GDR-C version and Jason-2 data are done.

4.1. Performances at crossovers

Ascending / descending SSH (Sea Surface Height) differences are computed at crossover points. These differences are computed for time differences less than 10 days between ascending and descending tracks. This allows us to minimize the contribution of the oceanic variability (mesoscale). Therefore the variance of the SSH differences at crossover points gives an information of the performance of the altimeter system. Computing the differences of these variances (using on the one hand GDR-E data and on the other hand GDR-C data), allows to measure the ability of the GDR-E data to improve the computation of the SSH.

The main SSH calculation for Jason-1 are defined below:

$$SSH_{GdrE} = Orbit_{GdrE} - Altimeter\ Range_{GdrE} - \sum_{i=1}^n Correction\ GdrE_i$$

$$\begin{aligned} \sum_{i=1}^n Correction\ GdrE_i &= \text{Dry troposphere correction} \\ &+ \text{Dynamical atmospheric correction} \\ &+ \text{Radiometer wet troposphere correction}_{GdrE} \\ &+ \text{Dual frequency ionospheric correction}_{GdrE} \text{ (filter 250 km)} \\ &+ \text{Non parametric sea state bias correction}_{GdrE} \\ &+ \text{GOT4.10 ocean tide correction (including loading tide)} \\ &+ \text{Earth tide height} \\ &+ \text{Pole tide height} \end{aligned}$$

$$SSH_{GdrC} = Orbit_{GdrC} - Altimeter\ Range_{GdrC} - \sum_{i=1}^n Correction\ GdrC_i$$

$$\begin{aligned} \sum_{i=1}^n Correction\ GdrC_i &= \text{Dry troposphere correction} \\ &+ \text{Dynamical atmospheric correction} \\ &+ \text{Radiometer wet troposphere correction}_{GdrC} \\ &+ \text{Dual frequency ionospheric correction}_{GdrC} \text{ (filter 250 km)} \\ &+ \text{Non parametric sea state bias correction}_{GdrC} \\ &+ \text{GOT00 ocean tide correction (including loading tide)} \\ &+ \text{Earth tide height} \\ &+ \text{Pole tide height} \end{aligned}$$

$$SSH_{pseudoGdrD} = Orbit_{POE-D} - Altimeter\ Range_{GdrC} - \sum_{i=1}^n Correction\ updatedGdrC_i$$

$$\begin{aligned} \sum_{i=1}^n Correction\ updatedGdrC_i = & \text{Dry troposphere correction}_{GdrC} \\ & + \text{Dynamical atmospheric correction}_{GdrC} \\ & + \text{Radiometer wet troposphere correction} \\ & \text{updated for Composite for cycles 1 to 374 and GdrC for cycles 500 to 537} \\ & + \text{Dual frequency ionospheric correction}_{GdrC} \text{ (iterative filter)} \\ & + \text{Non parametric sea state bias correction}_{updated\ GdrC\ with\ Tran2012} \\ & + \text{GOT4.8 ocean tide correction (including loading tide)} \\ & + \text{Earth tide height} \\ & + \text{Pole tide height} \end{aligned}$$

On Figure 6 (except for the map), a selection on $|latitude| < 50deg$, bathy $< -1000m$ and low variability areas has been done. The standard deviation of SSH differences is near systematically lower for GDR-E than GDR-C data, thus improving the coherence between ascending and descending passes (at time scales less than 10 days). The global SSH variance reduction (bottom of figure 6) is about 1.3 cm^2 . For cycles 284 and 528, the standard deviation of SSH differences is higher for GDR-E than GDR-C data (respectively 2.56 cm^2 and 2.39 cm^2): these values are not significant as the number of crossover points is very low due to SHM.

The global SSH variance reduction (bottom of figure 7) compared to pseudo GDR-D is about 0.2 cm^2 . Depending on cycle, the monitoring shows an increase for some period. This variance increase seems to be related to POE-E orbit standard which only slightly improves (=not for all cycles) performances at crossovers for Jason-1 period with GPS data compared to POE-D, and which has rather equivalent performances at crossovers for Jason-1 period without GPS data (from mid-2006 onwards) compared to POE-D.

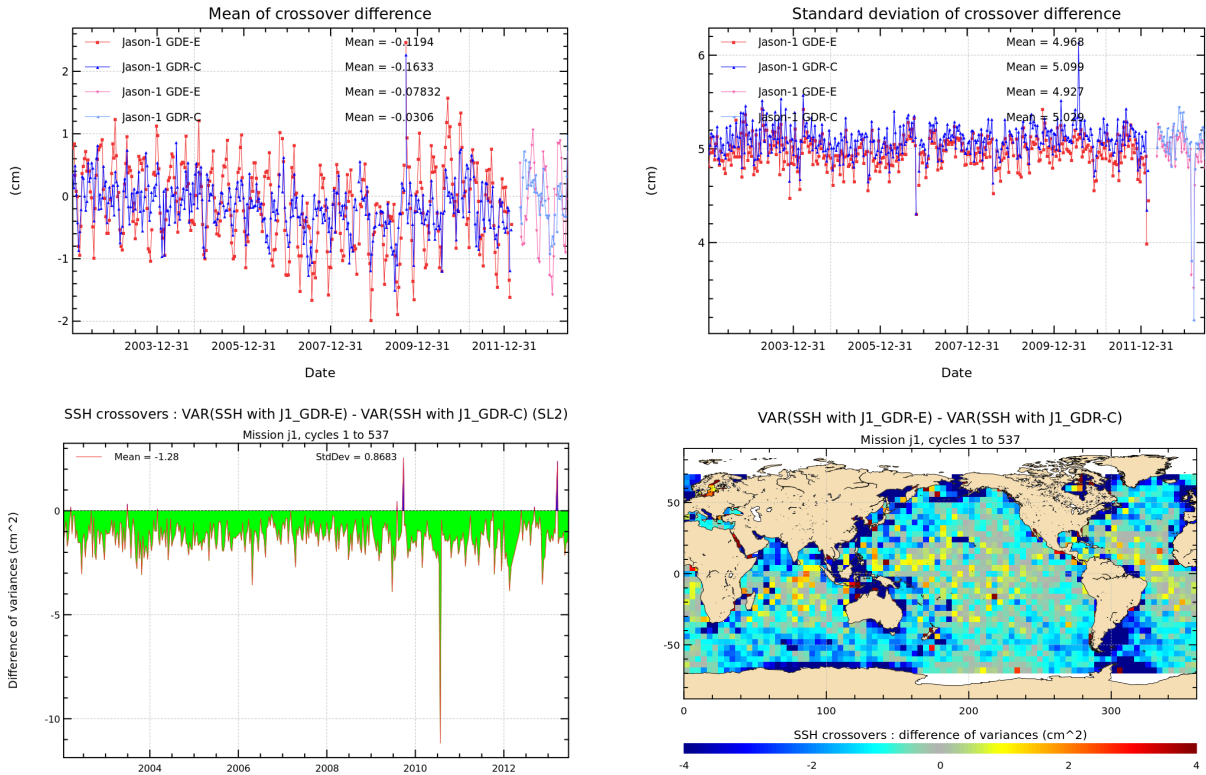


Figure 6: For monitorings, crossovers are only selected for open ocean (latitude less than $\pm 50^\circ$, bathymetry less than -1000 m and oceanic variability less than 20 cm). **Top:** Cycle per cycle monitoring of mean (left) and standard deviation (right) of SSH difference at crossovers with GDR-E (red) and GDR-C (blue) standards. **Bottom left:** Difference of SSH variance at crossovers between GDR-E and GDR-C. **Bottom right:** Map of difference of SSH variances (variance SSH_{GDR-E} - variance SSH_{GDR-C}).

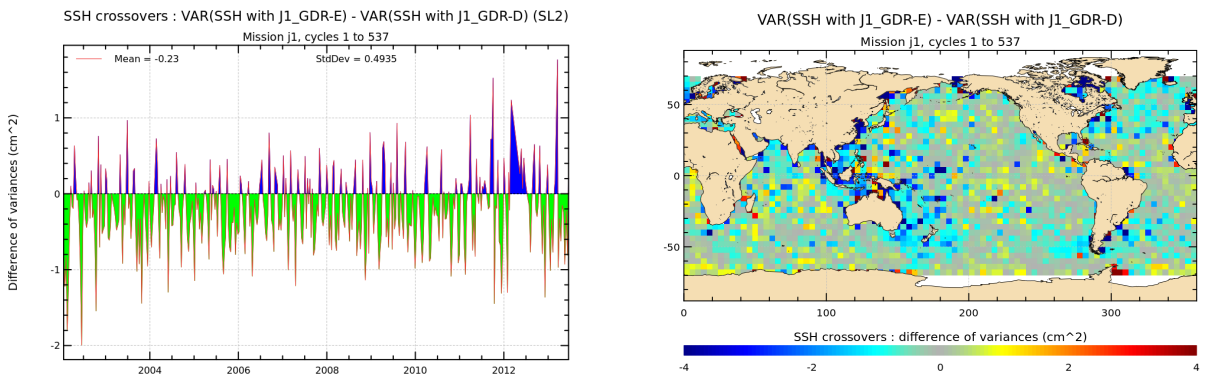


Figure 7: **Bottom left:** Difference of SSH variance at crossovers between GDR-E and pseudo GDR-D. Crossovers are only selected for open ocean (latitude less than $\pm 50^\circ$, bathymetry less than -1000 m and oceanic variability less than 20 cm). **Bottom right:** Map of difference of SSH variances (variance SSH_{GDR-E} - variance SSH_{GDR-D}).

The GDR-E data improve also the coherence of ascending/descending SSH differences as geographic patterns are reduced (see figure 8 showing the mean of ascending/descending SSH difference). These improvements (variance reduction and a mean close to zero with reduced geographical patterns) are mainly due to :

- POE-E orbit that contributes to about 0.36cm^2 of decrease of variance reduction in average [5.2.]
- Ocean Tide as using GOT4.10 instead of Got00 leads to a decrease of 0.87cm^2 of variance reduction in average [5.5.1].
- SSB and ionospheric correction that also slightly contributes to about 0.08cm^2 of decrease of variance reduction in average [5.4.4.] .

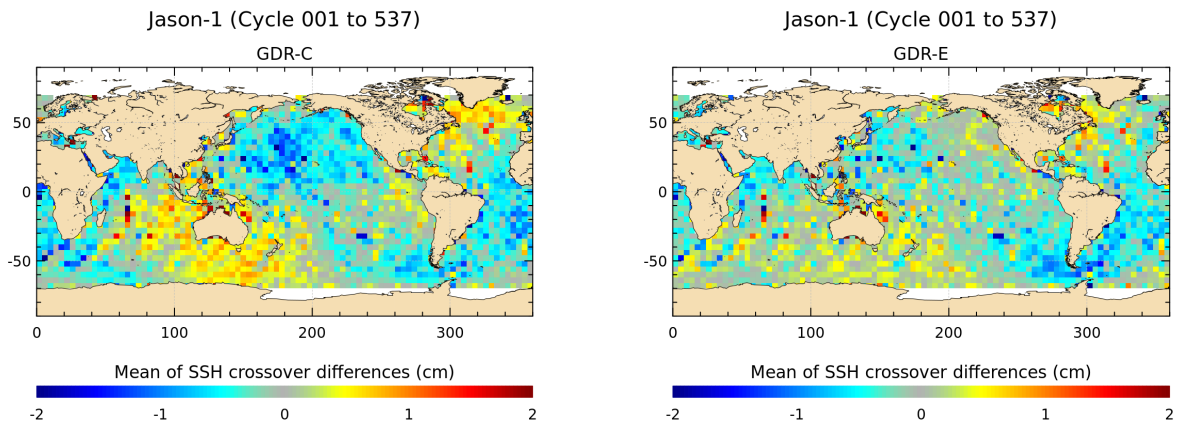


Figure 8: Mean at SSH crossovers for Jason-1 whole period **Left: GDR-C. Right: GDR-E.**

4.1.1. Jason-1/Jason-2 SSH crossover differences

Figure 9 shows the monitoring of multi-mission crossovers (between Jason-1 and Jason-2) using:

	J1	J2
red curve radiometer wet troposphere	GDR-E	updated GDR-D standards
pink curve ECMWF model wet troposphere	GDR-E	updated GDR-D standards
blue curve radiometer wet troposphere	updated Jason-1 GdrC product with GDR-D orbit + GOT 4.8 ocean tide + JMR replacement product	GDR-D standard

Table 3: Used Jason-1 and Jason-2 data for crossover analysis

The standard deviation between Jason-1/Jason-2 SSH crossovers (right of the figure) is slightly reduced when using Jason-1 GDR-E standards (+ updated Jason-2 standards). The mean of Jason-1 minus Jason-2 SSH crossover differences stays quite stable over the analyzed period. The drift that was visible from mid-2010 to 2012 with previous datasets (blue curve) is not visible with the new datasets (red curve). Note that the relative bias between Jason-1 and Jason-2 was +10.3 cm for GDR-D like standards. It is now reduced to ~ 1 mm using GDR-E like standards.

Since Jason-1 move to a geodetic orbit, the mean of Jason-1 minus Jason-2 SSH difference showed a jump of about 7mm (blue curve). It was mainly due to a more precise PRF value for Jason-1 for cycles after 500 (3.16mm), but also partly due to new JMR calibration file (about 1mm). This jump seems to disappear using the new dataset. Nevertheless, differences increase for the last 20 cycles (red curve). Using model wet troposphere instead of radiometer wet troposphere to compute Jason-1 minus Jason-2 differences of SSH crossovers shows quite more stable behavior until cycle 320 and over Jason-1 geodetic period, but the pink curve also shows a change in behavior from cycle 320 to 370. The relative difference between Jason-1 and Jason-2 crossovers is higher in average with model than using radiometer wet troposphere correction (-4mm instead of -1mm with radiometer wet troposphere).

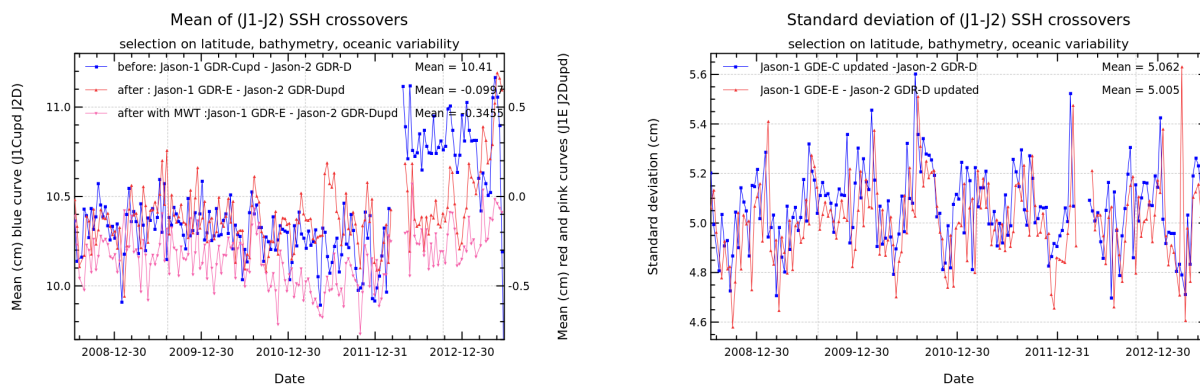


Figure 9: Monitoring of mean (**left**) and standard deviation (**right**) of Jason-1 minus Jason-2 SSH crossovers.

4.1.2. Estimation of pseudo time-tag bias

The pseudo time tag bias (α) is found by computing at SSH crossovers a regression between SSH and orbital altitude rate (\dot{H}), also called satellite radial speed:

$$SSH = \alpha \dot{H}$$

This empirical method allows us to estimate the potential real time tag bias but it can also absorb other errors correlated with \dot{H} . Therefore it is called “pseudo” time tag bias.

The monitoring of this coefficient estimated at each cycle is performed for Jason-1 GDR-C and GDR-E in figure 10. The origin of this pseudo time tag bias was found by CNES [10], a correction containing $\alpha \dot{H}$ in Jason-1 GDR-C products ([1]) has been already added to improve the Jason-1 SSH calculation, therefore the mean pseudo time tag bias for Jason-1 is close to zero. For Jason-1 GDR-E data, the datation was directly modified in order to correct it properly.

A 58,77days signal is visible on the right part of figure 10 for Jason-1 GDR-C and Jason-2 GDR-D pseudo datation bias. This signal disappear using GDR-E Jason-1 dataset (thanks to the use of Got4.10 ocean tide). A 180 days signal is reduced by a half from Jason-1 GDR-C to GDR-E (but is still visible). A 118 days signal is visible in pseudo datation bias with Jason-1 GDR-E dataset (visible with Jason-2 GDR-D too).

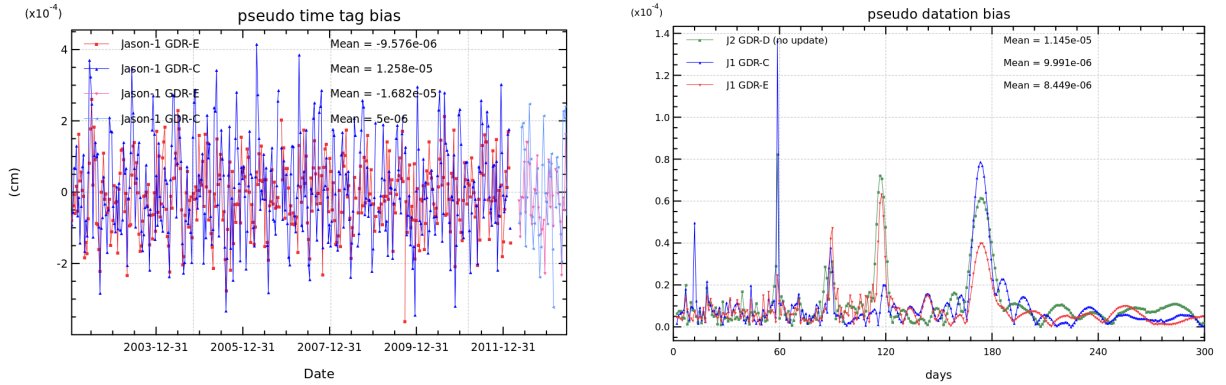


Figure 10: **Left:** Cycle per cycle monitoring of pseudo time-tag bias estimated cycle by cycle from GDR-C and GDR-E products for Jason-1. Unit is in seconds. **Right:** Periodogram of pseudo time tag bias.

4.2. Along-track performances of Sea Level Anomaly

4.2.1. SLA differences between GDR-E and GDR-C

The Sea Level Anomaly corresponds to the Sea Surface Height where the mean sea surface is removed ($SLA = SSH - MSS$). Due to the numerous changes (e.g. orbit, sea state bias, mean sea surface, ...) between GDR-E and GDR-C data, their SLA are different (10.14cm in average). These differences are due to :

- MSS : +2.40cm
- range : +6.39cm (internal path delay) and -3.2mm (correction due to PRF truncature)
- ssb: +0.65cm
- iono: +1.03cm

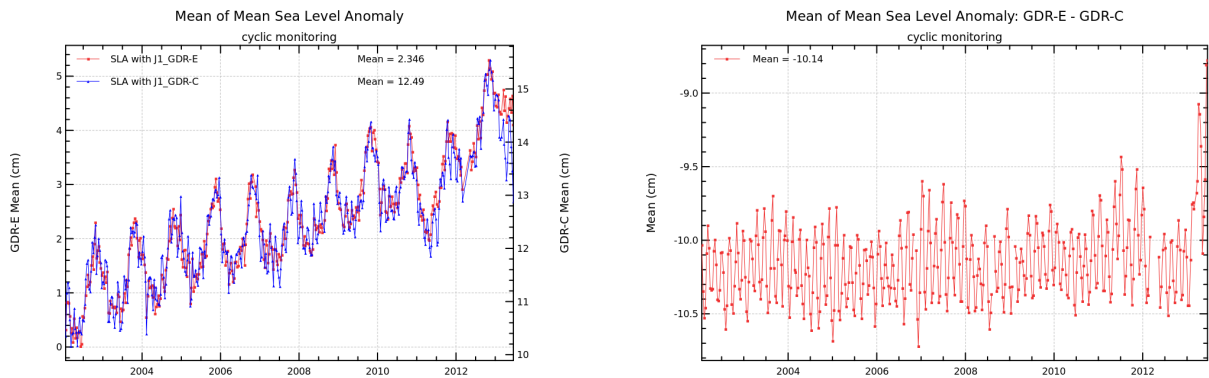


Figure 11: **Left:** Cycle per cycle mean of SLA with GDR-C (blue) and GDR-E (red) standards. **Right:** Monitoring per cycle of the difference of GDR-E SLA and GDR-C SLA

With GDR-C data, Jason-1 SLA standard deviation increases when the satellite is put on the interleaved ground track in 2009 (after flight formation phase with Jason-2). This SLA standard deviation increase is due to the use of MSS CLS01, as errors of this MSS are higher outside the historical T/P-Jason ground track. The Jason-1 mean sea surface were updated to MSS CNES/CLS 2011 in the GDR product since the move to the geodetic orbit in order to have a mean sea surface of good quality (MSS CNES/CLS 2011 also used data from the interleaved ground track, and so decreases Jason-1 SLA standard deviation significantly outside the historical groundtrack). As a consequence, the standard deviation of SLA is equivalent between Jason-1 GDR-C and Jason-2 data for the Jason-1 geodetic period (light blue and green curves).

Mainly thanks to the new mean sea surface (CNES/CLS 2011 referenced on 20 years) and the GOT4.10 global tide model, the standard deviation of GDR-E SLA is reduced (figure 12 red and pink curves, see also chapter 5.5.1. dedicated to the ocean tide).

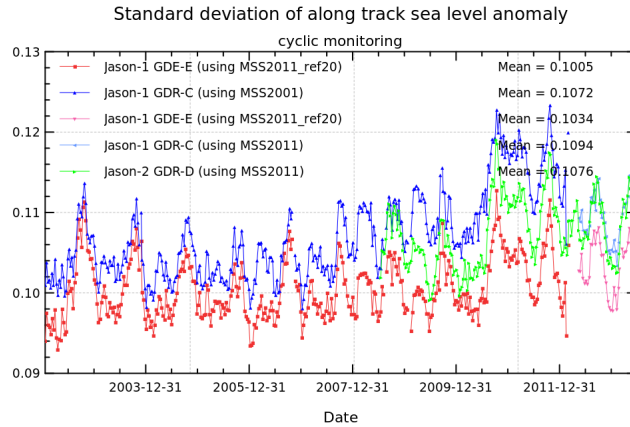


Figure 12: *Cycle per cycle standard deviation of along track SLA with GDR-C (blue) and GDR-E (red) standards.*

4.2.2. SLA differences between Jason-1 and Jason-2

When comparing Jason-2 and Jason-1 SLA over the formation flight phase (cycle 001 to 020), using on the one hand Jason-2 GDR-D and updated Jason-1 GDR-C standards (left side of figure 13) and on the other hand Jason-2 updated GDR-D and Jason-1 GDR-E standards (right side of figure 13), the differences between Jason-2 and Jason-1 are decreased for the reprocessed data. The main geographical correlated (left 13) differences between the two satellites came from the orbit and the sea state bias ([9]). Thanks to reprocessing, the same computation models are used for Jason-2 updated ssb (from N. Tran[8] presented at OSTST 2012 meeting) and GDR-E Jason-1 SSB, and these geographical correlated differences are reduced (right 13).

As during the formation flight phase, both satellites were on the same ground track with only 55 seconds apart, the satellites observe the same ocean under the same environmental conditions and differences of uncorrected SLA (Orbit -Range - MSS) can directly be made between Jason-1 and Jason-2. This is shown on bottom panel of figure 13. The remaining regional SLA differences (top right of figure 13) between Jason-1 and Jason-2 are not due to corrections as same geographical patterns are observed when computing the difference not taking into account the corrections.

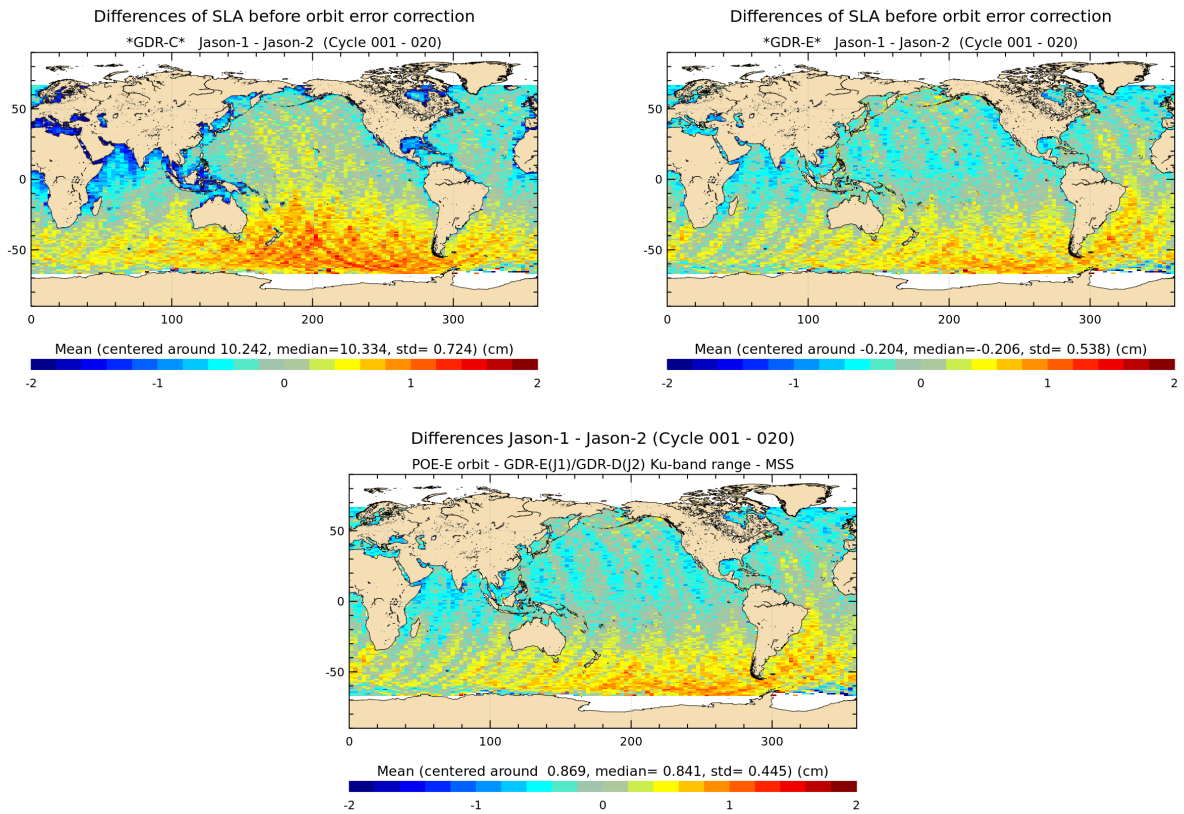


Figure 13: *SLA differences between Jason-1 and Jason-2 (before applying orbit error correction), **Left:** with GDR-D standards for Jason-2 and updated GDR-C standards for Jason-1, **Right:** with GDR-E standards for Jason-1 and updated GDR-D standards for Jason-2. **Bottom:** SLA differences between Jason-1 and Jason-2 (without any correction) with GDR-E standards.*

5. Details of the changes in GDR-E standard

In the following chapter the changes of the GDR-E standard (compared to GDR-C) are detailed. Therefore comparisons between Jason-1 GDR-E and GDR-C are done, but also between Jason-1 and Jason-2.

5.1. Concerning the datation of GDR-E products

In previous data versions, Jason-1 or Jason-2 data contained a pseudo time tag bias close to 0.3 milli-seconds. This was especially visible through a small north/south bias on ascending/descending mono-mission crossover points. In Jason-1 GdrC products, a pseudo altimeter datation bias correction is available which was determined empirically (see also chapter 4.1.2.). The origin of this pseudo time tag bias was found by CNES [10] in 2010. It has a mean of about 0.25 milli-seconds and is dependent on the altitude of the satellite. For Jason-1 GDR-E data (and for Jason-2 GDR-D data in 2012), the datation was directly modified in order to correct it properly. As shown on figure 10, Jason-1 GDR-E pseudo time tag bias is now close to zero (mean value).

5.2. Concerning the standard of GDR-E Precise Orbit Ephemeris (POE-E)

The quality of Precise Orbit Ephemeris is crucial for the quality of altimeter data products and the studies based upon these data. Inversely, studies using Sea Surface Height (SSH) calculation from altimeter or in-situ data enable:

- to give insight on orbit quality for the different missions,
- to compare different orbit solutions for one mission,
- and to give hints which mission is impacted by suspicious behavior, when comparing several missions.

The impact of the first improvement from POE-C to POE-D is detailed in Jason-1 2013 report ([3]). The impact of the second evolution from POE-D to POE-E is detailed in this chapter. POE-E orbit is close of POE-D orbit in terms of quality.

5.2.1. Comparison between GDR-E orbit and GDR-D orbit

The objective of this study is to evaluate POE-E orbit for Jason-1 (by comparison to POE-D standard), and observe and analyse the impact of the POE-E orbit for climate applications. Hereafter, the quality of POE-E orbit solution is assessed by comparing to POE-D solution. The following analysis were done on the same ensemble of data (reference (POE-D) and test (POE-E) orbits are valid).

	POE-D (Reference)	POE-E
Gravity model	EIGEN+GRGS.RL02bis_MEAN-FIELD	EIGEN+GRGS.RL03-v2.MEAN-FIELD
Non tidal TVG	one annual, one semi-annual, one drift terms for each year up to deg/ord 50	one annual, one semi-annual, one bias and one drift terms for each year up to deg/ord 80
Surface forces	Radiation pressure model: thermo-optical coefficient from pre-launch box and wing model, with smoothed Earth shadow model	Radiation pressure model: calibrated semi-empirical solar radiation pressure model
DORIS	DORIS weight is reduced by a factor 10 before DORIS instrument change	SAA DORIS beacons weight is divided by 10 before DORIS instrument change
Orbit solution	Doris/Laser/GPS till cycle 169 Doris/Laser after cycle 169	Doris/GPS till cycle 169 Doris after cycle 169

Figure 14: Main changes in final POE-E orbit standard compared to POE-D.

5.2.1.1. Crossovers

The temporal evolution of variance differences of Sea Surface Height at crossovers between POE-E and POE-D orbit is presented on figure 15. POE-E has no impact concerning short temporal scale (signals < 2 months).

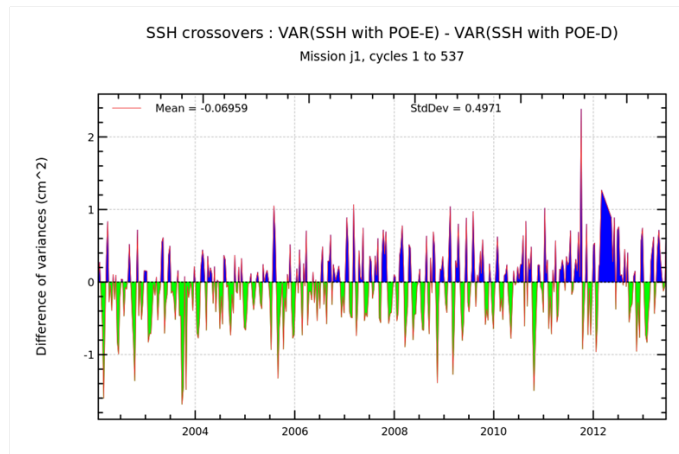


Figure 15: Final POE-E orbit standard. Difference of variance at crossovers

5.2.1.2. Impact on Global and Regional Mean Sea Level

5.2.1.3. Global Mean Sea Level

Figure 16 shows the temporal evolution of SLA mean calculated globally. The difference between POE-D and POE-E solution on GMSL is 0.07mm/yr, which represent a low impact.

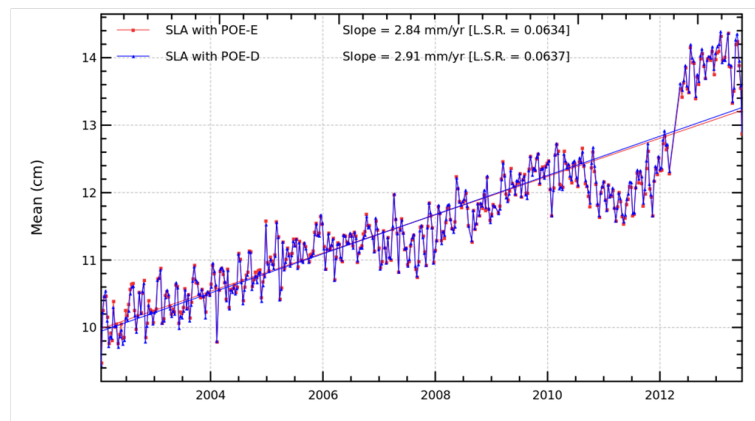


Figure 16: *Final POE-E orbit standard. Global Mean Sea Level*

5.2.1.4. Regional Mean Sea Level

Significant impact is detected on long-term trends (separating east and west hemisphere. Regions of strong positive (eastern box) and negative (western box) trend differences between the two orbit standards (see figure 17) are then selected.

The reduction in east/west differences between Altimeter and T/S (using POE-E instead of POE-D) is significant. Comparison to T/S seems to indicate that the significant impact on the long-term trend of the east/west regional mean sea level (between POE-E and POE-D) is a sign of improvement in the POE-E solution (figure 18).

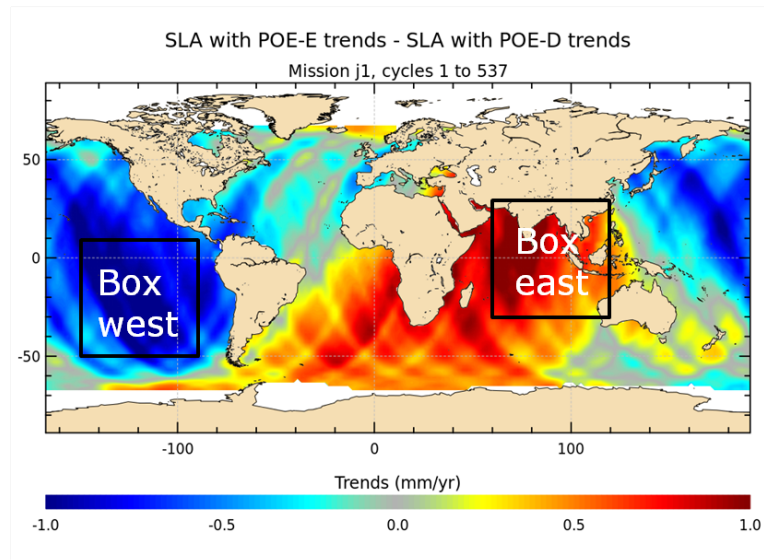


Figure 17: *Final POE-E orbit standard. Regional Mean Sea Level: location of studied boxes.*

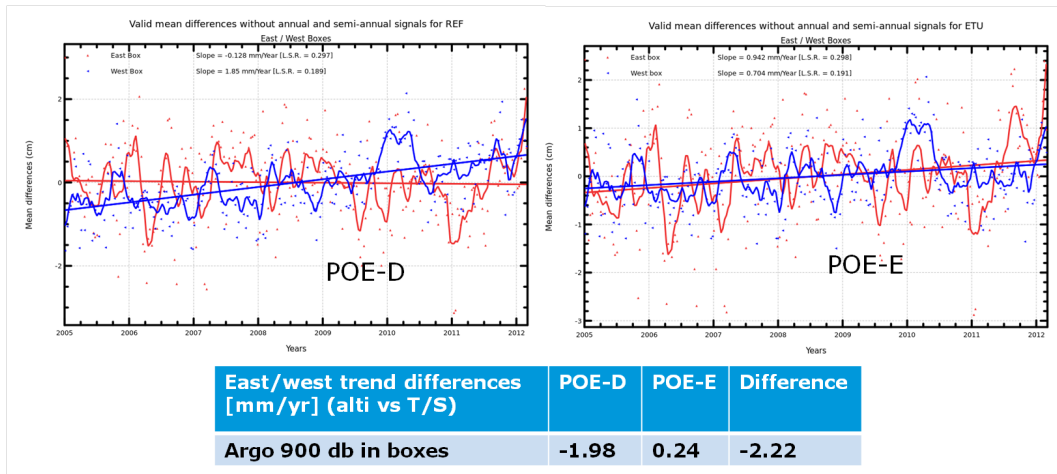


Figure 18: *Final POE-E orbit standard. Regional Mean Sea Level: East/West differences in boxes.*

5.2.1.5. Conclusions

POE-E orbit is close of POE-D orbit in terms of quality.

There is no clear impact on mesoscale performance at crossover points.

Concerning the MSL evolution:

- Low impact for the global MSL (reduction of 0.07 mm/yr), but differences between odd and even passes trend evolutions are slightly increased with POE-E
- Strong impact for the regional MSL trends (+/- 1 mm/yr). East/West gradient on geograph-

ical trends (Atlantic+Indian vs Pacific) is highlighted. POE-E is more homogeneous with T/S profile concerning east/west trends.

Comparisons with tide gauges show equivalent results for POE-D and POE-E

5.2.2. Conclusions about the evolutions from GDR-C orbit to GDR-E orbit

The mesoscale performance at crossover points has been first improve (-0.3cm² for variance at crossovers) with POE-D orbit compared to POE-C orbit, and is equivalent using POE-D or POE-E orbit, so that **mesoscale performance at crossover points is improved from POE-C to POE-E.**

Concerning the MSL evolution:

- Low impact for the global MSL (total reduction of 0.2 mm/yr with the two evolutions),
- differences between odd and even passes trend evolutions are slightly increased with POE-E instead of POE-C
- East/West gradient on geographical trends (Atlantic+Indian vs Pacific) were highlighted with POE-D. They are reduced from POE-D to POE-E (POE-E is more homogeneous with T/S profile concerning east/west trends). A difference of 0.24mm/yr is still visible on East/West difference of trends when compare to T/S profiles.

5.3. Concerning the radiometer related parameters

For the GDR-E product, JPL has provided the following inputs:

- radiometer surface type
- radiometer radial distance to land
- instrument correction quality flag or JMR data (one for 18.7GHz, one for 23.8GHz, one for 34.0GHz)
- radiometer along-track averaging flag
- radiometer antenna gain weighted land fraction in main beam (one for 18.7GHz, one for 23.8GHz, one for 34.0GHz)
- radiometer rain flag
- radiometer sea-ice flag
- radiometer brightness temperatures interpolation flag
- **radiometer wet tropospheric correction**
- atmospheric attenuation correction on Ku band backscatter coefficient
- atmospheric attenuation correction on C band backscatter coefficient
- 18.7GHz main beam brightness temperature and smoothed brightness temperature
- 23.8GHz main beam brightness temperature and smoothed brightness temperature

- 34.0GHz main beam brightness temperature and smoothed brightness temperature
- radiometer wind speed
- radiometer water vapor content
- radiometer liquid water content
- 18.7GHz antenna temperature
- 23.8GHz antenna temperature
- 34.0GHz antenna temperature

In this report, we will focus on radiometer wet troposphere correction and atmospheric attenuation.

5.3.1. Radiometer wet troposphere correction

The differences of radiometer wet troposphere correction between GDR-E and GDR-C come from a new near land algorithm and the use of new calibration coefficients. In GDR-C, a pre/post safhold bias of -1.6mm remains for wet troposphere correction. This has been addressed by the recalibration of the JMR (see red/pink (GDR-E) against blue (GDR-C) curves on figure 19).

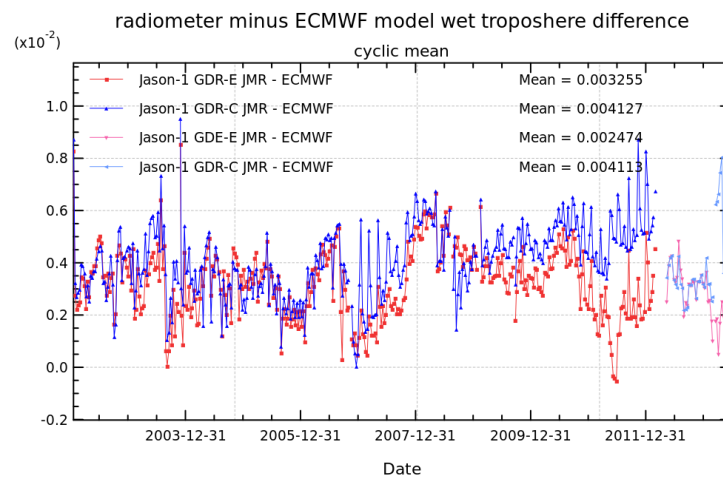


Figure 19: Cycle per cycle monitoring of radiometer minus model wet troposphere differences. Radiometer minus model for Jason-1 GDR-E and GDR-C.

The new coastal retrieval algorithm improves the quality of the radiometer wet troposphere correction, as on the one hand difference of radiometer minus ECMWF model wet troposphere stays for GDR-E quite stable when approaching the coast (left side of figure 20) and on the other hand the variance of SLA is reduced especially near coasts when using GDR-E instead of GDR-C radiometer wet troposphere correction (right side of figure 20). Differences near coasts are also visible on bottom panel of figure 20, which represents the mean of GDR-E minus GDR-C radiometer wet troposphere differences.

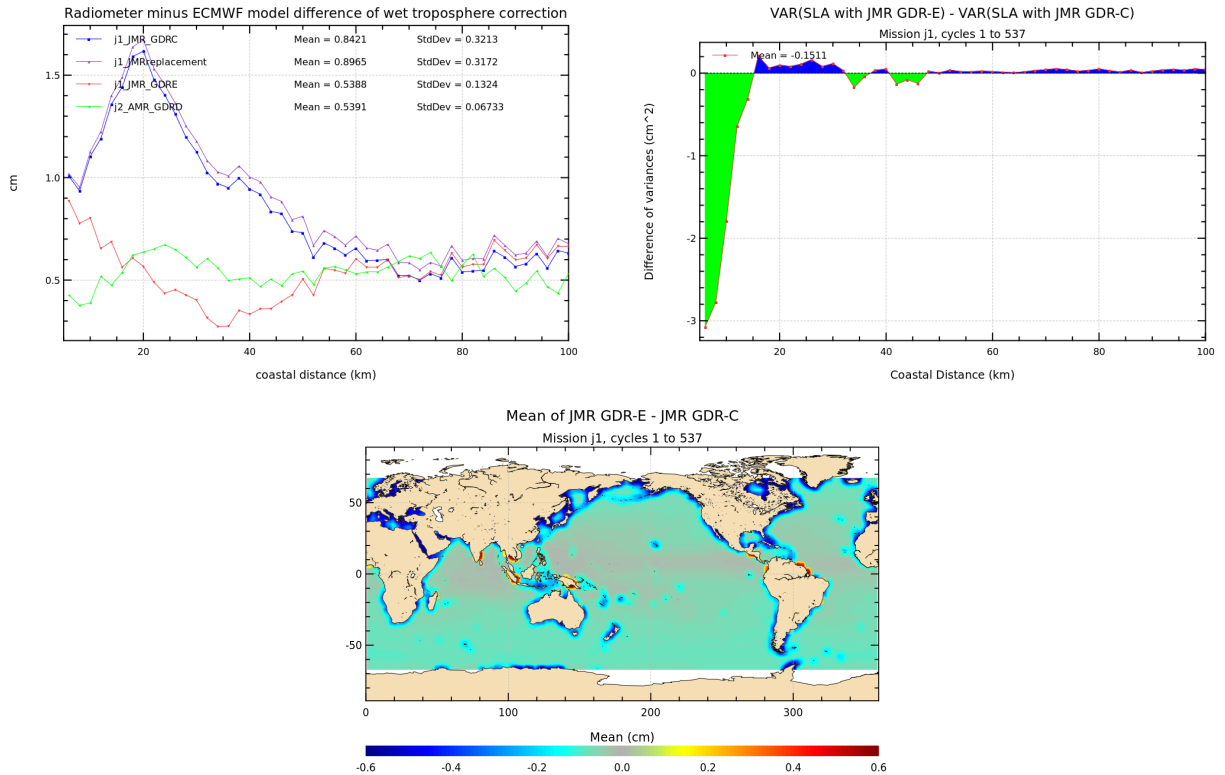


Figure 20: **Left:** Difference of radiometer minus ECMWF model wet troposphere correction as a function of coast distance for Jason-1 cycle 250 (Jason-2 cycle 011). **Right:** Difference of SLA variances - computed by using successively GDR-E and GDR-C radiometer wet troposphere - as a function of coastal distances between 0 and 100 km. **Bottom:** Map of differences between GDR-E - GDR-C radiometer wet troposphere

For GDR-C, a JMR replacement product corrected JMR instabilities which were observed after August 2008 safhold mode. Part of these improvements seem to be taken into account in GDR-E product (results are better than using original GDR-C JMR solution, for which daily differences could reach 8mm). Nevertheless comparisons with Jason-2 show more important differences (daily instabilities) than using the JMR replacement product for Jason-1 (see red curve, bottom left of figure 21). JPL radiometer expert stated that these ± 1 -2mm variations with respect to the replacement product are acceptable and fully inline with the accuracy of the calibration method. Also the differences observed with the model are within the range observed during other periods and comparisons with Jason-2 show quite stable cyclic monitoring at bottom right of figure 21. The standard deviation of these differences are equivalent with both solutions. Computing map of Jason-1 - Jason-2 wet troposphere differences mean over tandem phase shows a better coherence between the two mission solutions, with reduced geographically correlated patterns (from top left

to top right of figure 21)

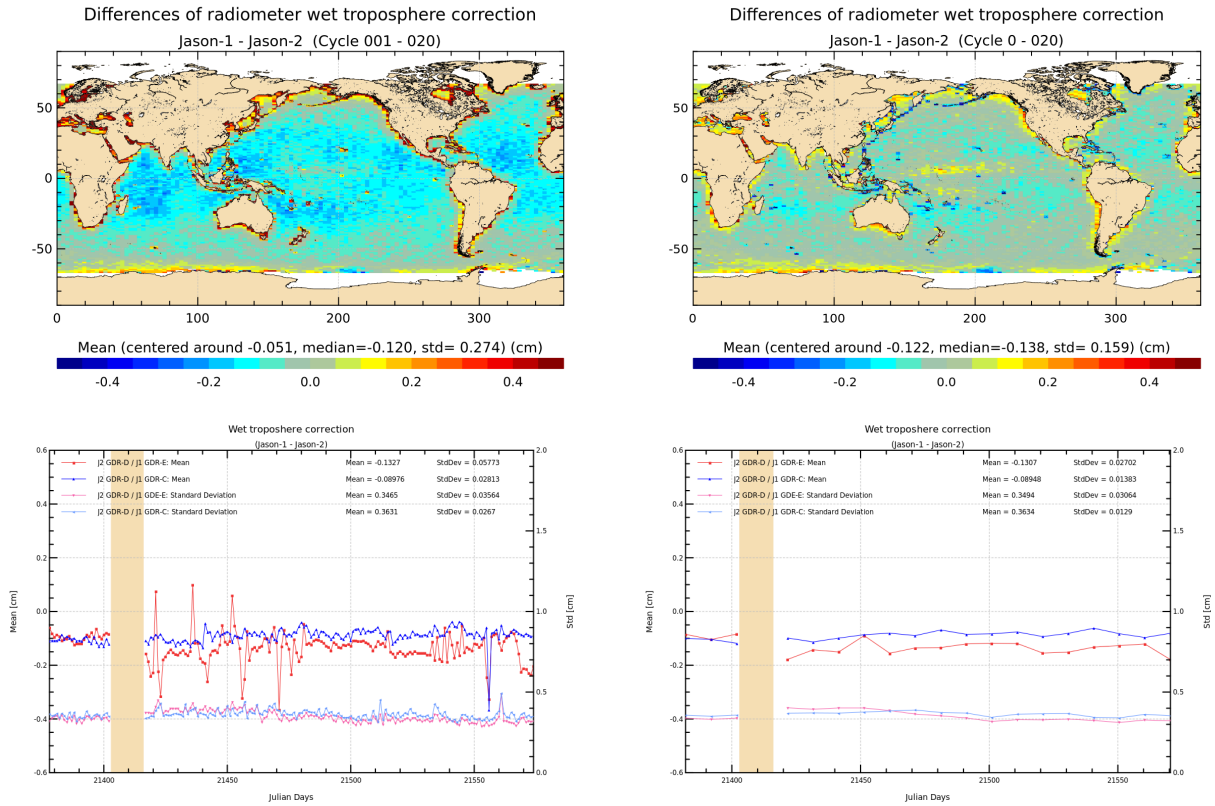


Figure 21: Mean of Jason-1 - Jason-2 wet troposphere differences over tandem phase. **Top left:** Map with J1 updated GDR-C and J2 GDR-D. **Top right:** Map with J1 GDR-E and J2 updated GDR-D. **Bottom left:** Daily monitoring **Bottom right:** Cyclic monitoring

The solution from ERA-interim model is available in Jason-1 GDR-E products. The advantages of this solution are presented by Legeais&al. in [24].

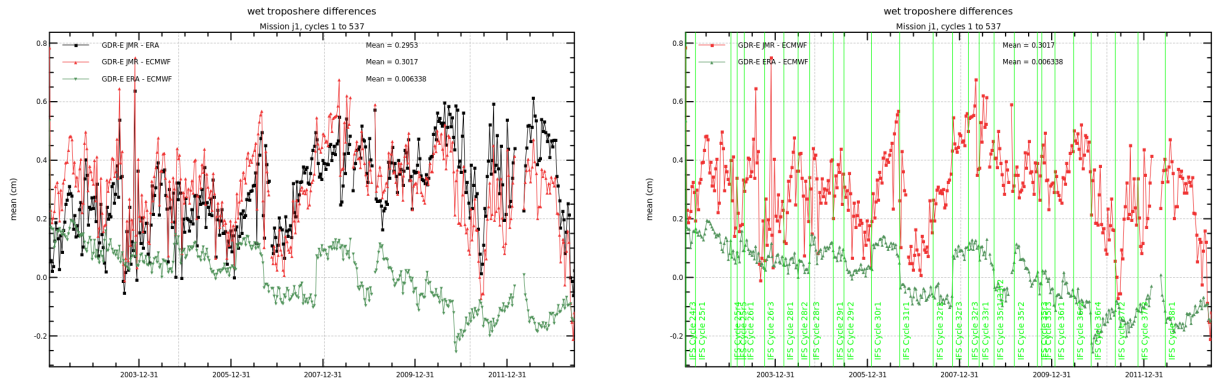


Figure 22: Cycle per cycle monitoring of radiometer minus model wet troposphere differences. **Left:** radiometer minus ERA or ECMWF operational model wet troposphere difference for GDR-E Jason-1. **Right:** radiometer or ERA model minus ecmwf wet troposphere model, and ecmwf model changes.

5.3.2. Atmospheric attenuation

As the atmospheric attenuation is derived from radiometer parameters, which have changed in GDR-E version, it is also different between GDR-E and GDR-C product version (see figure 23). Jason-1 GDR-E solution is also more coherent to Jason-2 GDR-D solution over the tandem phase (see figure 24). As backscattering coefficient is corrected for the atmospheric attenuation, this difference of about -0.012dB between GDR-E and GDR-C atmospheric attenuation will also impact the Sigma0 (see part 5.4.2.).

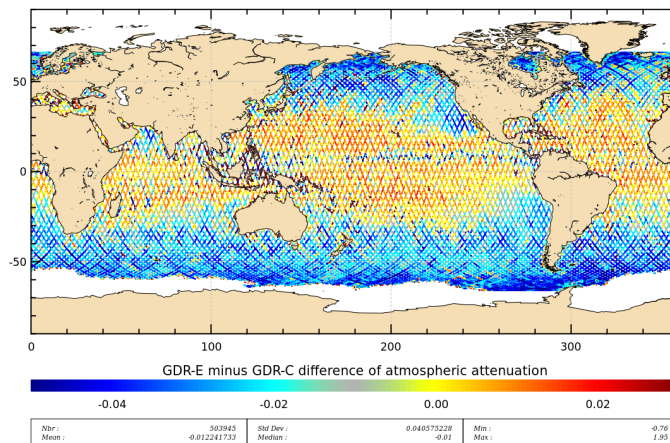


Figure 23: GDR-E minus GDR-C difference over Jason-1 cycle 250.

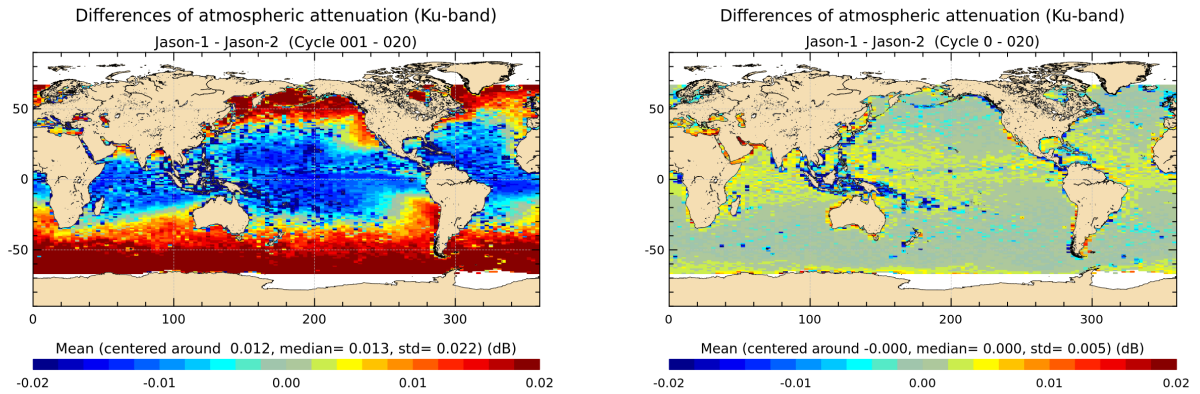


Figure 24: Mean of Jason-1 - Jason-2 atmospheric attenuation differences over tandem phase. **Left:** J1 GDR-C and J2 GDR-D. **Right:** J1 GDR-E and J2 GDR-D.

5.4. Concerning the altimeter related parameters and corrections derived from the altimeter related parameters

Note that waveforms are not retracked.

5.4.1. Altimeter Ku-band range

Altimeter range instrument correction and associated Ku- and C-band range take account for error in internal path delay. (+63.9 mm compared to version C). In addition, range_ku is corrected by 3.2 mm: this correction is due to PRF truncature (only applied over repetitive period). Except for bias and time tag, ranges are identical.

$$\begin{aligned} \text{Over repetitive period:} \quad \text{range_ku_gdre} &= \text{range_ku_gdrc} + 0.0639 - 0.0032 \\ \text{range_c_gdre} &= \text{range_c_gdrc} - 0.0032 \end{aligned}$$

$$\begin{aligned} \text{Over geodetic period:} \quad \text{range_ku_gdre} &= \text{range_ku_gdrc} + 0.0639 \\ \text{range_c_gdre} &= \text{range_c_gdrc} \end{aligned}$$

5.4.2. Ku-band sigma0

Sigma0 (Figure 25) is slightly modified as the Ku-band backscattering coefficient is corrected for the atmospheric attenuation, and a new atmospheric attenuation (Figure 24) is used.

There is a bias of about -0.012 dB between GDR-E and GDR-C Ku-band backscattering coefficient. The regional differences (bottom left of figure 25) are correlated to the atmospheric attenuation differences (see Figure 24).

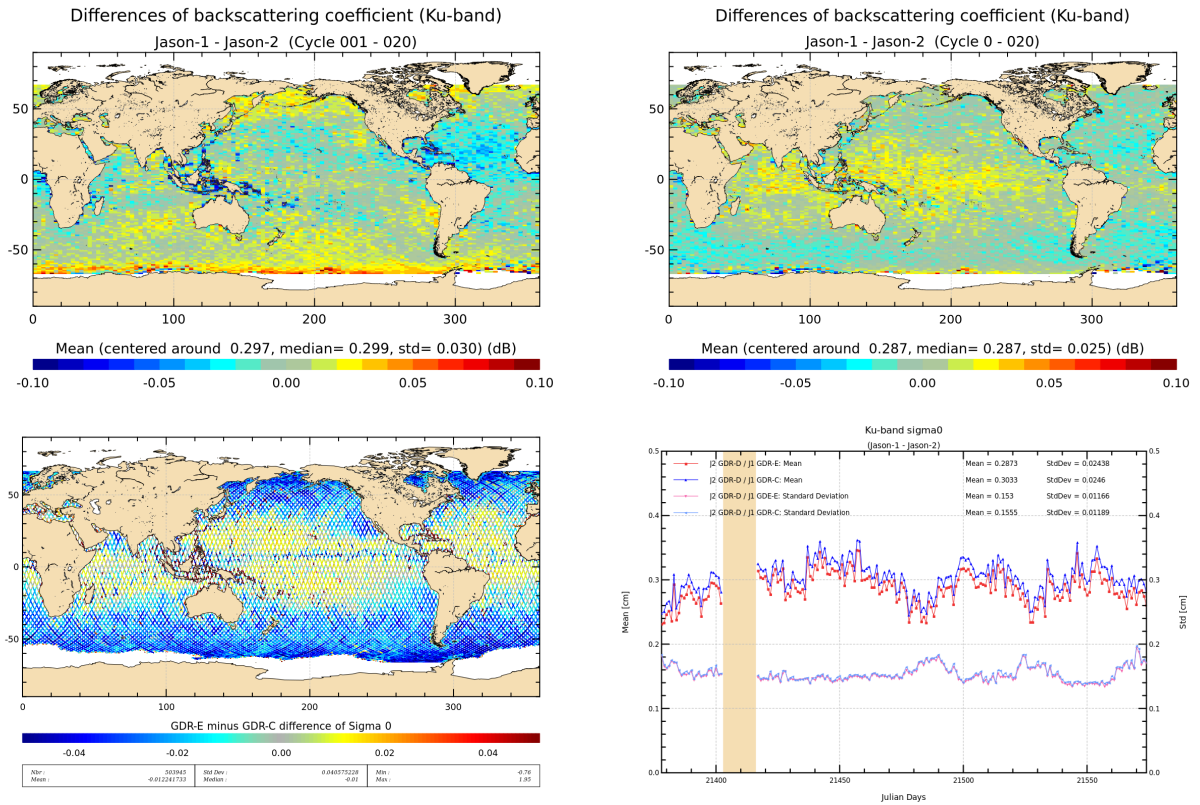


Figure 25: **Top:** Mean of Jason-1 - Jason-2 σ_0 differences over tandem phase. **Left:** J1 updated GDR-C and J2 GDR-D. **Right:** J1 GDR-E and J2 updated GDR-D. **Bottom left:** GDR-E minus GDR-C difference over Jason-1 cycle 250. **Bottom right:** Daily mean and standard deviation of Jason1 - Jason2 Ku-band backscattering coefficient difference over the tandem phase.

5.4.3. Altimeter wind speed

For GDR-E dataset, altimeter wind speed has been computed with the updated σ_0 value. Although Jason-1 GDR-E / Jason-2 GDR-D wind speed are now more homogeneous in Atlantic than previously, geographically correlated patterns are now visible at latitude around -50° (> 0) and in equatorial area (< 0). Also, the global bias between Jason-2 and Jason-1 altimeter wind speed (computed over the tandem phase) is increasing from 0.08m/s to 0.10m/s (see top of figure 26).

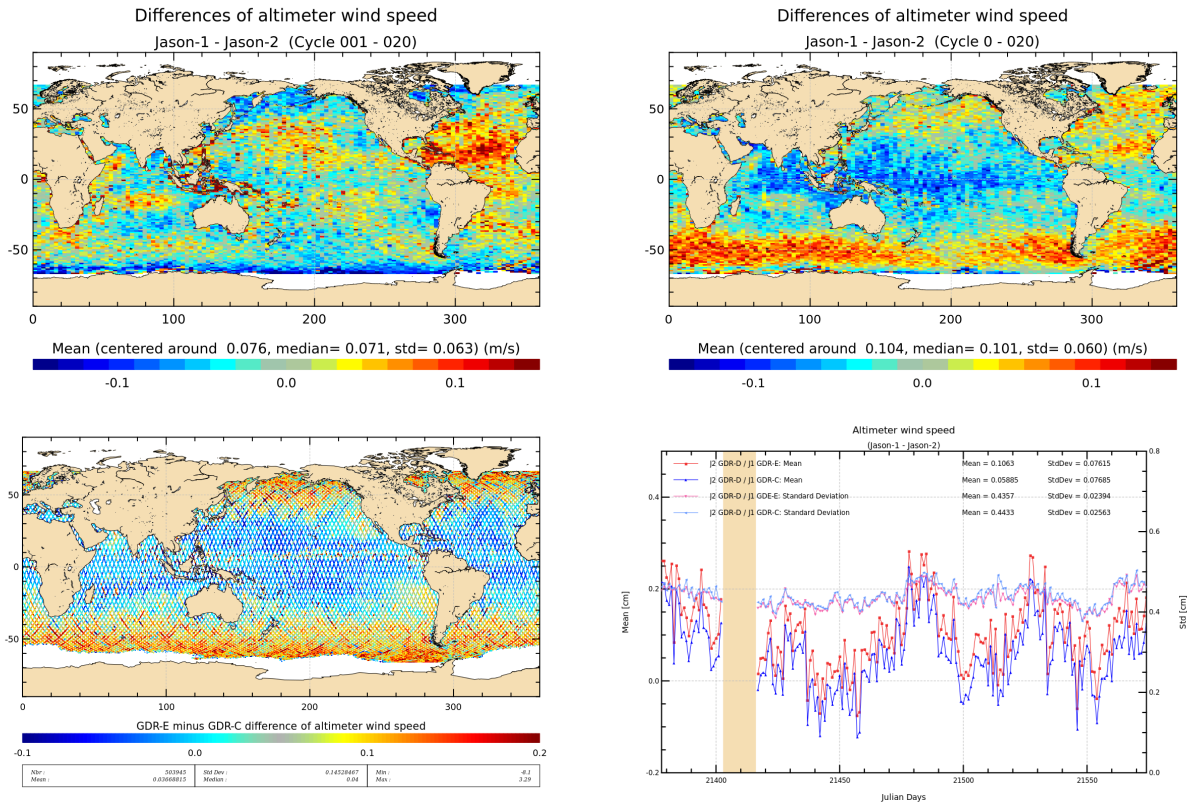


Figure 26: Mean of Jason-1 - Jason-2 wind speed differences over tandem phase. **Left:** J1 updated GDR-C and J2 GDR-D. **Right:** J1 GDR-E and J2 updated GDR-D **Bottom left:** GDR-E minus GDR-C difference over Jason-1 cycle 250. **Bottom right:** Daily mean and standard deviation of Jason1 - Jason2 Ku-band altimeter wind speed difference over the tandem phase.

5.4.4. Sea State Bias and Dual-frequency ionosphere correction

At the OSTST2012 meeting, Tran and al. [8] presented a new SSB model computed using one year of Jason-2 GDR-D data. This model seems slightly better than the SSB model used for the GDR-D product. A new SSB solution has been computed for Jason-1 in the same way of the one presented previously for Jason-2. **This solution was computed using GDR-E-like input data from cycle 1 to 111.** When using these updated sea state bias solution proposed by Tran and al. for both missions, the Jason-1 minus Jason-2 differences are much more homogeneous than before. Note that this homogeneization is mainly due to the updated Jason-2 SSB and to a lesser extent due to the updated Jason-1 SSB (see also [9]).

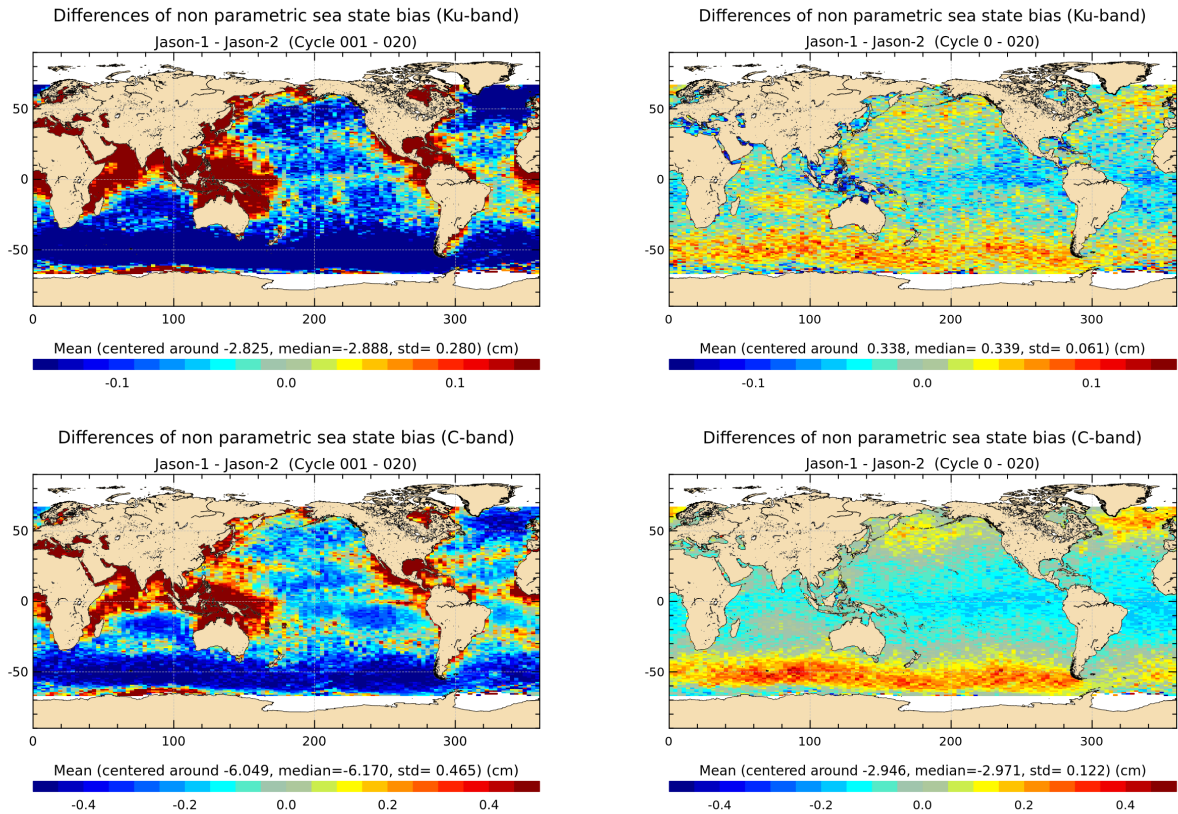


Figure 27: **Top:** Mean of Jason-1 - Jason-2 ssb (Ku band) differences over tandem phase. **Bottom:** Mean of Jason-1 - Jason-2 ssb (C band) differences over tandem phase. **Left:** J1 GDR-C and J2 GDR-D. **Right:** J1 GDR-E and J2 Tran2012

There is a bias of 1.16 cm between GDR-C and GDR-E ionospheric corrections, mostly due to bias difference applied on Ku and C-band ranges (see part 5.4.1.). Geographically correlated patterns on Jason-2 minus Jason-1 ionospheric correction difference over tandem phase are reduced (from top left to top right of figure 28).

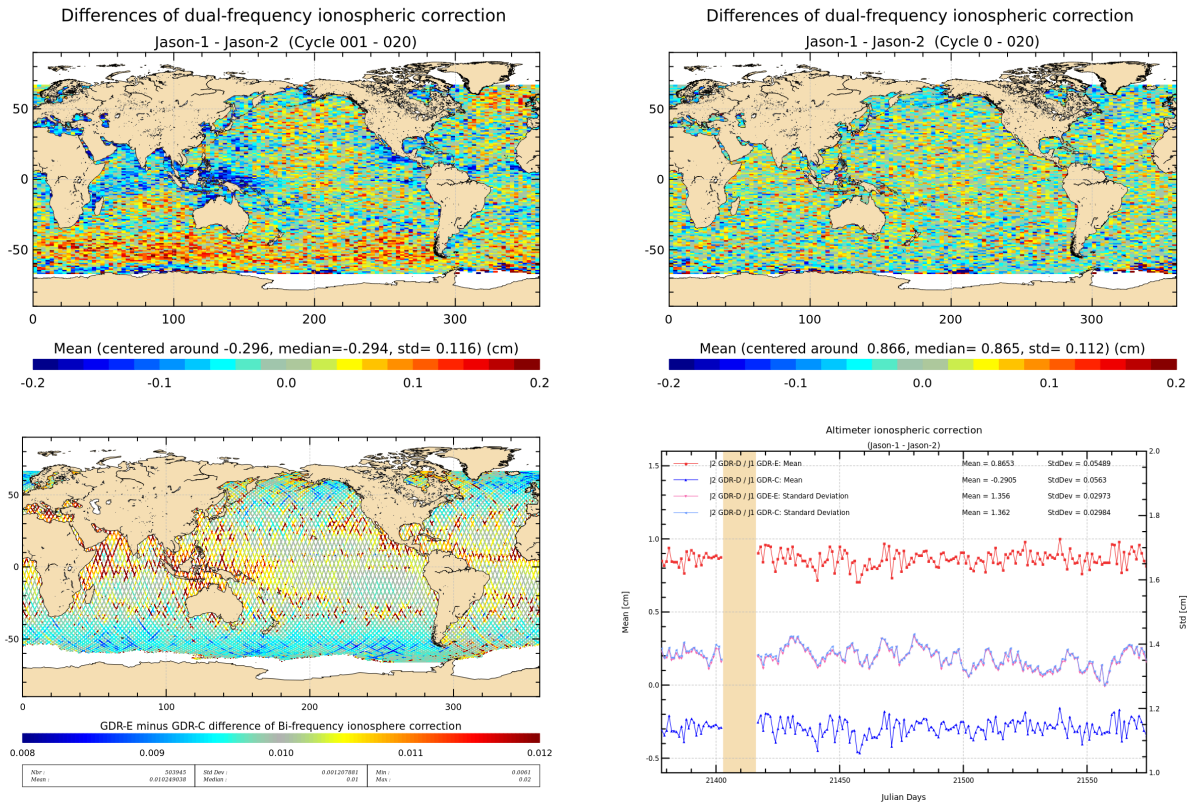


Figure 28: **Top:** Mean of Jason-1 - Jason-2 dual frequency ionosphere correction differences over tandem phase. **Left:** J1 updated GDR-C and J2 GDR-D. **Right:** J1 GDR-E and J2 updated GDR-D **Bottom left:** GDR-E minus GDR-C difference over Jason-1 cycle 250. **Bottom right:** Daily mean and standard deviation of Jason1 - Jason2 ionosphere correction difference over the tandem phase.

Concerning mesoscale performances (SSH differences at 10 days crossovers), when a selection on $bathy < -1000m$, $|LAT| < 50^\circ$, and $oceanic\ variability < 0.2m$ is applied (see figure 29), the reduction of SSH crossover variance when using GDR-E ssb and ionospheric correction, instead of GDR-C solutions leads to a global variance reduction of about 0.08 cm^2 .

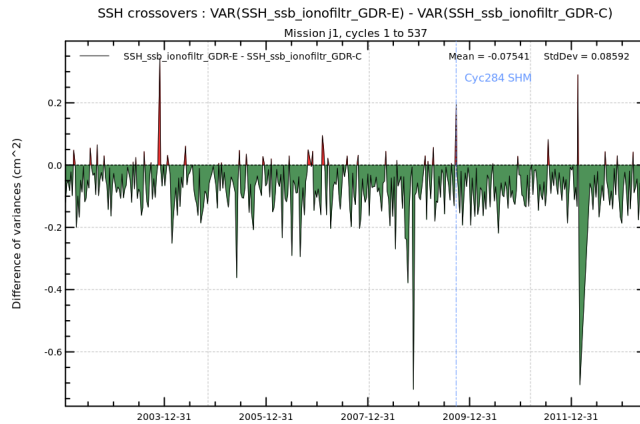


Figure 29: *Cycle by cycle monitoring of the difference of variance at crossover points with selection on bathy < -1000m, |LAT| < 50°, and oceanic variability < 0.2m. Impact of SSB + IONO*

5.5. Concerning other corrections

5.5.1. New global tide model (GOT4.10 and FES2014)

For GDR-E, the global tide model GOT4.10 has replaced the GOT00 model available in GDR-C products. The changes concern all waves.

Data coverage with new ocean tide model is better: there are more valid measurements near coasts and over lakes using GOT4.10 ocean tide than the previous solution.

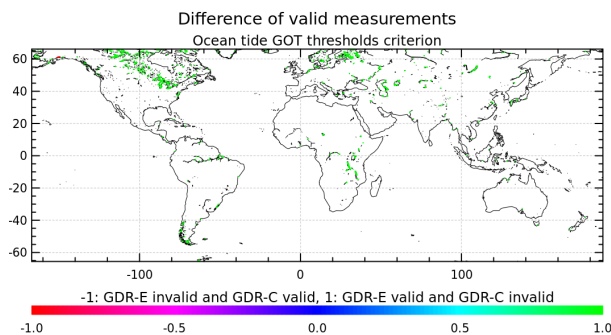


Figure 30: *Difference of valid measurements with ocean tide GOT thresholds criterion over cycle 250.*

Averaged over all the period, there is no global bias between the two ocean tide standards. Nevertheless a 58.77 days signal is visible on the global ocean tide differences (top left and bottom of figure 31).

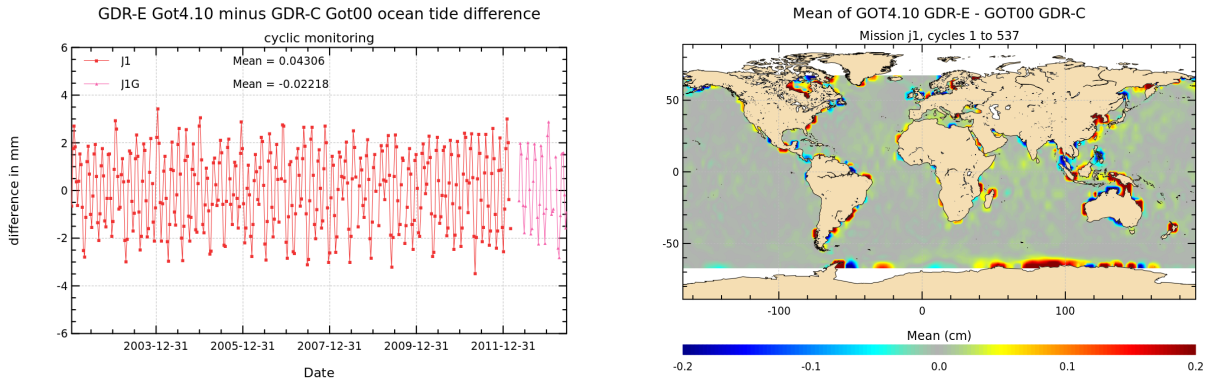


Figure 31: **Left:** Monitoring of mean of GDR-E (Got4.10) minus GDR-C (Got00) Jason-1 ocean tide differences. **Right:** Map of the difference

Using the GOT4.10 global tide model instead of the GOT00 one improves the coherence between ascending and descending passes. The right side of figure 32 shows the reduction of SSH crossover variance when using GOT4.10 instead of GOT00. The global variance reduction has a value of about 0.9 cm². (For cycles 284 and 528, the standard deviation of SSH differences is higher for GDR-E than GDR-C data: these values are not significant as the number of crossover points is very low due to SHM).

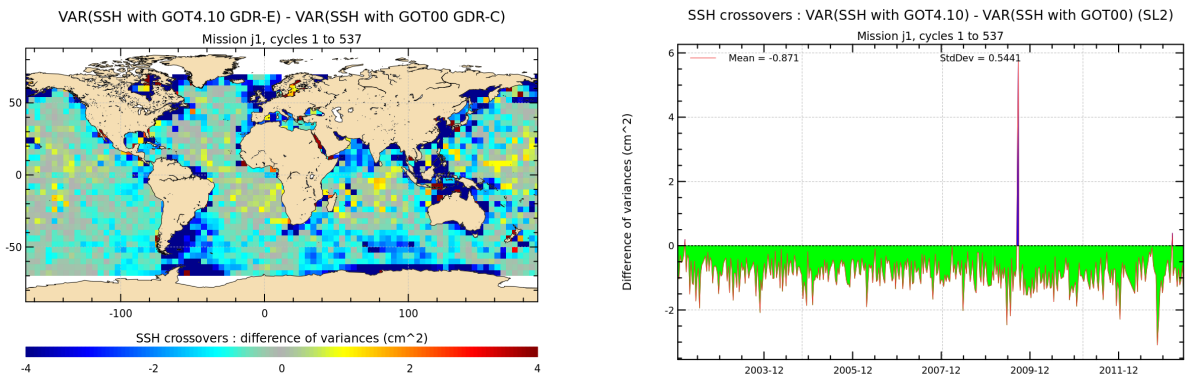


Figure 32: **Left:** Map of differences of SSH variances (SSH variance using GOT4.10 - SSH variance using GOT00) **Right:** cyclic monitoring of this difference.

The GOT4.10 global model compared to the GOT00 global model is indeed especially improved in coastal areas. This is visible on figure 33, showing that the SLA variance is strongly reduced for coastal areas.

Compared to GOT00 (and intermediate solution GOT4.8), the 58.77days signal on SLA is significantly reduced using GOT4.10 ocean tide (figure 34). Zawadzki&al explain in details in [25] the impact of the latest FES and GOT ocean tide models on the reduction of the 59-day signal in the mean sea level derived from TOPEX/Poseidon, Jason-1 and Jason-2 data.

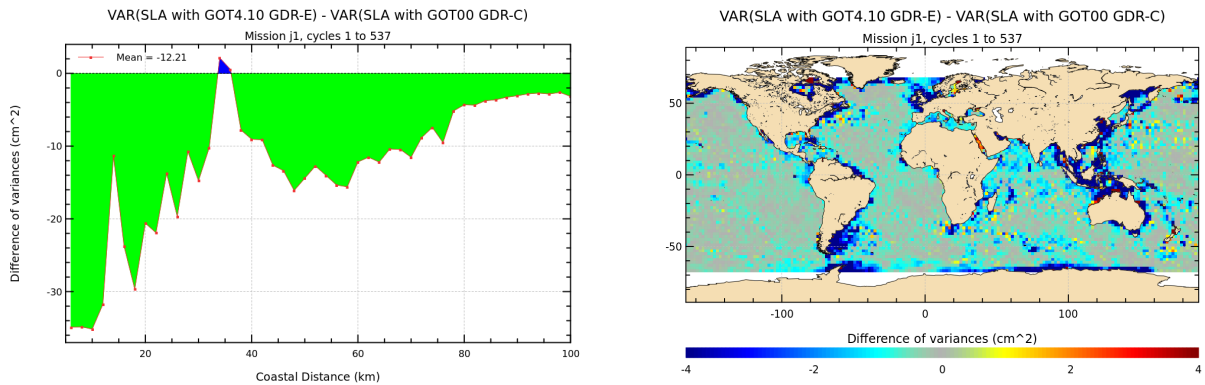


Figure 33: *Difference of SLA variances - computed by using successively GDR-E GOT4.10 and GDR-C GOT00.2 tide model* **Left:** *plotted in function of coastal distances between 0 and 100 km.* **Right:** *Map of the difference*

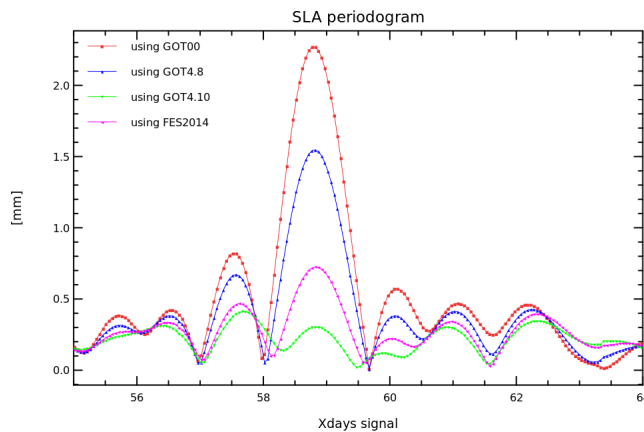


Figure 34: *Periodogram of SLA using different ocean tide solutions close to 59 days signal.*

Concerning FES2014 solution, mean at crossovers is quite equivalent to GOT4.10. Annual signal for standard deviation at crossovers is lower using FES2014 than with GOT4.10. Results are improved in many places, in deep ocean, in shallow waters, and at latitudes $>50^\circ$ (figure 35). Nevertheless, variance at SSH crossovers is slightly lower with GOT4.10 on the western coast of South America. Global Mean Sea Level is equivalent with both solutions (GOT4.10 and FES2014, not shown here). Regional differences between SLA using FES2014 or GOT4.10 is not significant. Standard deviation of SLA is slightly lower using FES2014 than with GOT4.10: the differences are mainly located near coasts (see figure 36).

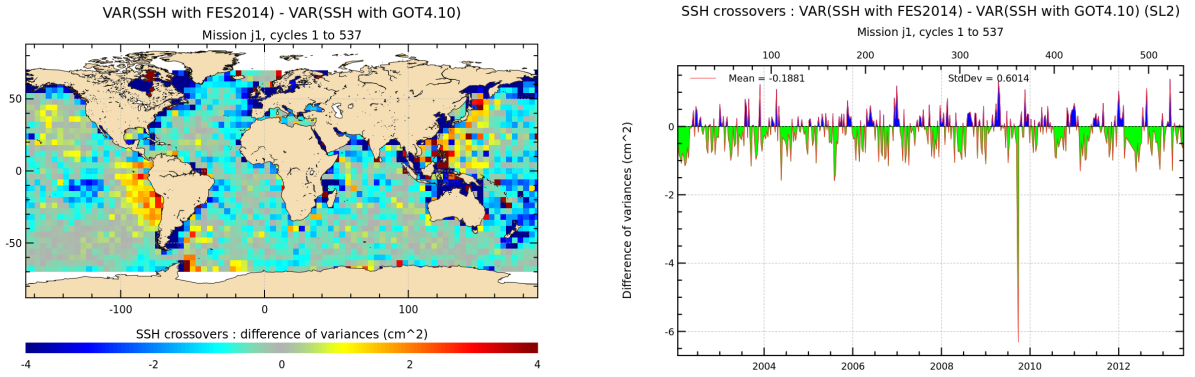


Figure 35: **Left:** Map of differences of SSH variances (SSH variance using FES2014 - SSH variance using GOT4.10) **Right:** cyclic monitoring of this difference.

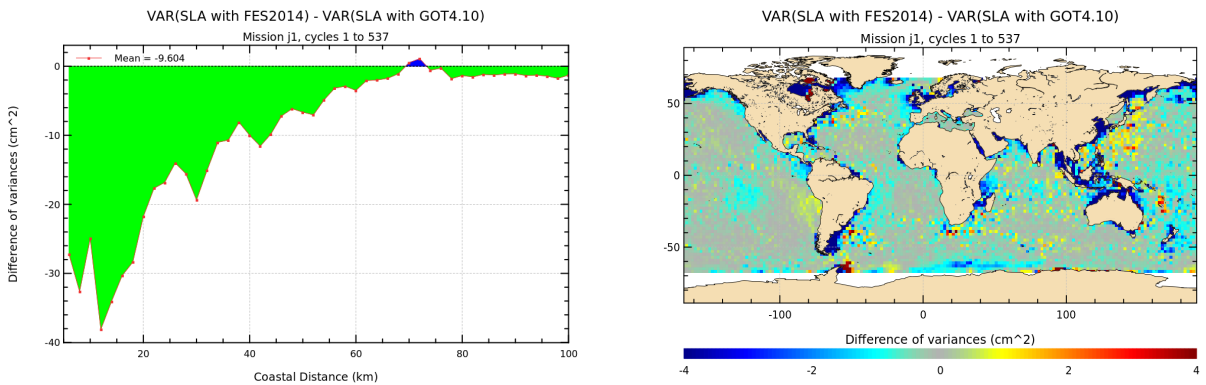


Figure 36: Difference of SLA variances - computed by using successively GDR-E GOT4.10 and FES2014 tide model **Left:** plotted in function of coastal distances between 0 and 100 km. **Right:** Map of the difference

5.5.2. Pole tide correction

In GDR-E, equilibrium model using mean pole of $X + iY = 0.042 + i0.293$ arcseconds. On figure 37 differences are visible over lakes and enclosed seas.

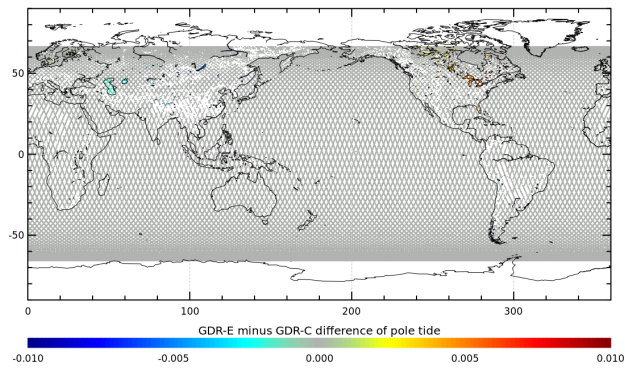


Figure 37: *GDR-E minus GDR-C pole tide difference over Jason-1 cycle 355.*

5.5.3. Long period non equilibrium tide

The long period non equilibrium tide in Jason-1 GDR-E product is based on FES2014. The global differences between the two dataset is shown on figure 38.

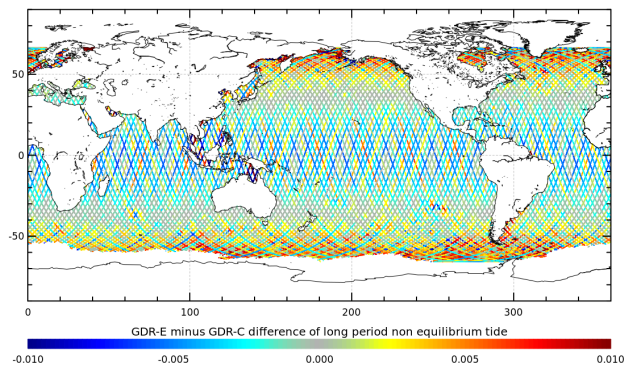


Figure 38: *GDR-E minus GDR-C long period non equilibrium tide difference over Jason-1 cycle 250.*

5.5.4. Mean sea surface

The mean sea surface of GDR-E is homogeneous over the whole Jason-1 mission, and contains the CNES/CLS 2011 referenced on 20 years version (instead of

- 2001 until cycle 374
- and 2011 on geodetic phase

for GDR-C) (see also Schaeffer & al. in [15], [16], [17]). The global mean bias between GDR-E MSS (CNES/CLS 2011 referenced 20years) and GDR-C MSS (CLS 2001) is mainly due to the change in the referenced period :

- from CLS 2001 to CNES/CLS 2011 MSS : 0.44cm.
- from CLS 2001 to CNES/CLS 2011 referenced 20years MSS: 2.40cm.

There are also some regional biases, shown on left of figure 39. Using the MSS CNES/CLS 2011 ref 20years instead of MSS CLS 2001 reduces the standard deviation of the SLA (see bottom part of figure 39).

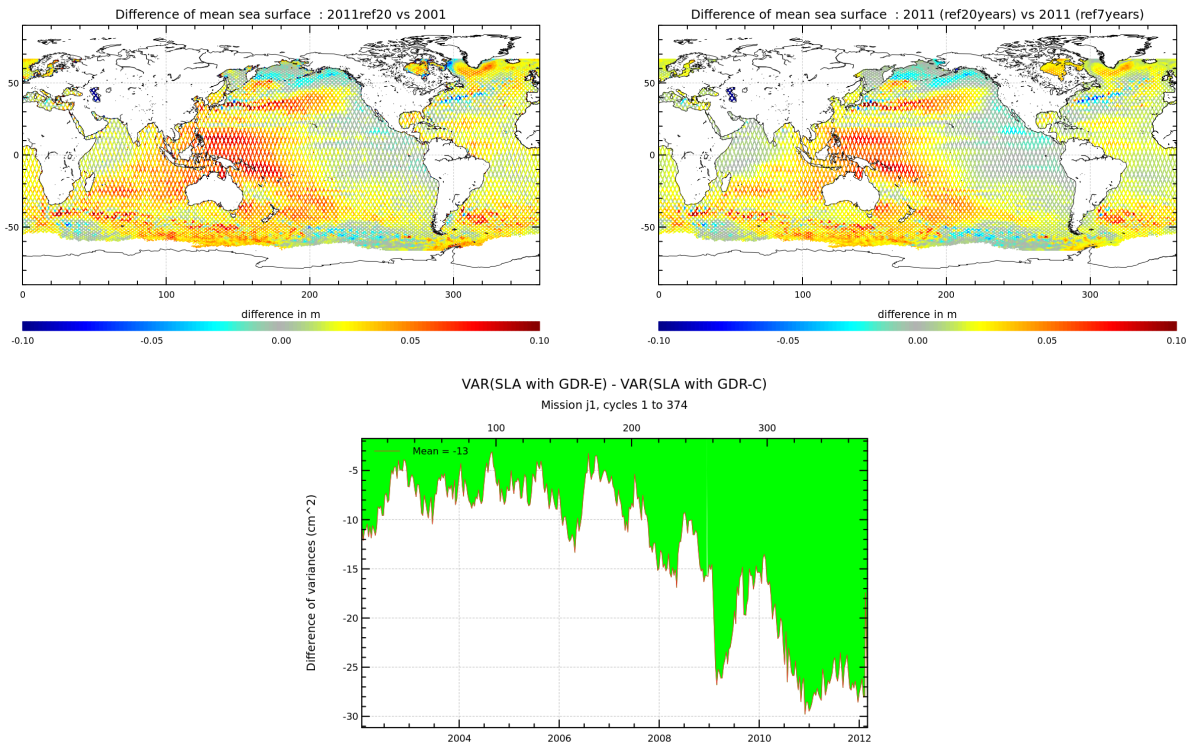


Figure 39: **Left:** Map of differences between MSS2011 referenced over 20 years and MSS2001 for Jason-1 cycle 250 **Right:** Map of differences between MSS2011 referenced over 20 years and MSS2011 for Jason-1 cycle 250 **Bottom:** Difference of variance of SLA for repetitive phase.

Figure40 shows the impact of the MSS solution on SLA spectrum. The choice of MSS solution impacts the error that is seen between 50 km and 600 km out of historical ground track. The impact on historical ground track is very low (2001 solution is a good one on historical ground track).

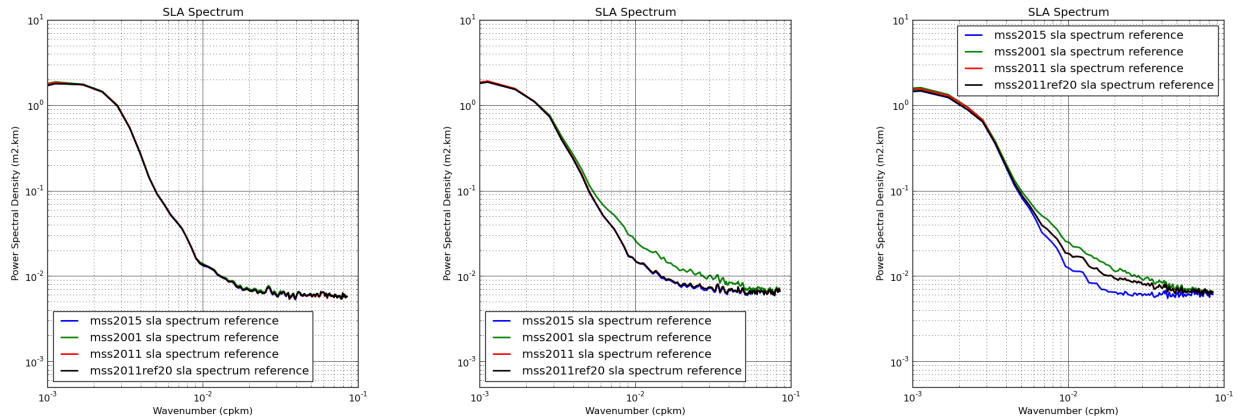


Figure 40: *SLA spectrum computed with one Jason-1 cycle (1Hz GDR data)* **Left:** Cycle 250: Historical ground-track **Middle:** Cycle 300: interleaved ground-track **Right:** Cycle 510: geodetic ground-track

5.5.5. Mean dynamic topography

The mean dynamic topography of Jason-1 GDR-E contains the CNES/CLS 2013 referenced on 20years version (instead of 2005 for GDR-C). Figure 41 shows the differences between the two versions over cycle 250.

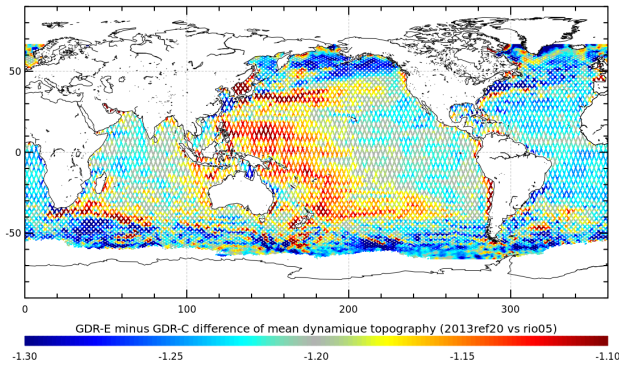


Figure 41: *GDR-E minus GDR-C MDT difference over Jason-1 cycle 250.*

5.5.6. Geoid based on EGM2008

Geoid in GDR-E takes into account EGM2008. Figure 42 shows the differences between the two versions over cycle 355.

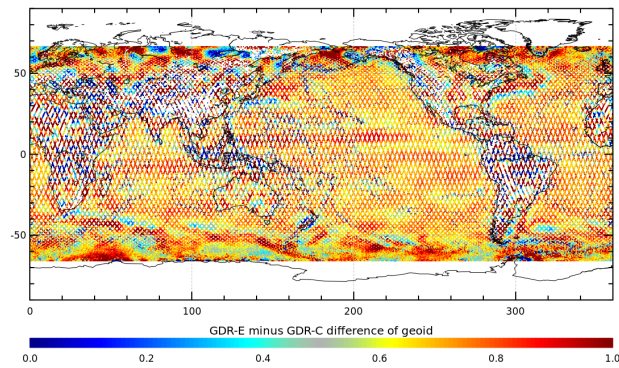


Figure 42: *GDR-E minus GDR-C geoid difference over Jason-1 cycle 355.*

5.5.7. Bathymetry from DTM2000.1

As in GDR-C, bathymetry in GDR-E is from DTM2000.1. Nevertheless, computation was done using a linear interpolation in previous dataset, interpolation by spline is used to compute GDR-E. Figure 43 shows the differences between the two versions over cycle 355.

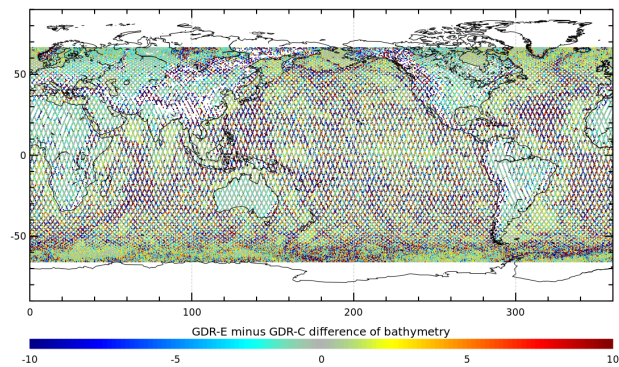


Figure 43: *GDR-E minus GDR-C bathymetry difference over Jason-1 cycle 355.*

5.5.8. Meteorological data: ERA-INTERIM

ERA-interim solutions have been studied by Carrere&al. [26], Legeais&al.[24], and for SL-CCI project (<http://www.esa-sealevel-cci.org/PublicDocuments/technical>). These studies show the advantages of these solutions for long term stability and at mesoscales.

The following items are available in Jason-1 GDR-E products:

- model_dry_tropo_corr_era (figure 44)
- model_wet_tropo_corr_era (For more details about model_wet_tropo_corr_era, see part 5.3.)
- inv_bar_corr_era (figure 45)
- hf_fluctuations_corr_era(figure 45)
- wind_speed_model_u_era (figure 46)
- wind_speed_model_v_era (figure 46)

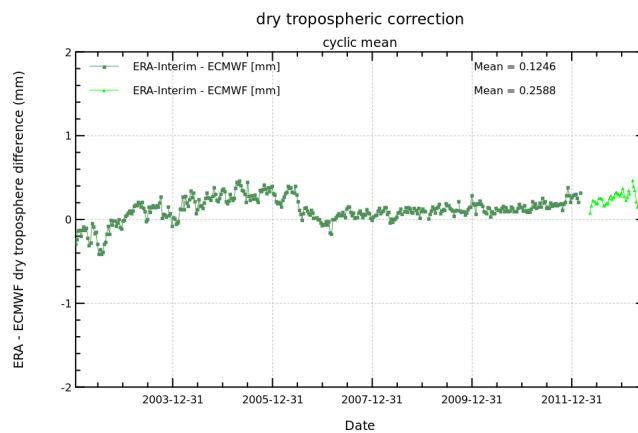


Figure 44: *Cycle per cycle mean of model dry tropospheric correction from ERA Interim products*

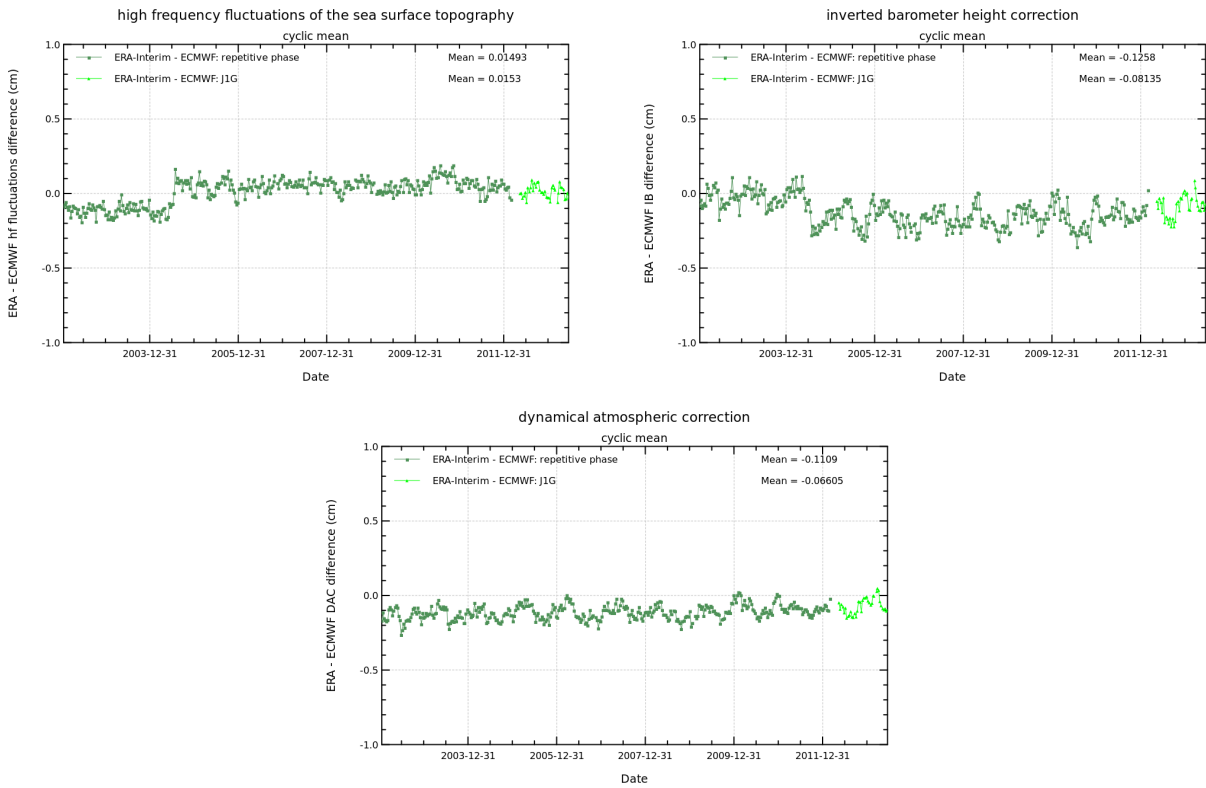


Figure 45: Cycle per cycle mean of **Left:** high frequency fluctuations of the sea surface topography derived from ERA Interim products. **Right:** inverted barometer height correction from ERA Interim products. **Bottom:** mog2d from ERA Interim products

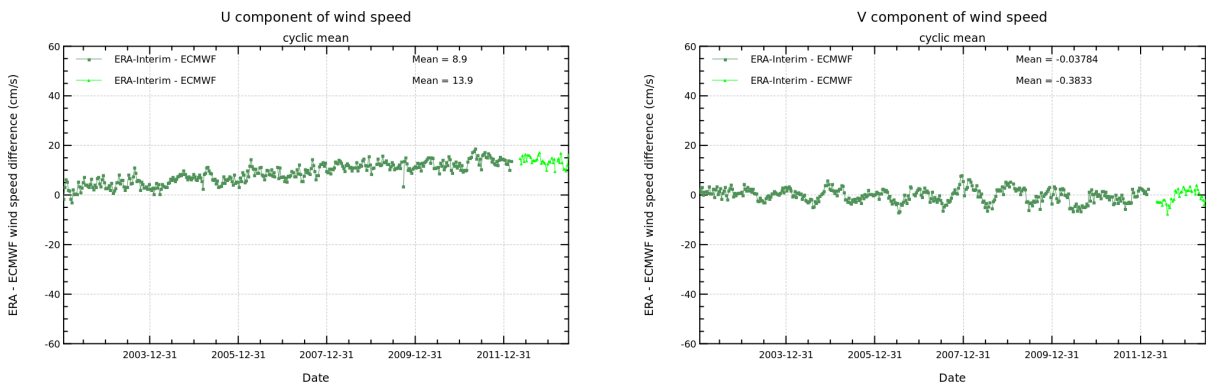


Figure 46: Cycle per cycle mean of model wind vector from ERA Interim products **Left:** U component. **Right:** V component.

6. Long Term Monitoring

The global mean sea level is one of the most important indicators of climate change as it incorporates the reactions from several different components of the climate system.

External data sources such as tide gauges allows to assess the altimeter MSL evolution and detect potential MSL drift. The changes concerning the MSL trends are presented here.

6.1. From J1 repetitive mission to geodetic drifting mission

As regards the Jason-1 MSL monitoring, a jump was visible on Jason-1 dataset when mission moved to the geodetic orbit. This jump was mainly attributed to a more precise PRF value for Jason-1 since may 2012, this part is directly corrected by a 3.2 mm bias in range value (see part 5.4.1.), but also partly due to new JMR calibration file in case radiometer wet troposphere solution is used. Nevertheless, a part of this jump was still unexplained. This uncertainty on Jason-1 MSL monitoring has no impact on L3/L4 GMSL computation (CMEMS products) as Jason-2 is the reference mission since year 2009. This jump was particularly visible on the monitoring of multi-mission crossovers (see part 4.1.1.) and seems to be significantly reduced using the new dataset. The process described in [3] is applied to the new dataset and the results are presented in table 4. The results show a bias of about -2.8mm to apply on geodetic part of SLA if computing with model wet troposphere (using either ECWMF model or ERA-Interim). Using radiometer wet troposphere reduces this bias by 1.3mm, the bias to apply is then -1.5mm. When using CNES/CLS2015 MSS, the bias falls under 1mm. This phenomenon has not been completely explained by now, but a part seems to be linked to the reference surface (MSS).

	Total bias (computed with radiometer wet troposphere)	Total bias (computed with model wet troposphere)	bias due to radiometer
GDR-C SLA	-3.8 mm	-1.8 mm	-2.0 mm
GDR-E SLA	-1.5 mm	-2.8 mm	+1.3 mm
GDR-E SSH - CNES2015 MSS	-0.6 mm	-1.9 mm	+1.3 mm

Table 4: *SLA global bias between repetitive and geodetic Jason-1 phases*

6.2. Global and Regional Mean Sea Level Trend

The description of the method and particular studies on this subject are detailed in [11]. The aim of this part is to synthesize how it was impacted by the reprocessing. The global mean sea level is calculated after removing the annual and semi-annual signals. In order to take into account the postglacial rebound, a correction of +0.3 mm/year is applied on the figures.

Coherence between ascending and descending passes:

Figure 47 shows the difference of MSL trends of Jason-1 computed by separating ascending and descending passes. These trends should be very close, as the same ocean is sampled. For GDR-C, there were negligible trend differences (less than 0.1 mm/yr) between odd and even passes (when removing annual and semi-annual signals). For GDR-E, the odd/even pass MSL trend difference is increased to 0.4 mm/yr, this is due to POE-E orbit (see part 5.2.1.).

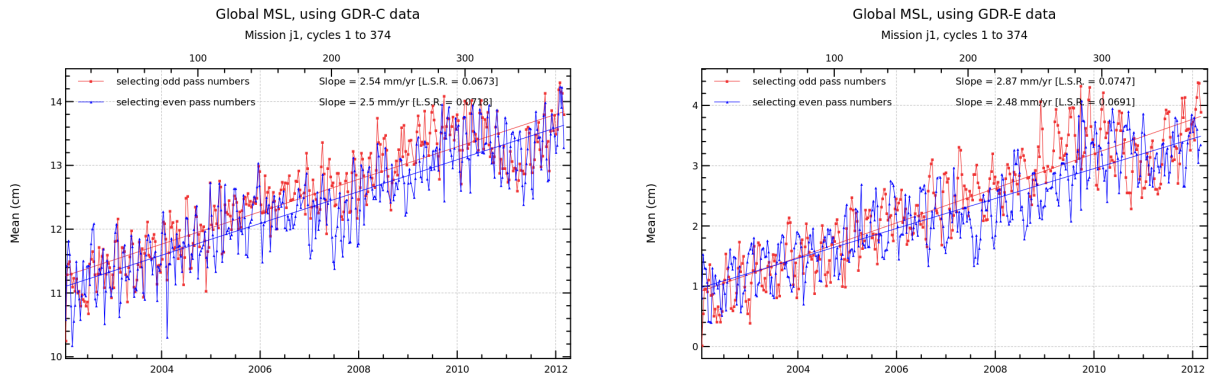


Figure 47: *Global Mean Sea Level difference between odd and even passes, annual and semi-annual signals removed. Left: GDR-C Right: GDR-E*

GMSL evolution from Jason-1 GDR-C to GDR-E:

The global MSL trend over repetitive phase using Jason-1 GDR-E increases by about 0.2 mm/yr compared to GDR-C GMSL when using radiometer wet troposphere correction (left part of figure 48). Taking into account the whole Jason-1 mission (including geodetic phasis, and correcting for the jump value described in part 6.1.), GMSL trend increases from 2.74 mm/yr to 3.08 mm/yr (+0.3 mm/yr).

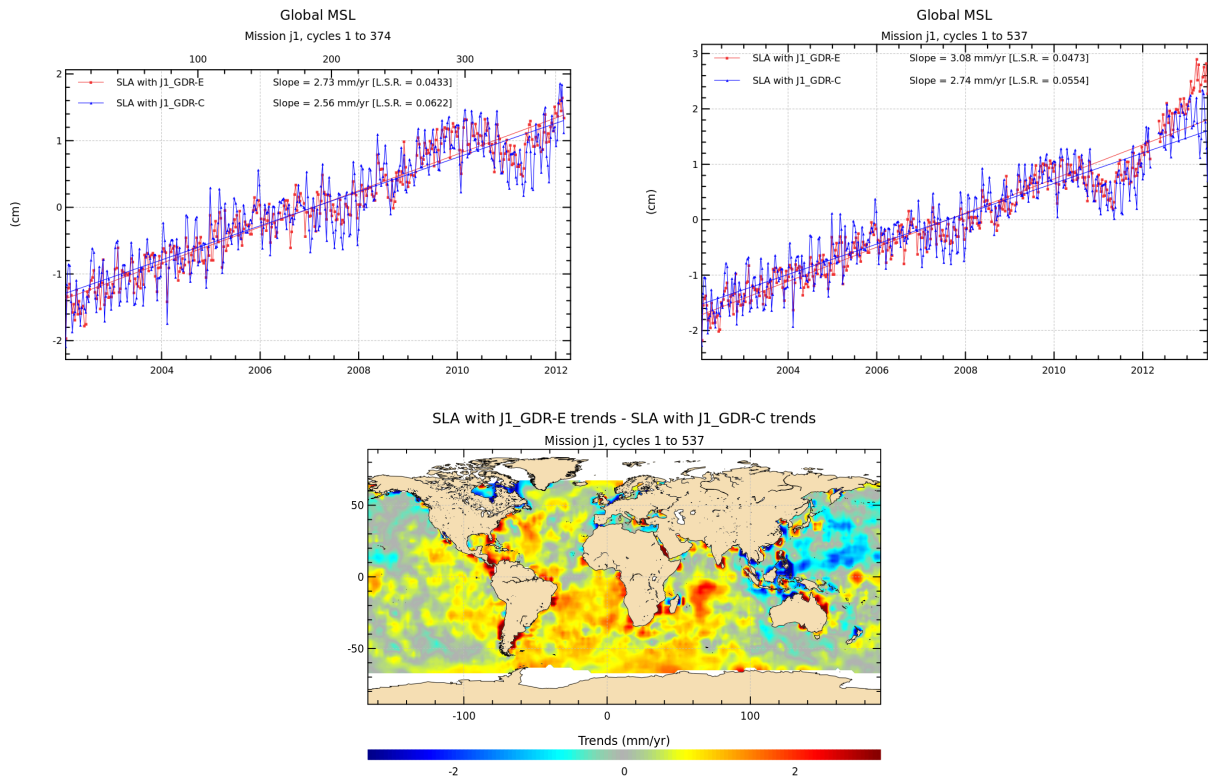


Figure 48: **Top:** Global MSL trends for J1 GDR-E versus GDR-C (annual and semi-annual signals are removed) **Left:** limited to repetitive phase **Right:** including geodetic phase, bias between repetitive and geodetic phase presented on dedicated part are applied. **Bottom:** Global MSL trends difference between J1 GDR-E and GDR-C

Comparison to Jason-2:

The difference of GMSL trend between Jason-1 and Jason-2 over the 5 years they flew together is reduced by a half (from $+0.83$ mm/yr for $J2_{GDR-D} - J1_{GDR-C}$ to -0.42 mm/yr for $J2_{GDR-D+} - J1_{GDR-E}$), see figure 49. Geographically correlated patterns of differences are reduced from bottom left to bottom right of figure 49.

On top left of figure 50 (same as top right of figure 49), Jason-1 and Jason-2 GMSL show a difference of behaviour for year 2013. This is due to JMR and AMR wet troposphere solutions differences. Using a model wet troposphere correction reduces the J2-J1 GMSL trend differences to 0.25 mm/yr (with either ECMWF or ERA-Interim model, bottom part of figure 50). Using radiometer wet troposphere correction when limited to 2008-2012 period for comparison, differences between Jason-1 and Jason-2 GMSL trends are under 1 mm/yr.

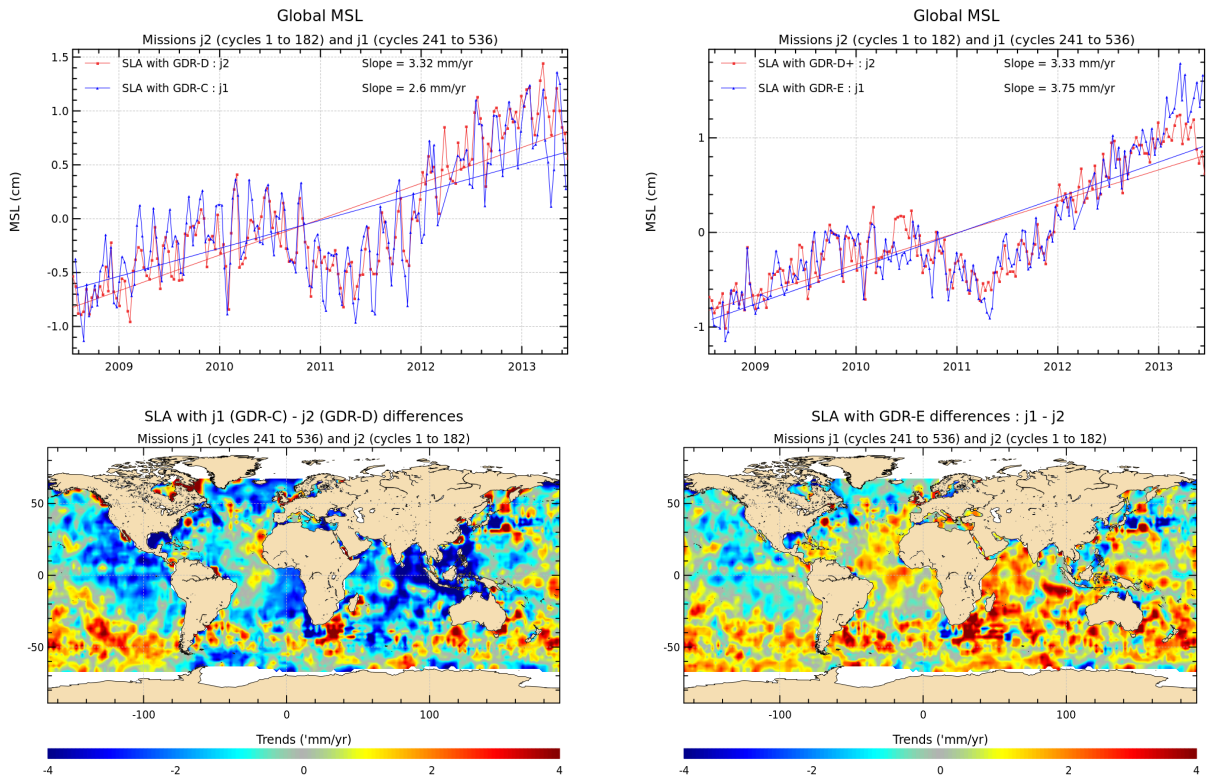


Figure 49: **Top:** Global MSL trends for J1 versus J2 (annual and semi-annual signals are removed) over common inflight period. Jump value in Jason-1 SLA is applied (bias presented on dedicated part are applied). **Bottom:** Maps of the Jason-1 minus Jason-2 MSL difference of trends. **Left:** J1 GDR-C and J2 GDR-D **Right:** J1 GDR-E and J2 updated GDR-D (GDR-E like).

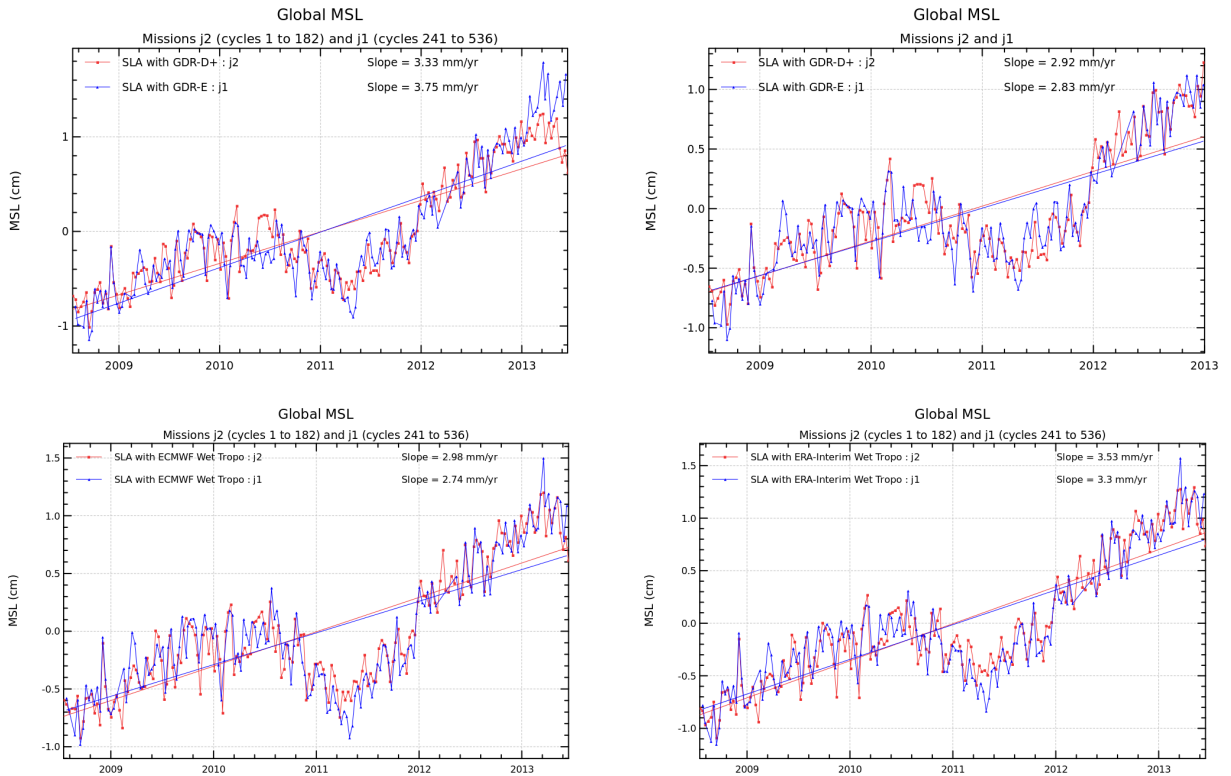


Figure 50: *Global MSL trends for J1 versus J2 (annual and semi-annual signals are removed) over common inflight period. Jump value in Jason-1 SLA is applied (bias presented on dedicated part are applied). Data used are J1 GDR-E and J2 updated GDR-D (GDR-E like). **Top left:** Whole common inflight period **Top right:** without year 2013. **Bottom left:** using ECMWF wet tropospheric correction. **Bottom right:** using ERA-Interim wet tropospheric correction.*

6.3. Tide Gauges Comparison

Figure 51 displays the time series of global average differences between Jason-1 and tide gauges, either keeping (left part of the figure) or removing (right part of the figure) the seasonal cycle. Concerning the long term trend differences (figure 51), results displayed show a change in behavior of the drift observed on Jason-1 time series, with a mean value of -0.3 mm/yr using GDR-E while it was $+0.3$ mm/yr considering GDR-C products, but with a method error of 0.7 mm/yr (Prandi, 2015 OSTST).

Therefore, residual signal of the difference between altimetry and tide gauges are neither increased nor reduced, which means that the temporal consistency between both datasets is the same when comparing to tide gauge measurements. Nevertheless, considering may to june 2013 (see bottom figure), the GDR-C serie seems to be slightly closer to TG measurements than GDR-E SLA, the difference of behaviour for this period could be related to the radiometer wet troposphere solution which is quite different in GDR-C and GDR-E products for this period (see figure 19).

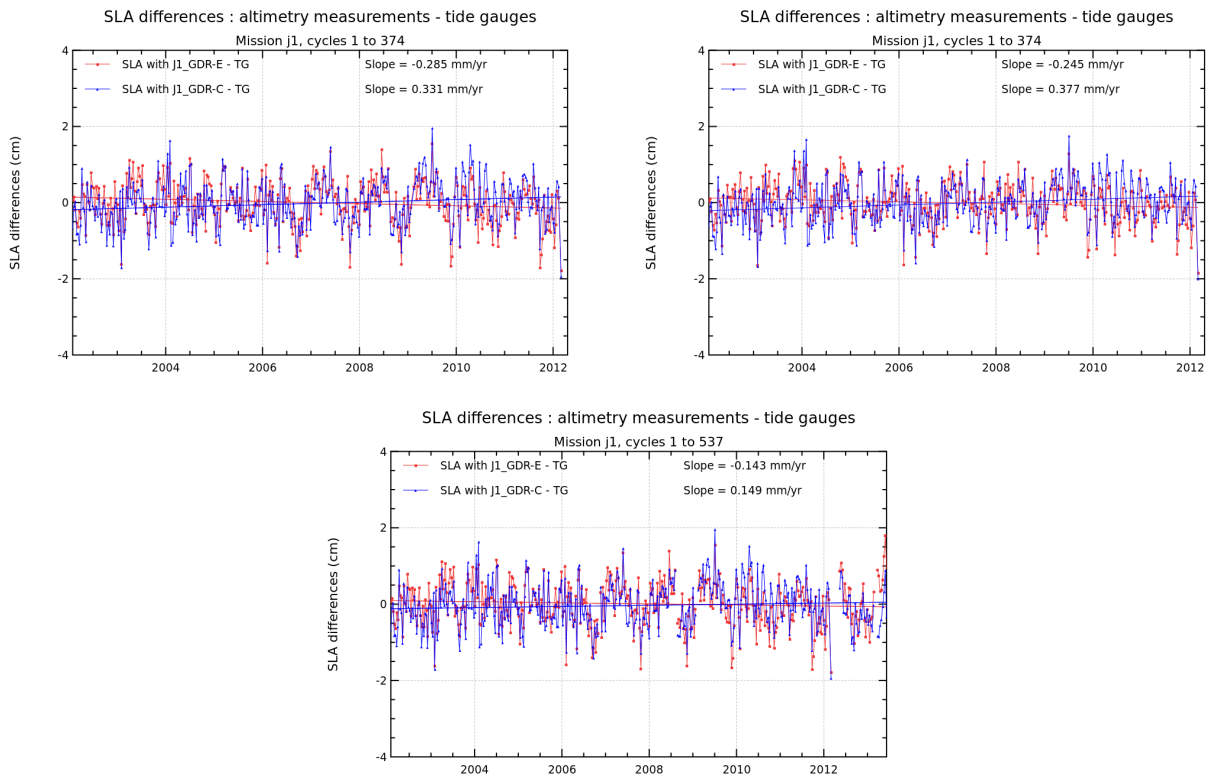


Figure 51: *Time series of global average differences between Jason-1 GDR-C (blue) or GDR-E (red) and tide gauges* **Top Left:** *Repetitive Phasis, no signal ajustment.* **Top Right:** *Repetitive Phasis, annual and semi-annual signals ajustments.* **Bottom:** *Whole Jason-1 mission.*

7. Table of uncertainties

This chapter is a synthesis of the error budget estimated for Jason-1 altimeter level 2 products. The global uncertainties estimation may change over the mission lifetime considering corrections improvements or on the other hand aging of devices. The global uncertainties have been estimated for several instrumental parameters but also geophysical corrections. In order to clarify and explain how each uncertainty has been calculated, dedicated sections have been performed with illustrations for each one described in the table 7.2., which sums up the uncertainties estimation of the Jason-1 altimeter mission using GDR-E product standard. It is also very important to mention that the uncertainties described here do not take into account long-term errors impacting climate implications as long term drift, periodic signals (annual, semi-annual or 60-day signal) and isolated jump for instance. We also do not describe the spatial repartition of uncertainties but only the mean error at global scale. For most of the parameters presented, the errors have been averaged spatially and temporally over a short period (10 days).

7.1. Comments

7.1.1. Description of the uncertainties sources

Several types of uncertainties can be defined in order to describe the error of altimetry measurements. These uncertainties are depending on time and spatial scales. For time scales, the following errors are defined:

- White noise: this uncertainty is uncorrelated on time and is due most of the time to the instrumental measurements (altimeter).
- Short-time temporal error (< 10 days) : these errors includes all the error uncorrelated and correlated on time for time scales lower than 10 days. It is important to define these errors for oceanographic applications in relationship with mesoscale or sub-mesoscale studies.
- Medium temporal errors (2 months - 1year) : these errors include all correlated temporal errors at medium scales such as for instance periodic signals (annual, semi-annual,..). The description of these errors is useful for climate application.
- Long-term errors (> 1 year) : these errors include inter-annual and drift. It is the most important for climate applications as the global mean sea level evolution.

The purpose of this chapter is not to describe all these errors. On the one hand, currently, we are not able to describe all the errors at these temporal scales and on the other hand there is not a clear way to merge all these errors together to calculate the average uncertainty. Therefore, our concern hereafter is to focus only on short-time temporal errors (< 10 days) and provide a synthetic view of these uncertainties. Indeed the Jason-1 cycle duration is about 10 days. The ocean is therefore globally covered within the 10 days period. Several diagnostics based on almost 10 days periods were already developed in the frame of the validation of the altimeter data (see also part 7.1.2.) and can be used for the estimation of the error budget. Notice also, that the spatial repartition of these errors has not been described. Only the global mean error have been calculated in order to simplify the approach.

7.1.2. Methods to determine the uncertainties

Several methods can be used in order to estimate the uncertainties of the different altimeter parameters and geophysical corrections. Furthermore, it is important to take into account spatial and temporal scales. In the following, only global uncertainties are considered. When not mentioned otherwise, uncertainties within a 10 days period (which equals a Jason-1 cycle) are computed.

7.1.2.1. Using tandem flight phase of Jason-2 with Jason-1

Concerning the altimeter parameters, the tandem flight phase, when Jason-1 and Jason-2 overflow the same ground track with only 55 seconds delay, is very useful. During the first 20 cycles of Jason-2, direct differences of Jason-1 and Jason-2 (collocated) 1 Hz measurements can be computed. Due to the short time delay, the assumption, that both satellites measure the same quantities can be made. These measurements contain errors compared to the unknown truth. Assuming that both missions contribute equally to the error and assuming that they are not correlated, the standard deviation of the Jason-1/Jason-2 differences divided by square-root of 2, gives the noise of the measured parameter. This error can potentially include the measurement noise (if it exists for the studied parameter), but also errors on time scales less than 10 days. Nevertheless, this is the minimum threshold of the error, since both missions might be impacted by the same errors, which can not be seen when just comparing Jason-2 and Jason-1. For instance, the similarity of altimeter and retracking method, as well as algorithms to retrieve the wet troposphere content derived from radiometers, the identical atmospheric and geophysical corrections (dry troposphere, ocean tides ...) prevent the estimation of the whole error budget.

7.1.2.2. Spectral Analysis

The spectral analysis of a signal allows to identify the repartition of the energy of this signal in the frequency spectrum and contains information about the spatial (wavelength in km) scales implied. The method consists in averaging N Fast Fourier Transform computed over samples of M along-track points. The length of the samples is 300 points or 15 s for 20 Hz data. The bandwidth analyzed with this method concerns frequencies between the inverse of the spectrogram window's size and Shannon frequency (inverse of two times the sampling period). These frequencies can also be converted into distances with the relation:

$$Distance = Ground_Satellite_Speed * Frequency$$

with Ground_Satellite_Speed equal to 7 km/s. For 20 Hz data, analyzed frequencies are:

- between 0.1 and 15 s
- between 0.07 Hz (1/15 seconds) and 10 Hz (20 Hz/2)
- between 700 m and 105 km

The power spectrum of a real physical signal containing measurement noise can be seen as decreasing spectrum added to a white noise spectrum which is an uniform plateau (energy equally distributed on all frequencies). The high frequency plateau can therefore be interpreted as the noise level of the data. The value of the plateau is

$$\alpha = 2 * \Delta t * \sigma^2 \tag{1}$$

where σ is the standard deviation of the white noise.

7.1.2.3. Analyzing rms of 20 Hz data

In the Jason-1 products, the rms of the 20 Hz altimeter parameters is available (for range, significant wave height, backscattering coefficient, ...). This rms of the elementary Ku-band parameters can be averaged over a certain period in function of significant wave height. Only valid measurements are used (using the method described in part 3.2.) The mean value of the rms of the 20 Hz altimeter parameters for significant wave height of 2 m (most of measurements have significant wave heights around 2 m), corresponds approximately to the 20 Hz measurement noise of the altimeter parameters. According to Zanife et al. ([40]), this value can be approximately related to the 1Hz using the decorrelation assumption of the high rate data over 1s. Assuming full decorrelation, the division by square root of 20 (20 elementary measurements) results in the 1 Hz data noise. Therefore, this approach give the same kind of information (white noise of altimeter parameter) than the spectral analysis just previously described. It is easily applicable but only for the range, SWH and Sigma-0 parameters.

7.1.2.4. Comparison with other corrections

For some corrections, several versions exist (for example dry troposphere correction derived from different models). The mean and standard deviation of the correction differences gives an indication of the accuracy and the noise of the correction. Furthermore at crossover points, the impact of using either one or another correction in the Sea Surface Height computation can be analyzed. Therefore the explained variance of a correction is analyzed for the ascending/descending SSH differences at crossover points. These differences are computed for time differences less than 10 days between ascending and descending tracks. This allows to minimize the contribution of the oceanic variability (mesoscale). Therefore the variance of the SSH differences at crossover points gives an information of the performance of the altimeter system. Computing the differences of these variances (one using one version of the correction, one using another version of the correction), allows to measure the ability of the correction to improve the computation of the SSH. This difference of variance has to be divided by 2, as errors on ascending and descending tracks are additive, supposing that they are independent. This type of analysis gives therefore access to errors concerning timescales less than 10 days (on average, the time differences at 10-day crossovers is 3.5 days for Jason missions). This means that analyzing 2 corrections where one has experienced improvements concerning long-term periods (e.g. annual signals, long-term trends, ...), this improvement will not be visible with this type of analysis.

7.1.2.5. Intercalibration with other altimeter missions

Another way to assess errors on parameters or corrections is to intercalibrate different altimeter missions. Especially correction (or parameter) differences at multi-mission crossover points with small temporal interval (1h or 3h) are useful. The drawback is that there are relatively few crossover points with such a small time interval. This gives access to errors concerning timescales of less than 1 or 3 hours.

7.1.2.6. Bibliography and theoretical considerations

Finally, several authors have already studied errors on several parameters and corrections. They will be mentioned along this chapter.

7.2. Jason-1 uncertainties summarize

The following table gives the noise estimation of the different corrections and parameters.

	GDR		Goal
	Spec	Perf	
Altimeter noise ^{1 2 3}	1.7 cm	>1.6cm	1.5 cm
Ionosphere ^{3 4}	0.5 cm	white noise: 0.2cm scales < 10days: 0.41cm	0.5 cm
Sea State Bias	2.4 cm (1.2%)	scales < 10days: 0.42cm	2.0 cm (1%)
Dry troposphere	0.7 cm	0.3 to 0.7cm	0.7 cm
Wet troposphere	1.2 cm	>0.2cm	1 cm
Altimeter range: RSS $\sqrt{(\sum_i \cdot \sigma_i)}$ (from tandem flight with J2)	3.3 cm	>1.9cm 2.3cm	3 cm
Rms Orbit (radial component) ⁵	2.5 cm	>1.0cm	1.5 cm
SSH: Total RSS	4.2 cm	<3.9cm	3.3 cm
Significant wave height ⁶	10% or 50cm	white noise: 11.2cm scales < 10days: 12.1cm	10% or 40cm
Wind speed	1.7 m/s	white noise: 1.03m/s scales < 10days: 0.31m/s	1.5 m/s
Sigma0 (absolute)		white noise: 0.08dB scales < 10days: 0.15dB	

Table 5: Table of uncertainties on Jason-1 summarize

¹Ku-band after ground retracking

²Averaged over 1 sec

³Assuming 320 MHz C bandwidth

⁴Filtered over 100 km

⁵Real time DORIS onboard ephemeris

⁶Whichever is greater

⁷On global mean sea level, after calibration

7.3. Details

7.3.1. Altimeter Noise

Uncertainties on the range measurements can depend on several sources: atmosphere state (rain, presence of water vapor, ...), non-gaussian distribution of the wave field, but also technical parameters such as altimeter calibration, platform mispointing, Doppler effect, The estimation of the altimeter range distance depends also on the retracking algorithm.

In order to determine altimeter noise, two methods can be used: the spectral analysis of the high-frequency content and the monitoring of rms of elementary Ku-band range measurements.

Considering the power spectrum of the uncorrected SLA (orbit - range - MSS) of 20 Hz data, and as the orbit and the mean sea surface (MSS) are low frequency quantities, the noise displayed on the spectrum, comes from the range. This method is not used here.

The monitoring of rms of elementary Ku-band range measurements is done, only valid data were used (using the method described in part 3.2. The cycle by cycle mean (left of figure 52) is 8.0cm in average. Assuming that the 20Hz measurements have uncorrelated noise, it corresponds to a noise of about 1.79cm at 1Hz.

The rms of the elementary Ku-band range (range_rms_ku) over 2011 was averaged in function of significant wave height (right of figure 52). For significant wave height of 2 m (as specified in the Error Budget), the mean of range_rms_ku is 7.22cm. Assuming full decorrelation, the division by $\sqrt{20}$ (20 elementary measurements) results in 1.61 cm for the 1 Hz data.

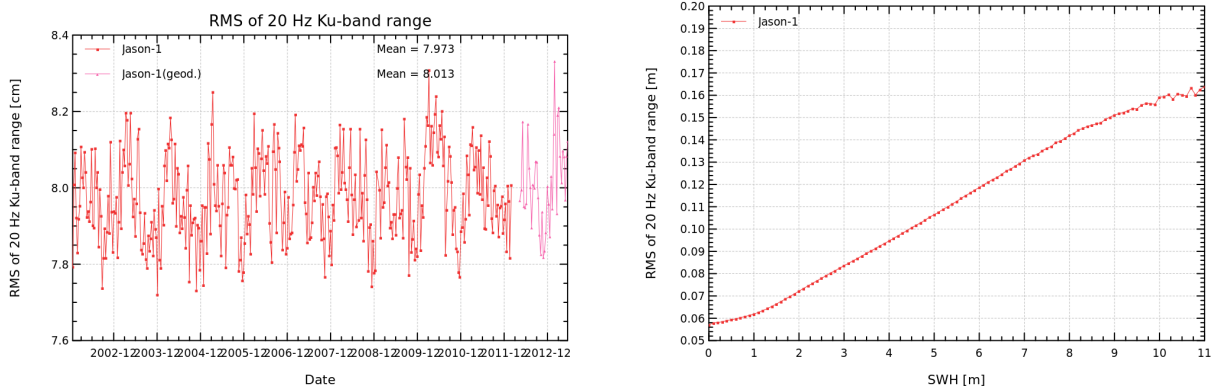


Figure 52: *Rms of elementary Ku-band range measurements* **left:** Mean per cycle monitoring. **right:** in function of significant wave height for Jason-1 GDR-E over 2011.

**The random noise of altimeter range is 1.6cm for significant wave height of 2m.
The total error (due to correlations) for time scales less than 10 days is higher.**

7.3.2. Ionosphere

White noise of ionosphere correction:

The ionospheric correction is dependant on the ranges (corrected for sea state bias) for Ku- and C-bands, as well as the frequencies used. The noise of the dual-frequency ionosphere correction can be computed theoretically by using the noise of the Ku- and C-band ranges. The Ku-band ionospheric correction formula is:

$$Iono_corr_Ku = \frac{1}{f_{Ku}^2} \left(\frac{f_{Ku}^2 * f_C^2}{f_{Ku}^2 - f_C^2} \right) (Range_Ku - Range_C) \quad (2)$$

$$\sigma_{Iono_corr_Ku} = \frac{1}{f_{Ku}^2} \left(\frac{f_{Ku}^2 * f_C^2}{f_{Ku}^2 - f_C^2} \right) \sqrt{\sigma_{Range_Ku}^2 + \sigma_{Range_C}^2} \quad (3)$$

For 2011, the rms of 20Hz range measurements for significant wave heights of 2 m, are 7.2 cm for Ku-band (see figure 52) and 15.6 cm for C-band (see figure 53). The computation gives therefore:

$$\sigma_{Iono_corr_Ku} = 0.179 \sqrt{7.2^2 + 15.6^2} \cong 3.08cm \quad (4)$$

at 20 Hz.

$$\sigma_{Iono_corr_Ku} = 3.08 / \sqrt{20} \cong 0.69cm \quad (5)$$

at 1 Hz.

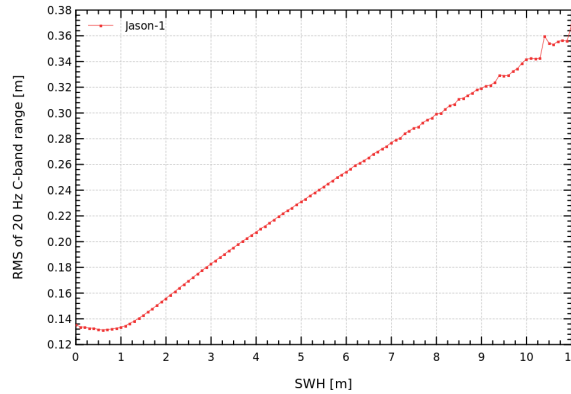


Figure 53: *Rms of elementary C-band range measurements in function of significant wave height for Jason-1 GDR-E over 2011.*

When filtered at 100 km $\rightarrow 100 \text{ km} / 7 \text{ km/s}^{-1} = 14.3 \text{ s}$: $\sigma_{Iono_corr_Ku} = 0.69 / \sqrt{14.3} \cong 0.2cm$.

Nevertheless, as this value only takes into account range noise, it presents the minimum threshold of the error.

Uncertainty of ionosphere correction (timescale less than 10 days):

Another way to determine noise on ionospheric correction is using the comparison between Jason-1 and Jason-2 during the tandem flight phase (Jason-1 cycles 240 to 259 Jason-2 cycles 001 to 020). As during this phase, Jason-1 and Jason-2 were only 55 seconds apart on the same track, computing collinear measurement differences is possible.

Top of figure 54 shows the cycle per cycle monitoring of the difference of the unfiltered ionospheric corrections. The standard deviation is 1.357 cm. Assuming that both altimeters contribute equally to the noise, the noise on ionospheric correction on either Jason-1 or Jason-2 is 0.960 cm.

Bottom of figure 54 shows the cycle per cycle monitoring of the difference of the filtered ionospheric corrections (300km). The standard deviation is 0.334 cm. Assuming that both altimeters contribute equally to the noise, the noise on ionospheric correction on either Jason-1 or Jason-2 is 0.236 cm.

To obtain the noise level for 100 km filtered data, this value has to be multiplied by $\sqrt{3}$. This results in a noise level of 0.41cm.

Note that there is a bias of about -8.6 mm between Jason-1 and Jason-2 ionosphere corrections.

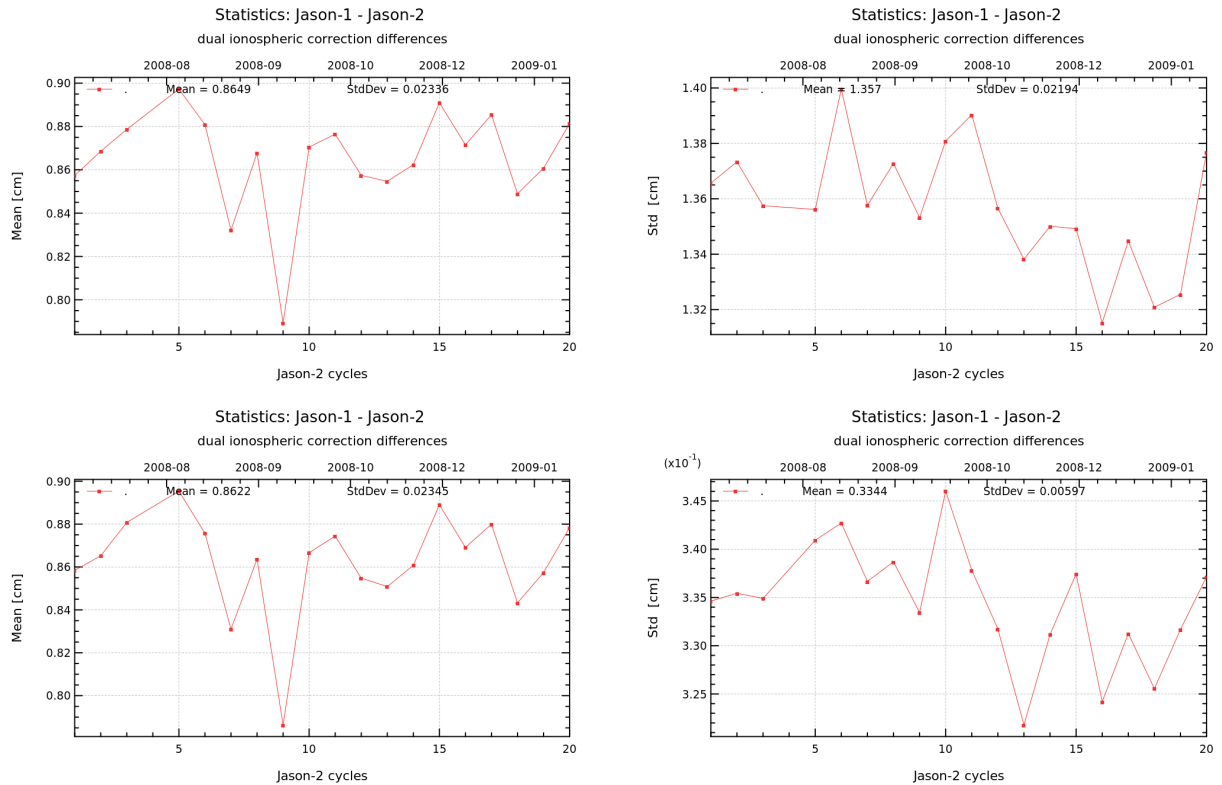


Figure 54: *Cycle per cycle monitoring (mean and standard deviation) of the Jason-1 minus Jason-2 unfiltered (top) and filtered (bottom) dual-frequency ionospheric correction.*

The uncertainty on ionosphere correction (for time scales less than 10 days) is about 0.96cm. By filtering it falls to 0.41cm. The white noise is about 0.2cm at 100km.

7.3.3. Sea State Bias

The non-parametric sea state bias available on Jason-1 products is determined from a look-up table dependant on altimeter wind speed and significant wave height. Its quality is therefore directly dependant on the quality of this input values. The noise of the resulting parameter therefore comes from the error made on the significant wave height and wind speed estimation and the model estimation error.

Historically, Chelton ([35]) considered 1% SWH for SSB uncertainty in his 1994 reference paper. It corresponds to a 2 cm SSB noise level for 2m SWH. This high value is mainly due to the uncertainty of the constant offset term α_0 in the regression used for the parameter based sea state bias models. This error figure corresponds therefore rather to a bias. For non parametric models there is also an uncertainty on the determination of the constant (SSB for (SWH, Wind) = 0). Therefore non-parametric SSB solutions can have biases of several mm to several cm. Hereafter for the computation of the error figures, we do not take into account constant biases.

SSB estimation noise due to input noise

Estimating the absolute sea state bias correction error is relatively difficult. Since most SSB estimators are computed as a function of SWH and altimeter Wind Speed, the first approach is to use a Gaussian assumption, and a direct dependence between the random noises on the input parameters. Taking a SWH value of 2m and a wind speed of 8m/s, the SSB model (table) gives a SSB value of -9.105375 cm for Jason-1 GDR-E. During the Jason-1/Jason-2 tandem flight phase, sea state bias differences between Jason-1 and Jason-2 had a mean value of 1.6 mm and a standard deviation of 5.9 mm (see figure 55), assuming that both missions contribute equally to the noise, the noise on Jason-1 sea state bias is 4.2 mm.

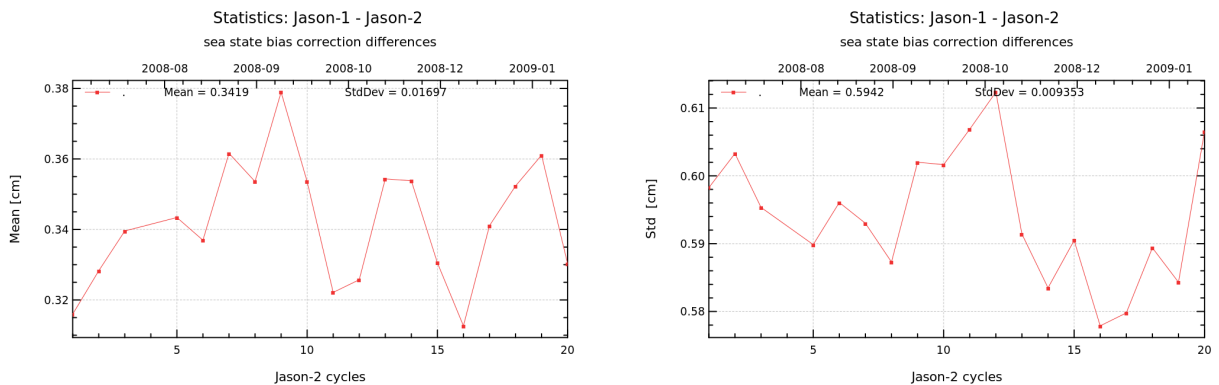


Figure 55: *Cycle per cycle monitoring (mean and standard deviation) of the Jason-1 minus Jason-2 non-parametric sea state bias correction.*

The uncertainty of ssb (for time scales less than 10 days) is about 0.42cm.

7.3.4. Dry Troposphere Correction

The dry troposphere correction available in the products comes from analysed atmospheric pressure fields and model for S1 and S2 atmospheric tides (operational ECMWF model).

The dry troposphere correction value is proportional to the pressure value. To assess the error made on the dry tropospheric correction (basically due to the error in the pressure field), a theoretical approach is possible. Salstein et al. ([39]) stated a rms error of 2-3 hPa in the pressure fields, which translates to an error of approximately 0.7 cm in the dry tropospheric correction.

As the dry troposphere correction comes from a model, there is no white noise.

The study of the uncertainty of dry troposphere solution has been done and presented in [12]:

The uncertainty on the dry troposphere correction (for timescales less than 10 days) is between 0.3 cm (comparison between models) and 0.7 cm (theoretical considerations)

7.3.5. Wet Troposphere Correction

Uncertainties of the radiometer wet troposphere correction (for timescales < 10 days)

To determine noise on radiometer wet troposphere correction the comparison between Jason-1 and Jason-2 during the tandem flight phase is used, as already in chapter 7.3.2.. As during this phase, Jason-1 and Jason-2 were only 55 seconds apart on the same track, computing collinear measurement differences is possible. Figure 56 shows the cycle per cycle monitoring of the difference of the radiometer wet troposphere corrections. The standard deviation is 0.349 cm. Assuming that both altimeters contribute equally to the noise, the noise on wet troposphere correction on either Jason-1 or Jason-2 is 0.247 cm.

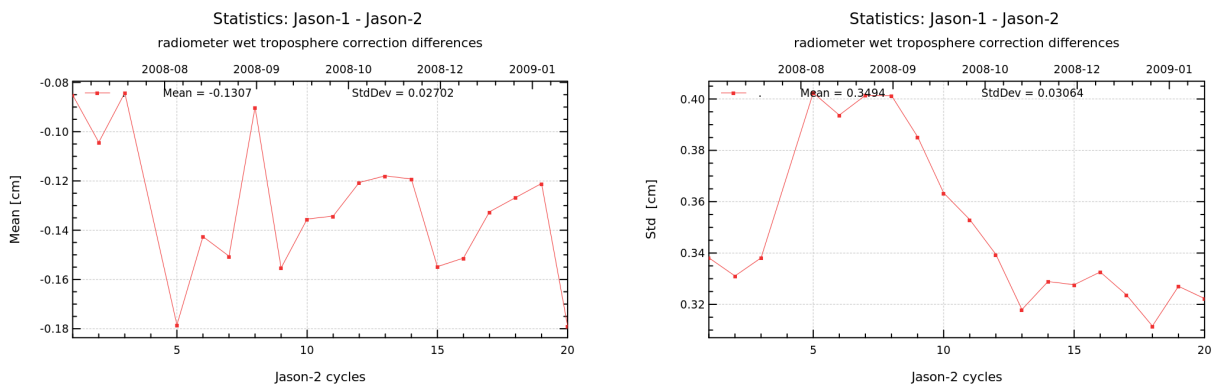


Figure 56: *Cycle per cycle monitoring (mean and standard deviation) of the Jason-1 minus Jason-2 radiometer wet tropospheric correction.*

Jumps and drifts of the radiometer wet troposphere correction

The present study is focalized on uncertainties for timescales less than 10 days. Nevertheless errors on longer timescales exist. The radiometer wet troposphere correction for example is impacted by drifts and jumps. The jumps and drifts are easily recognizable on Figure 57, where radiometer and ECMWF model wet troposphere correction are compared. This variability can include the effect of the JMR ageing but it also includes ECMWF changes (for green curves). The standard deviation of radiometer minus model wet troposphere differences is more stable with ERA-Interim than with operational ECMWF model.

The error of the radiometer wet troposphere correction (for timescales less than 10 days) is at least 0.2 cm.

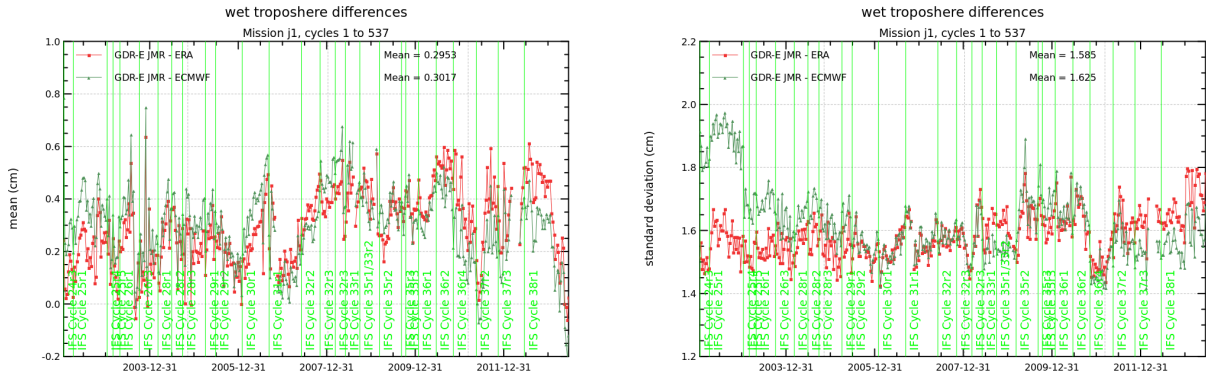


Figure 57: Cycle per cycle monitoring of the radiometer minus model (ECMWF or ERA-Interim) wet tropospheric correction difference for Jason-1 GDR. Vertical lines indicate a change in ECMWF model. **Left:** mean. **Right:** standard deviation.

7.3.6. Significant Wave Height

White noise of significant wave height:

In order to assess the noise of 1Hz significant wave height (SWH), the rms of the elementary Ku-band SWH (swh_rms_ku) over 2011 was averaged in function of significant wave height. Only valid data were used (using the method described in in part 3.2. For significant wave height of 2 m, the mean of swh_rms_ku is 50.0 cm. Assuming full decorrelation, the division by square root of 20 (20 elementary measurements) results in 11.2 cm for the 1 Hz data.

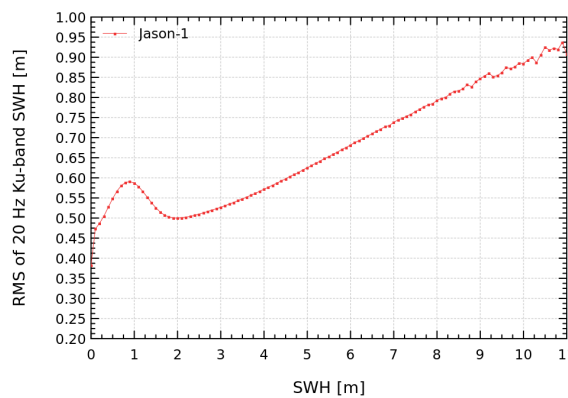


Figure 58: Rms of elementary Ku-band SWH measurements in function of significant wave height for Jason-1 GDR-E over 2011.

Uncertainty of significant wave height (timescales less than 10 days):

During the tandem flight phase, the standard deviation of the Jason-1 minus Jason-2 significant wave height difference was 17.17 cm (right part of figure 59). Assuming that both missions contribute equally to the noise, the noise on Jason-2 SWH is 12.1 cm.

The uncertainty of significant wave height (for timescales less than 10 days) is about 12.1cm.
The white noise is about 11.2 cm.

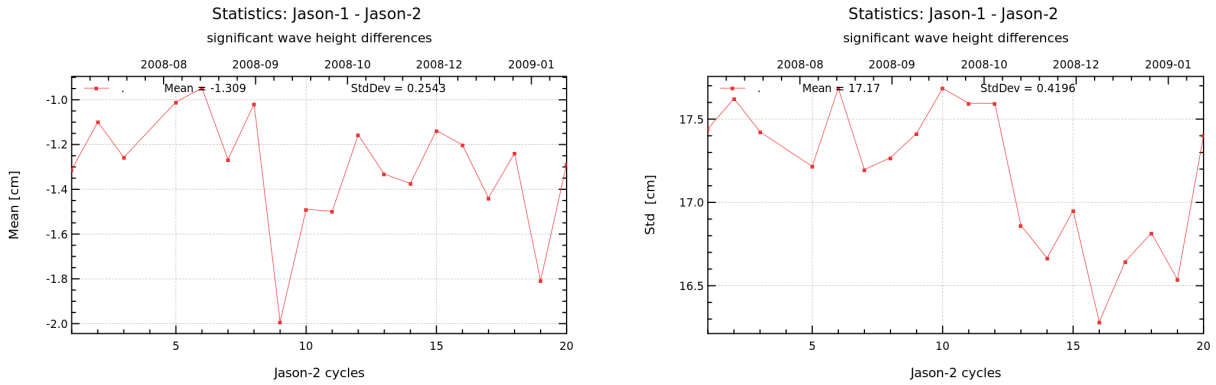


Figure 59: Cycle per cycle monitoring (mean and standard deviation) of the Jason-1 minus Jason-2 significant wave height.

7.3.7. Backscattering coefficient

White noise of backscattering coefficient:

In order to assess the noise of 1Hz backscattering coefficient (σ_0), the rms of the elementary Ku-band σ_0 ($\sigma_{0_rms_ku}$) over 2011 was averaged in function of significant wave height. Only valid data were used (using the method described in part 3.2.)For significant wave height of 2 m, the mean of $\sigma_{0_rms_ku}$ is 0.372 dB. Assuming full decorrelation, the division by square root of 20 results in 0.08 dB for the 1 Hz data.

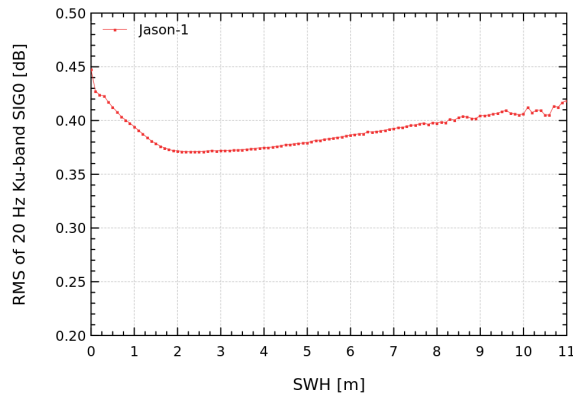


Figure 60: Rms of elementary Ku-band σ_0 measurements in function of significant wave height for Jason-2 GDR over 2011.

Uncertainty of backscattering coefficient (for time scales less than 10 days):

During the tandem flight phase, the standard deviation of the Jason-1 minus Jason-2 backscattering coefficient difference was 0.154 dB (right part of figure 61). Assuming that both missions contribute equally to the noise, the noise on Jason-1 backscattering coefficient is 0.15 dB. Note, that the error of backscattering coefficient is probably higher for Jason-1 than Jason-2, as Jason-1 experienced some increased mispointing periods (due to unavailability of star trackers). This also impacts the backscattering coefficient.

The error of σ_0 (for time scales less than 10 days) is about at least 0.15dB. The white noise is about 0.08dB.

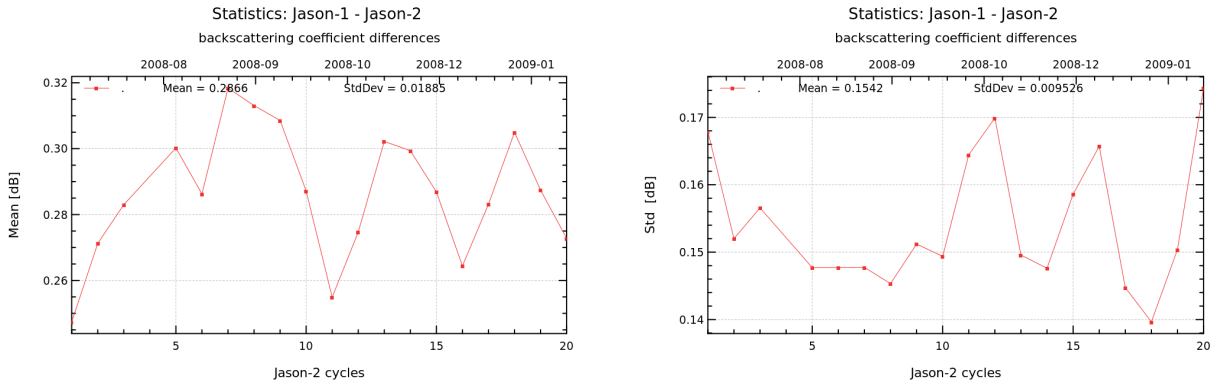


Figure 61: Cycle per cycle monitoring (mean and standard deviation) of the Jason-1 minus Jason-2 backscattering coefficient.

7.3.8. Altimeter wind speed

Noise of altimeter wind speed:

To assess the noise on altimeter wind speed, model and altimeter wind speed (both available in products) are compared for Jason-1 over 2011. Cycle per cycle standard deviation of this difference is shown in figure 62. Its mean value is 1.46 m/s. Assuming that both correction types contribute equally to the noise (which is not true as the model wind speed correction is smoother than the altimeter wind speed), the noise of altimeter wind speed is 1.03 m/s.

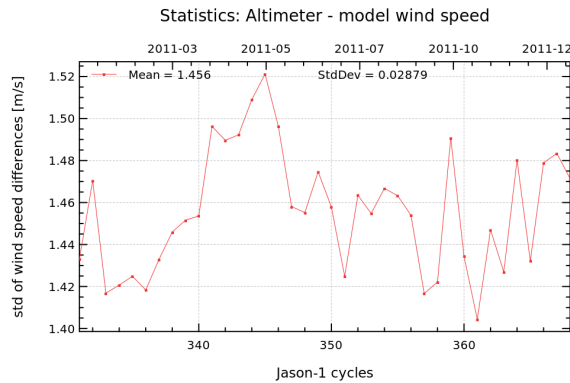


Figure 62: Cycle per cycle monitoring of std of altimeter - model wind speed for Jason-1 GDR-E over 2011.

Uncertainty of altimeter wind speed (for time scales less than 10 days):

During the tandem flight phase, the standard deviation of the Jason-1 minus Jason-2 altimeter wind speed difference was 0.44 m/s (right part of figure 63). Assuming that both missions contribute equally to the noise, the noise on Jason-1 altimeter wind speed is 0.31 m/s. This is a minimum value of the error.

The error of the altimeter wind speed (for time scales less than 10 days) is about 0.31m/s. The white noise is about 1m/s.

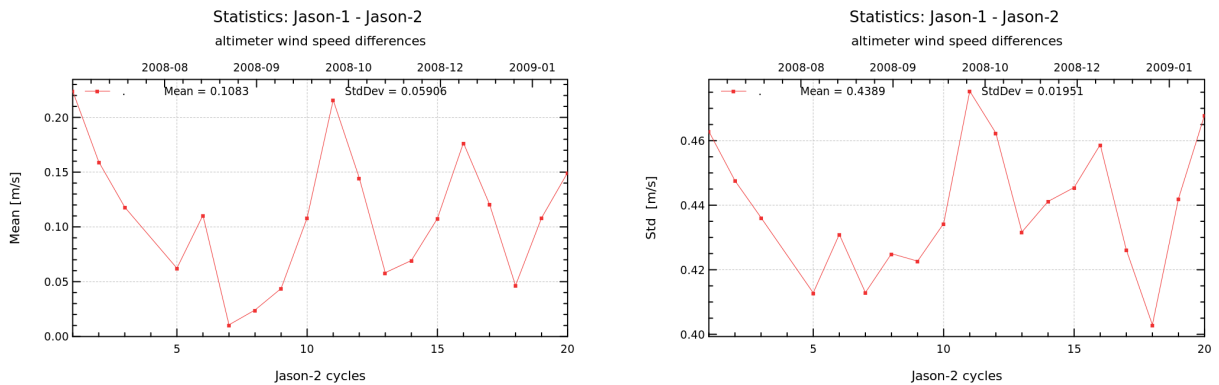


Figure 63: *Cycle per cycle monitoring (mean and standard deviation) of the Jason-1 minus Jason-2 altimeter wind speed.*

7.3.9. Uncertainty on the raw Sea Surface Height (for time scales less than 10 days)

Generally, the raw SSH error specifications (Table 7.2.) were computed by the square root of the sum of the squared individual errors ($\sqrt{(\sum_i \sigma_i)}$). This seems not very fortunate, as noises and correlated errors were mixed up. This can lead to an under-estimation of the error, as the white noise is only a part of the error. Furthermore, the values are not really uncorrelated (e.g. the ionosphere correction is computed using range and sea state bias). Concerning the observed/computed error budget, often only minimum thresholds of the error values are available. So this method leads to a minimum threshold of the error on raw sea surface height. Computing with this method the raw SSH error, yields 1.9 cm for GDR (when using ionosphere correction filtered over 300 km).

Hereafter we use the tandem formation phase between Jason-2 and Jason-1. The sea level anomaly (SLA) contains the parameters and corrections presented in Table 7.2., as well as the mean sea surface. Note that the ionosphere correction used for the SLA computation was filtered over 300 km. The standard deviation of the Jason-1 minus Jason-2 sea level anomaly (SLA) difference is 3.3 cm for GDR. Assuming that both missions contribute equally to the errors, the SLA error is 2.3 cm for GDR. This is a minimum value, especially as some corrections like for example the ECMWF dry troposphere correction are identical for both missions. Nevertheless they are higher than the value computed with the previous method. This would confirm the hypothesis that some items which contribute to error on the SSH were not taken into account.

The uncertainty on sea level anomaly (for timescales less than 10 days) is at least 1.9 cm for GDR when using the method which sums the individual errors. Using the tandem formation phase, the error rises to 2.3 cm for GDR. This is also minimum values.

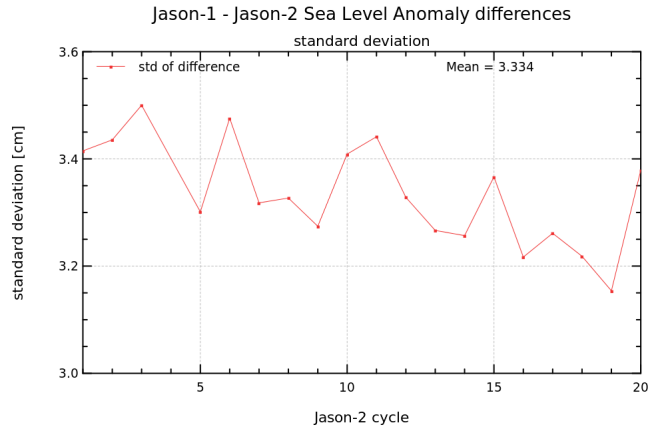


Figure 64: Cycle per cycle monitoring (standard deviation) of the Jason-1 minus Jason-2 sea level anomaly.

7.3.10. Uncertainty on the final SSH (for timescales less than 10 days)

In the previous chapter, the error of the raw sea surface height was computed using the tandem flight phase. This did only give access to the error of a part of the sea surface height computation, as many corrections (like tides) are the same for both satellites. In order to compute the error of the total sea surface height, mono-mission crossover points are used. Standard deviation of ascending/ descending sea surface height (which includes all corrections) yields 5.5 cm for GDR (Figure 65). Generally, range values at crossover points are interpolated per spline and allowing for a 3 cm noise, which reduces the standard deviation. Hereafter no noise was allowed during spline interpolation. As errors on sea surface height are on both tracks (ascending and descending), dividing the standard deviation by $\sqrt{2}$ gives the errors of Jason-1 final sea surface height: 3.9 cm for GDR. This is a maximum value.

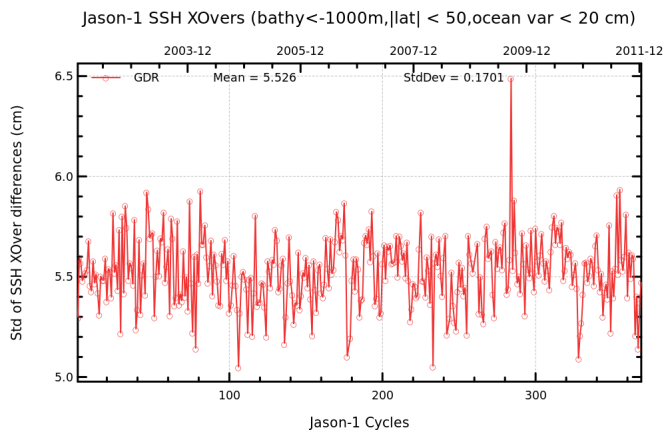


Figure 65: Cycle per cycle monitoring standard deviation of ascending / descending sea surface height differences for Jason-2 OGDR, IGDR and GDR products.

The error of the final sea surface height is less than 3.9 cm for GDR.

7.3.11. System drift

Ablain et al, 2009 and 2015 ([30], [31], [32]) found an error of 0.5 mm/year (in a confidence interval of 90%) for the global mean sea level rate for the period of 1993-2008. For shorter period the error of the mean sea level rate is higher. For regional mean sea level too: systematic uncertainties range between 1 to 3 mm/yr.

Source of error for the MSL calculation	MSL trend uncertainties from 1993 to 2008	
	Minima	Maxima
Orbit:Cnes POE (GDR B) for Jason-1 and GSFC (ITRF2000) for T/P.	0.10 mm/yr	0.15 mm/yr
Radiometer Wet troposphere correction: JMR and TMR (with drift correction).	0.20 mm/yr	0.30 mm/yr
Dynamical atmospheric and dry troposphere corrections using ECMWF pressure fields.	0.05 mm/yr	0.10 mm/yr
Sigma0 drift impacting altimeter wind speed and sea state bias correction	0.05 mm/yr	0.10 mm/yr
Bias uncertainty to link TOPEX A and TOPEX B, and TOPEX and Jason-1.	0.10 mm/yr	0.25 mm/yr
Total error budget	absolute sum	0.50 mm/yr
	quadratic sum	0.32 mm/yr
	inverse formalism	0.6 mm/yr in a confidence interval of 90%

Figure 66: *MSL trend uncertainties from 1993 to 2008 for each correction or model impacting the MSL calculation.*

8. Conclusion

An overview of the impact of the GDR-E version of Jason-1 altimeter system over ocean has been presented in this report. 11.5 years of reprocessed Jason-1 data (standard GDR-E) were analyzed. As they are distributed in NetCDF format, they are easier to use than the precedent versions. Comparisons have been done with previous version data (GDR-C). Taking advantage that Jason-2 and Jason-1 flew on the same ground track with only 55 seconds apart during the formation flight phase (from 12th of July 2008 to 26th of January 2009), particular comparisons with Jason-1 data have been done over this period. From 10th of February 2009 to 3rd of March 2012, Jason-1 flew on an interleaved ground track with a time shift of 5 days compared to Jason-2 ground track, so that comparisons with Jason-1 data have also been done over this period.

The **main objective** of the reprocessing of the Jason-1 altimetric mission was to further improve the data, and in particular the sea level calculation. Despite the waveforms have not been retracked, the reprocessing allows several modifications that correct some problems and improve several standards, following the OSTST community's requests. Jason-1 GDR in version 'E' contain the latest standards available, as well as complementary standards, such as corrections from or based on ERA interim model.

Concerning data coverage, data availability of GDR-E products is the same as the data availability of GDR-C products, except for cycle 175 (one pass intentionally removed from GDR-E). Percentage of invalidated data is similar between GDR-E and GDR-C. Nevertheless, GDR-E products have about 0.04% more valid data.

The mesoscale **performance** is improved: ascending/descending SSH differences are more coherent, with reduced geographically correlated patterns. In addition, the variance of ascending/descending SSH differences at 10 days crossovers is reduced by 1.3 cm². The main contributors to this improvement are the GOT4.10 ocean tide (-0.87 cm²), the POE-E orbit (-0.36 cm²) and new sea state bias and ionosphere correction (-0.08 cm²). Furthermore, data are enhanced in coastal regions thanks to an amended algorithm to compute the radiometer wet troposphere correction (Brown, 2010) and FES2014 ocean tide solution. Computation of the sea level anomaly is more representative thanks to the use of the CNES/CLS 2011 Mean Sea Surface referenced to a 20 years period. Comparisons with Jason-2 show that reprocessed Jason-1 data are geographically more homogeneous to Jason-2 measurements than previous Jason-1 GDR-C version. This is especially the case for sea state bias and ionosphere correction. Regional differences exist still for the orbit component, but as the orbit computation was optimized for best processing for each mission homogeneity between missions was only a secondary priority.

Global mean sea level trend is increased by 0.3 mm/yr. The GDR-E trend is closer to Jason-2 GMSL trend than data from previous GDR-C version:

- using model wet troposphere correction, difference between Jason-1 and Jason-2 GMSL is now around +0.25 mm/yr;
- when using radiometer wet troposphere corrections the GMSL monitorings lead to a difference of -0.4 mm/yr, reduced to +0.1mm/yr without taking into account year 2013.

Furthermore the sub-annual variability in the GMSL trend is improved, as the 58.77-day signal is reduced thanks to the GOT 4.10 tide model, this is also the case when using FES2014 model (Zawadzki, 2015. [25]).

In the future, further improvements of the data are still possible, using for instance further improved corrections: mean sea surface (which takes also into account the interleaved phase from Jason-1, as well as geodetic phases from Jason-1, Cryosat-2 and Envisat), ocean tides, orbit,... Also, on the retracking side, improvement is possible. For GDR-E no retracking was done, but promising retracking algorithms exist, such as numerical retracking (Boy et al., 2014. [18]) used within a prototype to produce experimental Jason-3 SIGDR product. These retracking methods could also be applied to other past missions, such as TOPEX.

9. References

References

- [1] AVISO and PODAAC User Handbook. IGDR and GDR Jason-1 Products. Edition 4.2, June 2012. SMM-MU-M5-OP-13184-CN (AVISO), JPL D-21352 (PODAAC). Available at http://www.aviso.oceanobs.com/fileadmin/documents/data/tools/hdbk_j1_gdr.pdf.
- [2] Dumont, J.-P., V. Rosmorduc, N. Picot, S. Desai, H. Bonekamp, J. Figa, J. Lillibridge, R. Sharroo, 2011 (Issue 1 rev 8.): OSTM/Jason-2 Products Handbook. CNES: SALP-MU-M-OP-15815-CN. EUMETSAT: EUM/OPS-JAS/MAN/08/0041. JPL: OSTM-29-1237. NOAA/NESDIS: Polar Series/OSTM J400. Available at http://www.aviso.oceanobs.com/fileadmin/documents/data/tools/hdbk_j2.pdf
- [3] Roinard H., Philipps S., Ablain M., Valladeau G., and Legeais J.-F., Jason-1 validation and cross calibration activities (Annual report 2013). Reference: CLS.DOS/NT/13-226. Nomenclature: SALP-RP-MA-EA-22269-CLS. Available at http://www.aviso.oceanobs.com/fileadmin/documents/calval/validation_report/J1/annual_report_j1_2013.pdf.
- [4] E. Bronner and G. Dibarboure, May 24th, 2012: Technical Note about the Jason-1 Geodetic Mission. *SALP-NT-MA-EA-16267-CNv1.0*. Available at: http://www.aviso.oceanobs.com/fileadmin/documents/data/duacs/Technical_Note_J1_Geodetic_Mission.pdf
- [5] Ollivier and M. Guibbaud, Envisat RA2/MWR reprocessing impact on ocean data. SALP-RP-MA-EA-22083-CLS. CLS.DOS/NT/12.064. Available at http://www.aviso.oceanobs.com/fileadmin/documents/calval/validation_report/EN/EnvisatReprocessingReport.pdf
- [6] Ollivier et al., JASON-2 / ENVISAT CROSS-CALIBRATION *Oral presentation at OSTST meeting, Venice, Italy*.
- [7] Tran N. , Philipps S. , Bronner E. and Picot N. (2012) Impact of GDR-D standards on SSB corrections, *Oral presentation at OSTST meeting, Venice, Italy*.
- [8] Tran N., Philipps S., Bronner E., Picot N. (2012) Impact of GDR-D standards on SSB corrections, *Oral presentation at OSTST meeting, Venice, Italy*) (http://www.aviso.oceanobs.com/fileadmin/documents/OSTST/2012/oral/02_friday_28/01_instr_processing_I/01_IP1-Tran.pdf)
- [9] Roinard, H., S. Philipps. Jason-2 reprocessing impact on ocean data (cycles 001 to 145). Comparison of Jason-2 Gdr-D with Gdr-T, as well as with Jason-1 Gdr-C and Envisat Gdr v2.1. SALP-RP-MA-EA-22140-CLS. CLS.DOS/NT/12.222.
- [10] Boy, Francois and Jean-Damien Desjonquieres. 2010. Note technique datation de l'instant de reflexion des echos altimetres pour POSEIDON2 et POSEIDON3 *Reference: TP3-JPOS3-NT-1616-CNES*
- [11] <http://www.aviso.altimetry.fr/en/data/products/ocean-indicators-products/mean-sea-level.html>
- [12] Philipps, S., H. Roinard, M. Ablain, G. Valladeau, and J.-F. Legeais. Jason-2 validation and cross calibration activities (Annual report 2013). Reference: CLS.DOS/NT/13-227. Nomenclature: SALP-RP-MA-EA-22270-CLS. Available at http://www.aviso.altimetry.fr/fileadmin/documents/calval/validation_report/J2/SALP-RP-MA-EA-22270-CLS_1_0-RapportAnnuel_J2_2013.pdf.
- [13] Valladeau, G.. Validation of altimetric data by comparison with tide gauge measurements for TOPEX/Poseidon, Jason-1, Jason-2 and Envisat. SALP-NT-MA-EA-22157-CLS, CLS.DOS/NT/12-259.
- [14] Legeais J.-F. and S. Dupuy. 2012 annual report: Validation of altimeter data by comparison with in-situ T/S Argo profiles for T/P, Jason-1, Jason-2 and Envisat missions. CLS-DOS/NT/12-261. SALP-RP-MA-EA-22176-CLS.
- [15] Schaeffer, P., Y. Faugere, J.-F. Legeais, A. Ollivier, T. Guinle, and N. Picot (2012). The CNES-CLS11 Global Mean Sea Surface Computed from 16 Years of Satellite Altimeter Data. *Marine Geodesy* **35**: sup1, 3-19. Available at <http://www.tandfonline.com/doi/abs/10.1080/01490419.2012.718231>

-
- [16] DUACS/Aviso team ‘A new version of SSALTO/Duacs products available in April 2014’ <http://www.aviso.altimetry.fr/fileadmin/documents/data/duacs/Duacs2014.pdf>
 - [17] M.-I. Pujol, Y. Faugere, J. Legeais, M.-H. Rio, P. Schaeffer, E. Bronner, N. Picot. ‘A 20-YEAR REFERENCE PERIOD FOR SSALTO/DUACS PRODUCTS’, OSTST2013 http://www.aviso.altimetry.fr/fileadmin/documents/OSTST/2013/oral/pujol_ChgtRef.pdf
 - [18] Boy, F., N. Picot, J.-D. Desjonqueres, P. Thibaut, J.-C. Poisson, S. Peyridieux. Towards Jason-3 waveforms processing: Assessment of the Numerical Retracking performances. Oral presentation at OSTST Konstanz, Germany, October 27-31, 2014. Available at http://meetings.aviso.altimetry.fr/fileadmin/user_upload/tx_ausyclsseminar/files/28Ball1615-2_Jason-3_Numerical_retracking.pdf
 - [19] GCOS: Systematic Observation Requirements for Satellite-Based Data Products for Climate (2011 Update) - Supplemental details to the satellite-based component of the ‘Implementation Plan for the Global Observing System for Climate in Support of the UNFCCC (2010 Update)’, GCOS-154, WMO, December 2011.
 - [20] Menard, Y., L.-L. Fu, et al. (2003). ‘The Jason-1 Mission Special Issue: Jason-1 Calibration/Validation.’ *Marine Geodesy* 26(3-4): 131-146.
 - [21] Morrow, R., P. Bonnefond, L.-L. Fu, J. Willis, T. Guinle and G. Shirliffe. 2013. Jason-1 : 11.5 years of scientific achievements. Oral presentation at OSTST Boulder, CO, USA, October 8-11, 2013. Available at http://www.aviso.altimetry.fr/fileadmin/documents/OSTST/2013/oral/Morrow_v2.pdf
 - [22] Morrow, R and Pierre-Yves Le Traon, Recent advances in observing mesoscale ocean dynamics with satellite altimetry, *Advances in Space Research*, Volume 50, Issue 8, 15 October 2012, Pages 1062-1076, ISSN 0273-1177, <http://dx.doi.org/10.1016/j.asr.2011.09.033>. Available at (<http://www.sciencedirect.com/science/article/pii/S0273117711007150>) N. Picot, K. Case, S. Desai and P. Vincent, E. Bronner, 2012, ‘AVISO and PODAAC User Handbook. IGDR and GDR Jason Products’, SALP-MU-M5-OP-13184-CN (AVISO), JPL D-21352 (PODAAC). Edition 4.2. Available at http://www.aviso.altimetry.fr/fileadmin/documents/data/tools/hdbk_j1_gdr.pdf
 - [23] Official Announcement, 2013. Long-Running Jason-1 Ocean Satellite Takes Final Bow. Available at [http://www.aviso.altimetry.fr/en/news/front-page-news/news-detail.html?tx_ttnews\[tt_news\]=1490&cHash=cc974e0130b20df2292ac7a40ed07d92](http://www.aviso.altimetry.fr/en/news/front-page-news/news-detail.html?tx_ttnews[tt_news]=1490&cHash=cc974e0130b20df2292ac7a40ed07d92) or <http://www.jpl.nasa.gov/news/news.php?release=2013-213> GDR status. Oral presentation at OSTST Boulder, CO, USA , October 8-11, 2013. Available at http://www.aviso.altimetry.fr/fileadmin/documents/OSTST/2013/oral/GDR_status_2013_Picot.pdf
 - [24] Legeais J-F., Abalin M., Thao S. Evaluation of wet troposphere path delays from atmospheric reanalyses and radiometers and their impact on the altimeter sea level. <http://www.ocean-sci.net/10/893/2014/os-10-893-2014.pdf>
 - [25] Lionel Zawadzki, Michaël Ablain, Loren Carrere, Richard D. Ray, Nikita P. Zelensky, Florent Lyard, Amandine Guillot, Nicolas Picot. Reduction of the 59-day error signal in the Mean Sea Level derived from TOPEX/Poseidon, Jason-1 and Jason-2 data with the latest FES and GOT ocean tide models. <http://www.ocean-sci-discuss.net/os-2016-19/os-2016-19.pdf>
 - [26] Carrere, L., Faugere, Y., and Ablain, M.: Major improvement of altimetry sea level estimations using pressure derived corrections based on ERA-interim atmospheric reanalysis, *Ocean Sci. Discuss.*, doi:10.5194/os-2015-112, in review, 2016. <http://www.ocean-sci.net/12/825/2016/os-12-825-2016.pdf>
 - [27] Legeais, J.-F., Prandi, P., and Guinehut, S.: Analyses of altimetry errors using Argo and GRACE data, *Ocean Sci.*, 12, 647-662, doi:10.5194/os-12-647-2016, 2016. <http://www.ocean-sci.net/12/647/2016/os-12-647-2016.pdf>
 - [28] Abdalla, S., P. Janssen, and J.-R. Bidlot. 2010. Jason-2 OGDR Wind and Wave Products: Monitoring, Validation and Assimilation. *Marine Geodesy*. Vol. 33 (S1):239-255.
 - [29] Abdalla, S., P. Janssen, and J.-R. Bidlot. 2011. Altimeter Near Real Time Wind and Wave Products: Random Error Estimation. *Marine Geodesy*. Vol. 34:393-406.
 - [30] Ablain, M., A. Cazenave, G. Valladeau, and S. Guinehut. 2009. A new assessment of the error budget of global mean sea level estimated by satellite altimetry over 1993-2008. *Ocean Sci.* 5: 193-201. <http://www.ocean-sci.net/5/193/2009/os-5-193-2009.pdf>

-
- [31] Ablain, M., Cazenave, A., Larnicol, G., Balmaseda, M., Cipollini, P., Faugere, Y., Fernandes, M. J., Henry, O., Johannessen, J. A., Knudsen, P., Andersen, O., Legeais, J., Meyssignac, B., Picot, N., Roca, M., Rudenko, S., Scharffenberg, M. G., Stammer, D., Timms, G., and Benveniste, J.: Improved sea level record over the satellite altimetry era (1993-2010) from the Climate Change Initiative project, *Ocean Sci.*, 11, 67-82, doi:10.5194/os-11-67-2015, 2015. <http://www.ocean-sci.net/11/67/2015/os-11-67-2015.pdf>
 - [32] Zawadzki, L. and Ablain, M.: Accuracy of the mean sea level continuous record with future altimetric missions: Jason-3 vs. Sentinel-3a, *Ocean Sci.*, 12, 9-18, doi:10.5194/os-12-9-2016, 2016. <http://www.ocean-sci.net/12/9/2016/os-12-9-2016.pdf>
 - [33] Ablain, M., S. Philipps, N. Picot, E. Bronner. 2010. Jason-2 Global Statistical Assessment and Cross-Calibration with Jason-1. *Marine Geodesy*. Vol. 33 (S1): 162-185.
 - [34] Cerri, L., J.P. Berthias, W.I. Bertiger, B.J. Haines, F.G. Lemoine, F. Mercier, J.C. Ries, P. Willis, N.P. Zelensky, and M. Ziebart. Precision Orbit Determination Standards for the Jason Series of Altimeter Missions. *Marine Geodesy*. Vol. 33 (S1):379-418.
 - [35] Chelton, D.B. 1994. The sea state bias in altimeter estimates of sea level from collinear analysis of TOPEX data. *JGR* vol. 99, C12, pp. 24995-25008.
 - [36] Gaspar, G., F. Ogor, P.-Y. LeTraon, and O.-Z. Zanife. 1994. Estimating the sea state bias of the TOPEX and POSEIDON altimeters from crossover differences. *JGR* vol. 99, C12, pp. 24981-24994.
 - [37] Lambin, J. and C. Tourain. 2007. OSTM/ Jason-2 System Performances Budget. TP3-J0-NT-909-CNES.
 - [38] Lillibridge, J., R. Scharroo, G. Jacobs, L. Russell, and V. Tabor. 2011. *Marine Geodesy*. Vol. 34:191-213.
 - [39] Salstein, D., R. Ponte, K. Cady-Pereira. 2008. Uncertainties in atmospheric surface pressure fields from global analyses. *J. Geophys. Res.*, 113, D14107, doi:10.1029/2007JD009531.
 - [40] Zanife, O.Z., P. Vincent, L. Amarouche, J.P. Dumont, P. Thibaut, S. Labroue. 2003. Comparison of the Ku-Band Range Noise Level and the Relative Sea-State Bias of the Jason-1, TOPEX, and Poseidon-1 Radar Altimeters. *Marine Geodesy*. Vol. 26, 201-238.
 - [41] Alexandre Couhert; Luca Cerri; Jean-Francois Legeais; Michael Ablain; Nikita Zelensky; Bruce Haines; Frank Lemoine; William Bertiger; Shailen Desai; Michiel Otten; Towards the 1 mm/y Stability of the Radial Orbit Error at Regional Scales. *Advances in Space Research*, 2014. doi:10.1016/j.asr.2014.06.041 <http://www.sciencedirect.com/science/article/pii/S0273117714004219>
 - [42] Amarouche, L., L. Zawadzki, A. Vernier, G. Dibarboure, S. Labroue, M. raynal, and J. Poisson. Reduction of the Sea Surface Height spectral hump using a new Retracker decorrelating ocean estimated parameters (DCOR). Oral presentation at OSTST Konstanz, Germany, October 27-31, 2014. Available at: http://meetings.aviso.altimetry.fr/fileadmin/user_upload/tx_ausyclseminar/files/28Ball1615-3.DCORE-OSTST2014_v5.pdf